Evolution of the UG2 unit, Bushveld Complex, South Africa: mineral composition and petrological evidence.

A thesis submitted in partial fulfilment of the

requirements of the degree of

Master of Science

from

Rhodes University

by

Simon J. Everitt

December 2012

Abstract

Several disequilibrium textures are found to occur within the hanging wall and footwall of the UG2 chromitite layer of the Bushveld Complex, South Africa. These textures include plagioclase chadacrysts found included within orthopyroxene and clinopyroxene as well as the orthopyroxenes exhibiting round crystal boundaries that appear to be resorbed. Textures found within the UG2 stratigraphy such as linear boundaries and 120° triple junctions at interfaces of adjacent plagioclase or pyroxene grains also suggest that recrystallization has taken place. The presence of both disequilibrium textures and recrystallization textures would suggest that a complex emplacement history has occurred. Ideally, this would be expected to be manifested by minerals of the same type but which are texturally distinct showing different composition. However this has been found not to be the case; minerals that suggest disequilibrium textures show similar compositions to the minerals which appear to have formed in equilibrium. This is also the same for recrystallized crystals which show the same compositions as crystals that have not been recrystallized. For example tabular clinopyroxene, which has a compositional range of En 44.6 to En 50.5, is indistinguishable from clinopyroxene occuring as discontinuous rims, En 44.3-48.2, and as intergranular necking connecting primocrysts of orthopyroxene (En 44.3-50.4). Similarly, plagioclase occurring as inclusions with An 66.3-76.0 is indistinguishable from plagioclase occurring as zoned or recrystallized interstitial grains (An 69.0- An 77.4). Compositional variation has however, been found to be controlled to an extent by stratigraphy in that minerals show different compositions within one layer to the same minerals within another layer, consistent with an evolving magma composition. It is concluded therefore that while composition is not texturally controlled it is to an extent stratigraphy controlled and that the evidence collected within the study supports two models for the formation of chromite within the Bushveld complex. The evidence is consistent with a combination of the magma mixing model and magma injection model to account for the textures and compositional variations found within the study. The evidence may also show support for models involving late modification of minerals by magmatic fluids but not as prominently as for the models mentioned above.

Acknowledgments

Dr Stephen Prevec and Dr Gelu Costin are thanked for their help and guidance throughout this study. Dr Roger Scoon is thanked for supplying the drill core on which this study is based, and Anglo Pt is thanked for access to additional drill core from Driekop. The use of the Jeol JXA 8230 Superprobe instrument, purchased by Rhodes University with sponsorship from NRF/NEP grant 40113 (UID 74464), is kindly acknowledged.

Contents

1. Introduction

The Bushveld Complex has been studied in detail for many decades and in spite of this there still remains much debate as to the genetic processes involved in the formation of the chromitite layers and the often associated PGE-sulphides. Eales and Cawthorn (1996) summarised the studies done and concluded that there must be several processes taking place at the same time to produce the distinct chromite-rich layers. Previous work suggested that specific magma compositions can be identified as possible parent magmas which may have formed the mineralised Upper Critical Zone (see summary in Costin and Eales, 2012), however compositional and textural data described by Eales et. al. (1991) and discussed by Mondal and Mathez (2007) suggest that the Upper Critical Zone did not crystallise by in situ crystallisation of a liquid into a solid but rather that a mixing of magmas took place due to an injection of new magma. This is backed up by isotopic evidence indicating that mixing of genetically distinct magmas has occurred at and above the Merensky Reef at the top of the Upper critical zone. Prevec et al. (2005) and Seabook et al. (2005) using isotopic evidence indicate that silicates within the Merensky Reef consist of mixtures of genetically distinct phases. As mentioned above Eales et. al. (1991) described textural and compositional variation specifically within plagioclases from the Upper Critical Zone rocks. These textural and compositional variations along with previously described textural evidence indicate a polyphase crystallisation history.

Due to the abundance of evidence described and put forward by several papers there have been a wide variety of models put forward to explain the origin of the mineralised layers and the processes involved. These models include the ephemeral pressure model put forward by Cameron (1977), the magma mixing model by Irvine (1977), the crystal mush model by Hunter and Hamilton (1987) and the model by Eales (2000) which suggests that chromite accumulation is due to crystal charged magmas being injected into the Bushveld complex. Later models include the emplacement of mineralised horizons into existing crystal-liquid piles (crystal mushes) (Mitchell & Scoon, 2004) and the late modification by magmatic fluids (Chutas et al. 2011).

Accordingly the aim of this thesis is, broadly, to examine evidence which will help explain how the Bushveld complex was emplaced. This specifically involves the examination of textural and compositional variation of mineral phases amongst the silicate minerals of the UG2 hangingwall and footwall. In conjunction with examining the silicate mineral phases the UG2 chromitite layer is also being studied to observe if there are any significant variations between textures and compositions throughout the UG2 layer.

This study utilised core provided by R.N. Scoon and additional material collected by the author from the Anglo Pt Driekop exploration camp. These cores include the hangingwall, UG2 layer and the footwall. The methodology of this study involved core logging, petrological examination of thin sections and mineral compositional analysis by electron

probe microanalysis. The microprobe data will allow for mineral compositions to be determined for the observation of mineral variations, evolution and phases. These data complement the Mossbauer spectral data on iron oxidation state, collected by the author in an earlier paper (Adetunji et. al., 2013), which may be used to demonstrate mineral evolution.

The aims of this thesis have been chosen to coincide with the economic nature of the Bushveld complex as they will help to understand how emplacement took place and there for a greater understanding of how the economic minerals were formed and why, allowing for better exploration techniques and mining models. The thesis is being produced in conjunction with a complimentary study by Mark Rains which is looking at similar minerals and evidence within the overlying Merensky reef and its surrounding hangingwall and footwall. This will allow for a comparison of evidence and findings and allow for a model for emplacement to be produced.

2. Geological Setting

The Bushveld complex of South Africa is the largest mafic layered intrusion, and covers an area of approximately 68,000km^2 (Hunter, 1975). Five separate chambers or limbs are recognizable through outcrop and sub-outcrop. The focus of this thesis is the Eastern Limb of the complex and more specifically the Upper Critical Zone of the Rustenburg Layered suite.

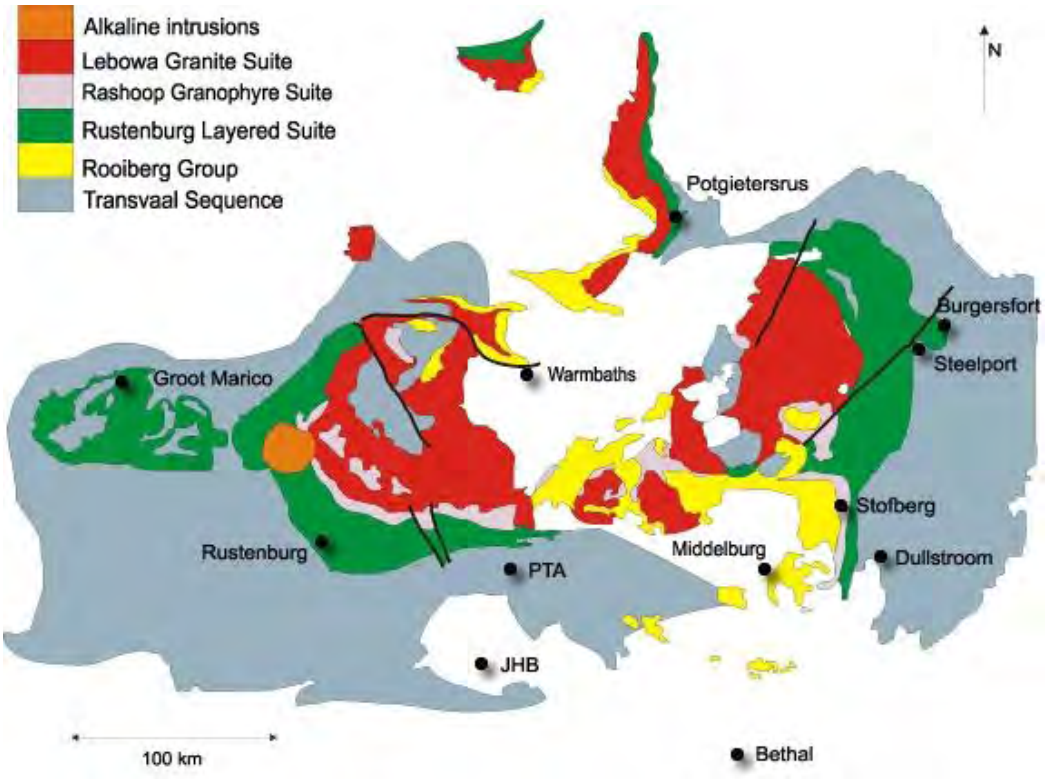

Figure 1a: Simplified stratigraphy of the Bushveld complex (after Kinnaird, 2005).

The Rustenburg Layered Suite includes the basal Marginal Zone and a succession of mafic-ultramafic rocks which have been divided into the Lower Zone, Lower Critical Zone, Upper Critical Zone, Main Zone and Upper Zone. The suite has a maximum thickness of 9km and conservative estimates estimate that its volume is in the range of 150,000km^3 to 400,000km^3 (Harmer, 2000). The range of volumes is due to the unknown volume of mafics that may or may not continue below the suite. The suite's age has been determined as 2054Ma $\pm$3Ma using both SHRIMP and IDTIMS data from the Critical Zone (Armstrong et al. 2000).

Figure 1b: Simplified stratigraphy of the Eastern lobe of the Rustenburg layered suite (after Kinnaird, 2005).

The Upper Critical Zone is the upper portion of the Critical Zone and is distinguished from the Lower Critical Zone by the presence of cumulus plagioclase. This occurrence appears between the MG3 and MG2 chromitite layers. The Upper Critical Zone is characterised by

distinct cyclic layering of chromitites, norites, pyroxenites and anorthosites. The focus within the Upper Critical Zone is the UG2 chromitite layer and it hanging and footwall (Kinnaird,2005)

The UG2 hanging wall is a pyroxenite which consists of cumulus orthopyroxene, interstitial plagioclase and clinopyroxene and minor, variable amounts of phlogopite as well as other accessory phases. The footwall is also a pyroxenite layer similar to the hanging wall, however there are several distinct differences between the two layers. The first difference is the chromite content of both layers; the footwall contains chromite throughout which occurs as <0.5mm subhedral grains which are interstitial and inclusions within orthopyroxene. The chromite content in the hanging wall is distinctly less and can only be found occurring within 2m of the UG2 chromitite and is completely absent from the overlying pyroxenites and norites. The second is that the footwall exhibits centimetre-sized oikocrysts of clinopyroxene, which can be observed in outcrop. The hanging wall contains about the same amount of clinopyroxene as the footwall however it occurs as coronas on the orthopyroxene and as vastly smaller oikocrysts that are found interstitially between the orthopyroxene. The third difference is the homogeneous nature of the footwall which contains a modal average of about 70% orthopyroxene, whereas the hanging wall varies between 40% and 70% with an average of approximately 55-60% orthopyroxene. Due to the modal variations being gradational, leucocratic layers are not distinct from the pyroxenite and are included as part of the pyroxenitic units. Lastly, textures within the hanging and footwall rocks differ. The footwall containss orthopyroxene as both subhedral, elongate tabular grains and also as smaller, irregular grains among larger ones. The hanging wall exhibits more equant, subhedral to rounded orthopyroxene which appears' better sorted' and finer in grain size.

The granular pyroxenes are surrounded by a matrix of intergrown plagioclase grains which range in size from 0.1mm-1mm. In many of the hanging wall rocks the plagioclase also occurs as rounded to slightly elongate lath shaped inclusions in poikilitic pyroxenes, hence also known as chadacrysts. These inclusions occur within both the orthopyroxene and clinopyroxene (Mondal and Mathez, 2007).

As mentioned in the introduction there have been several models proposed to explain the emplacement of the Bushveld complex and more specifically the formation of the chromitite layers found within the critical zone. Cameron, (1977) suggested that an ephemeral pressure increase in the magma chamber could account for the formation of chromitites in the Bushveld, a concept later developed by Lipin (1993). Cameron (1980) stated that a reversal of normal fractionation trend such as that seen in the Critical Zone could not be due to a simple change of temperature, as a rise in temperature would cause crystallization to cease and a fall in temperature would simply accelerate the normal fractionation trend. Reversal requires a change in bulk composition of the system or a change in total pressure. Bulk composition can take place through assimilation of the wall

rocks, by the diffusion of gasses into and out of the magma, and by pulses or injections of parent or new magma into the chamber. Changes in total pressure might be due to tectonic deformation of the chamber, by the rupturing of the chamber walls which allows the lateral escape of magma and therefore a decrease in the magma column height. Pressure change may also be due to an increase in magma column height through the injection of new magma into the chamber or by build-up and release of pressure due to surface eruption. Any one or combination of the above mentioned mechanisms can cause compositional changes between pyroxenite and chromitite; however the patterns of change are not necessarily the same (Cameron, 1980).

Irvine (1977) suggested that the mixing of a chemically primitive magma on the olivine-chromite cotectic with a more evolved magma may result in a mixture saturated in chromite alone. This is a result of the manner in which the olivine-chromite cotectic is curved (Mondal and Mathez, 2007). This mixing of magmas results in a magma composition that lies within the chromite stability field and for a brief interval would only crystallize chromite. The chromite being relatively dense could settle fairly efficiently allowing for a monomineralic layer of chromite to form on the floor of the chamber (Robb, 2005).

The crystal mush model by Hunter (1987) suggests that most crystal accumulation within large layered intrusions takes place on the floor where crystal mushes develop. These mushes either develop by in situ crystallization or by crystal sedimentation (settling). There are no definitive textural differences between these two methods except where crystal shape orientation occurs as a result of directional growth from a substrate. Mushes inherit primary texture characteristics that influence the subsequent texture within the crystal pile.

The paper by Eales (2000) suggests adopting a model that allows for the injection of crystal charged magmas into the resident magmas within the Bushveld chamber. These crystal charged liquids are suggested to be evolved within a deeper magma chamber which is undergoing crystallization. This helps to explain the high average chromite content found within the Critical Zone which may be due to the introduction of excess chromite in the form of suspended chromite microphenocrysts (Eales, 2000).

More recent papers by Chutas et al. (2011) and Maier et al. (2012) use isotopic data to suggest that isotopic disequilibrium is present. It is assumed that the crystal assemblage was isotopically homogeneous and that a two stage process is envisaged to explain the isotopic disequilibrium. The first stage involves crustal contamination which is thought to have migrated through the crystal mush as it underwent textural modification driven by crystal aging and recrystallization. The radiogenic overprint mainly affected those grains that were actively growing. While both pyroxene and plagioclase are radiogenically enriched it is the plagioclase that is slightly more enriched due to the partitioning preference of Sr for plagioclase. Due to this overprint likely being imposed on the pre-existing stratigraphic increase in Sr in the initial assemblage, the bulk Sr associated with the alteration event cannot be determined precisely. The second stage is the late contamination of young lead.

As the crystal pile continues to cool the orthopyroxene begins to undergo very fine exsolution of clinopyroxene. It is assumed that the presence of lamellae greatly increases that grain boundary area of the two exsolved pyroxenes allowing easy migration of younger lead into pyroxene. This infiltration of lead could have continued long after the Bushveld complex had cooled to ambient temperatures (Chutas et al. 2011). This model suggests a change in the rock composition but only as isotopic enrichment of already formed and forming crystals. This disequilibrium has led to overprinting of Sr and Pb and the formation of clinopyroxene rims forming through exsolution of orthopyroxene.

2.1. Evidence for disequilibrium

The main features of these chadacryst occurrences in the Western Limb of the Bushveld complex are that the inclusions are commonly 0.02mm-0.25mm in size and they are spheroidal, ovoid or irregular in shape suggesting resorption. The inclusions occur within cumulus pyroxenite grains, pyroxenite orthocumulates and norites. Inclusions most commonly show reverse zoning, but normally zoned and unzoned inclusions are also found. An compositions range from 60-75 which is similar in composition to the cumulus and intercumulus plagioclase of the host rocks. (Eales et al. 1991)

Microprobe analysis of both inclusions and cumulus plagioclase show no distinct compositional variations between the two distinct textures. Some bias is shown in the Fe content of the chadacrysts in that as many as 70% of the inclusions show Fe-enrichment relative to the cumulus plagioclase. Compositional differences can be seen as a regional trend, with more calcic inclusions being present in the northwest and more sodic compositions towards the southeast.

The inclusion of lath shaped or blade-like plagioclase crystals by pyroxenes is often observed within gabbro's, dolerites and some coarse grained basalts (Eales et al. 1991). The intergrowth of these minerals is these instances suggest the early crystallization of plagioclase or cotectic crystallization with the pyroxenes. However in the case of the Bushveld rocks the inclusions imply that the plagioclase existed at an earlier stage within melts before resorption and encapsulation by orthopyroxene took place prior to the filling of pore space by interstitial, cumulus plagioclase.

There are several possible origins of these inclusions among which the following seem the most plausible. The first is that the inclusions represent aberrations in the normal order of crystallisation phases; this may be due to a different parent magma being involved which has a different crystallisation sequence. The alternate parent magma may be present in underlying parts of the Bushveld. The second is that the inclusions represent plagioclase that nucleated within a bottom zone which was enriched with the components of feldspar, and then the consequent growth of pyroxenites in-situ on the floor of the complex. The third is that the inclusions are a result of sub solidus recrystallization, or a result of solution and reprecipitation in crystal mushes as described by Hunter (1987). The fourth possible

origin is that the inclusions represent feldspar crystals that settled out from higher liquid layers within a stratified liquid column. Lastly the inclusions may be as a result of mixing of an evolved, residual liquid with a more primitive liquid.

Some of these possible origins have been rejected due to the lack of evidence to account for the Sr-isotopic disequilibrium which seems to prevail within the feldspar population. These discounted theories also do not account for resorption or the preservation of the crystal zoning in both cumulus pyroxenes and feldspars. Furthermore they do not account for the preservation of primary foliation of well zoned, bladed crystals parallel to the layering. (H.V.Eales et al. 1991)

3. Methodology

The methods used in this study include the selection of sampling sites and collection of samples for thin and polished thin sections, and electron microprobe analytical work.

3.1 Sampling

The first step that had to be taken was to log both drill cores that were provided. This was done by using a standardised input form in Excel. Logging was done to give an overview of the stratigraphy in the core and to determine where major units are in relation to each other and additionally where major textural differences occur e.g. grain size increase. Both core logs are provided in Appendix A with a separate log for each core, the logs have been summarised below in figure 3a within the petrology section. The sites for thin sections have been determined using these core logs so that all major units are represented as well as areas of interest, such as textural differences.

These sites are then marked out and cut into blocks with the same dimensions as the final slide. These blocks were submitted to the Rhodes thin sectioning facility where they were ground down and adhered to glass slides to produce the thin sections. These slides are initially left uncovered and unpolished and petrological descriptions are produced, along with photomicrographs which illustrate the textures and minerals described. Comparisons of slides allow for textural differences to be noted within the same unit and between units as well as differences between minerals. Slides were then selected to be polished for use in the electron microprobe. The slides were selected because of textural differences from the norm, where there is an abundance of inclusions, as described in the petrology section. Slides are also selected to give a good representation of the major units. The slides were then sent back to the Rhodes thin sectioning facility where they were polished in preparation for use in the electron microprobe. Once the slides were polished sites were selected within the silicate slides where discontinuous rims, oikocrysts, triple junctions and inclusions occur. These sites were selected using a microscope and marked around the site in question with a permanent fine marker so they can be identified in the microprobe. In the

case of chromitite slides no sites were preselected due the abundance of textures within a slide and the relative ease in finding the textures within the electron microprobe. Preselecting sites for the chromite was also not done due to the lack of textural correlation with the silicate mineralogy. This means that chromite grains were sampled at random; however they are selected throughout the slide giving a good representation of the whole slide and textures found within the slide. A total of 14 slides were taken between the two cores which represent the hangingwall, UG2 chromitite, Footwall and pegmatoid. The table below shows where the slides were taken from in terms of unit and height within the core.

Stratigraphy	Slide	Core	Summary
Hangingwall	P1	WH-1	Top of hangingwall. Norite.
	P2	WH-1	Middle of hangingwall. Norite to pyroxenite.
	P3	WH-1	Hangingwall near UG2 contact. Pyroxenite
UG2 Chromitite	C1	WH-1	Top of UG2. Chromitite.
	C2	WH-1	Middle of UG2. Chromitite.
Pegmatoid	P4	WH-1	Pegmatoid within UG2. Pyroxenite with large tabular orthopyroxene grains.
UG2 Chromitite	C3	WH-1	Lower UG2. Chromitite.
	U1	Eastern Bushveld Core	Lower UG2. Chromitite.
	U2	Eastern Bushveld Core	UG2 footwall contact. Pyroxenite in contact with chromitite.
	C4	WH-1	UG2 footwall contact. Pyroxenite in contact with chromitite.
Footwall	U3	Eastern Bushveld Core	Top of footwall. Pyroxenite.
	Ftw	WH-1	Top of footwall with Chromitite seamlet. Pyroxenite hosting chromitite seamlet.
	U4	Eastern Bushveld Core	Footwall 15cm below contact. Pyroxenite

	U5	Eastern Bushveld Core	Footwall 30cm below contact. Pyroxenite.

Figure 2: Table summarising thin section locations and content.

3.2 Electron microprobe

Once the sites were selected the slides were carbon coated in preparation for the electron microprobe. The electron microprobe or EPMA (electron probe microanalyser) in question is a Jeol JXA 8230 Superprobe which uses 4 WD spectrometers. The EPMA data acquisition was performed at Rhodes University, Department of Geology. Analytical conditions employed were: acceleration voltage 15 kV, probe current 20 nA, counting time 10 sec on peak and 5 sec on background (except for Ni, where the counting time was 20 s and 10 s, respectively). Pyroxene, feldspar and chromite were analysed with spot beam size (<1 micron). The standards used for measuring the characteristic Kα radiations were natural minerals: forsteritic olivine std. for Si and Mg in pyroxene; fayalite std. for Fe in all silicates; diopside std. for Ca in pyroxene; orthoclase std. for Al in all silicates and chromite's. In all analysed minerals the following standards were used: chromite for Cr; sphene for Ti, rhodonite for Mn, orthoclase for K and albite for Na. In most of the cases where an element concentration is below 5%, a large diffracting crystal with high sensitivity was used: LIFL for Ni and Mn in both silicates and chromite's; PETL for Ti and Cr in silicates, V in chromite; TAPL for Na in pyroxene. The ZAF matrix correction method was used for quantification.

Once the data was collected offline quantitative corrections were performed on the data by Dr Gelu Costin. The corrected data was then accessed by the author using the SPview software where it was saved into Excel format and normalised using a pre-existing calculation format. SPview also allowed for the data points to be seen on the photos taken by the EPMA when sampling. This allowed for sites to be differentiated based on textural evidence. This then allowed for comparisons in compositions in minerals to be observed and in what textures the different compositions are taking place. Data was then also put through the MINPET software where it is calculated into cations and classified. The classifications were done visually using graphs.

4. Petrology

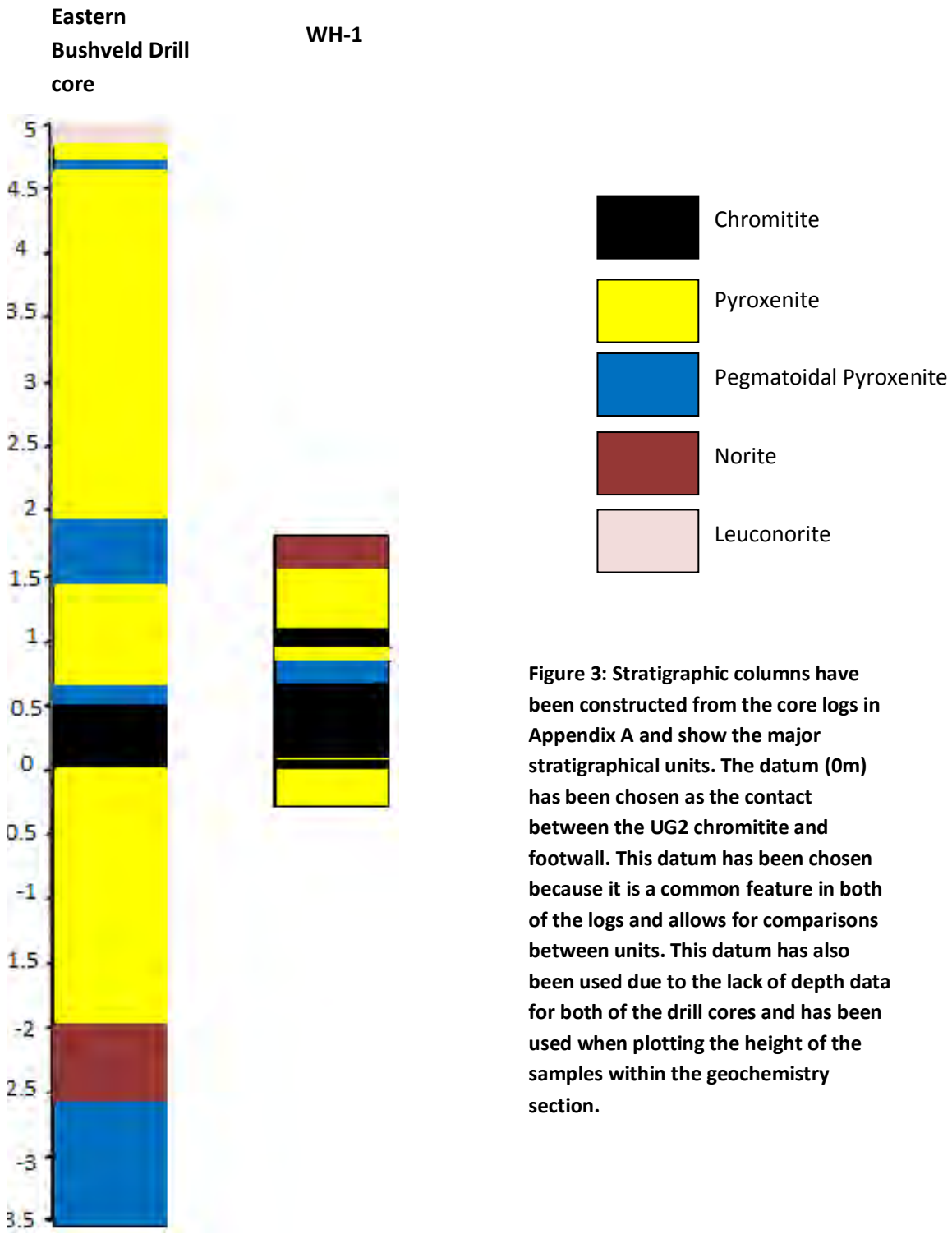

Figure 3: Stratigraphic columns have been constructed from the core logs in Appendix A and show the major stratigraphical units. The datum (0m) has been chosen as the contact between the UG2 chromitite and footwall. This datum has been chosen because it is a common feature in both of the logs and allows for comparisons between units. This datum has also been used due to the lack of depth data for both of the drill cores and has been used when plotting the height of the samples within the geochemistry section.

4.1 Core Logs

The core logs provided in Appendix A outline the major units within the stratigraphy from both cores. The logs also provide basic textural descriptions from looking at the core samples in hand specimen. These have then been used to create a simplified stratigraphic column (Figure 3) to enable better comparisons between the units of each core. The petrological descriptions below have been split into four basic sections which incorporated the units from the logs. These sections are the hangingwall, pegmatoid, UG2 chromitite and footwall. The hangingwall and footwall are generally comprised of the same rock type, pyroxenite, and show similar textures within both sections as can be seen from both the core logs and figure 3. These pyroxenites are composed of clinopyroxene, orthopyroxene and plagioclase with varying abundances of each mineral. These abundances have been summarised below in the sections and help to determine the rock type. The pegmatoid has been included due to its presence in both cores and because it is a textural change which in WH-1 takes place in the middle of the UG2. The pegmatoid when compared across both cores, as seen in figure 3, appears in different stratigraphic order. In the Eastern Bushveld core the pegmatoid is found to occur above the UG2 with the main body of the pegmatoid still below the UG2, whereas in the WH-1 core it is found in the middle of the UG2. The main body of the pegmatoid has not been observed within the WH-1 due to the lack of footwall. The pegmatoid appears sporadic in its occurrence within the Eastern Bushveld core. The main boddy occurs well below the UG2 which is consistent with the stratigraphy described by Mondal and Mathez (2007). The layers of pegmatoid above and within the UG2 however are not described. This may mean that the sporadic nature of the pegmatoid observed in this core is localised. This layer differs from the haningwall and footwall in that it contains large very coarse grains of orthopyroxene and clinopyroxene. The rock type however, is the same as both the hangingwall and footwall (pyroxenite) and shows similar mineral abundances. This unit does not share the same textures as the other units, as described in the petrology below, and is the reason for its inclusion within the study. The final unit included is the UG2 chromitite layer. This unit is one of the most economic layers in the Bushveld complex due to its high grade chromite and abundance of PGE-sulphides. The study has been tailored around this study and as such is the reason for the study as mentioned above. The chromitite in hand specimen appears to be a homogeneous layer with no textural variation or significant changes in mineral abundances and assemblages. The layer does however have stratigraphic differences as illustrated in figure 3. The differences include overall thickness of the layer and the fact that in WH-1 it appears to split into several seams. Overall both cores contain the major units which have allowed for comparisons to be made between them, however there are major differences in the occurrence of units between the cores and the position in which they occur most notably in the case of the UG2 chromitite.

4.2 Mineral Textures

Orthopyroxene:

The textures found within the orthopyroxene are coarse-grained tabular subhedral or anhedral grains and finer-grained, rounded anhedral grains. The coarse-grained tabular grains make up the bulk of the orthopyroxene grains and can often be found to form triple junctions. The figure 4 below shows basic sketches of the two textures. The coarse-grained tabular grains are also found to contain inclusions of plagioclase. The finer-grained, rounded grains are not as common and generally occur where there is abundance of plagioclase.

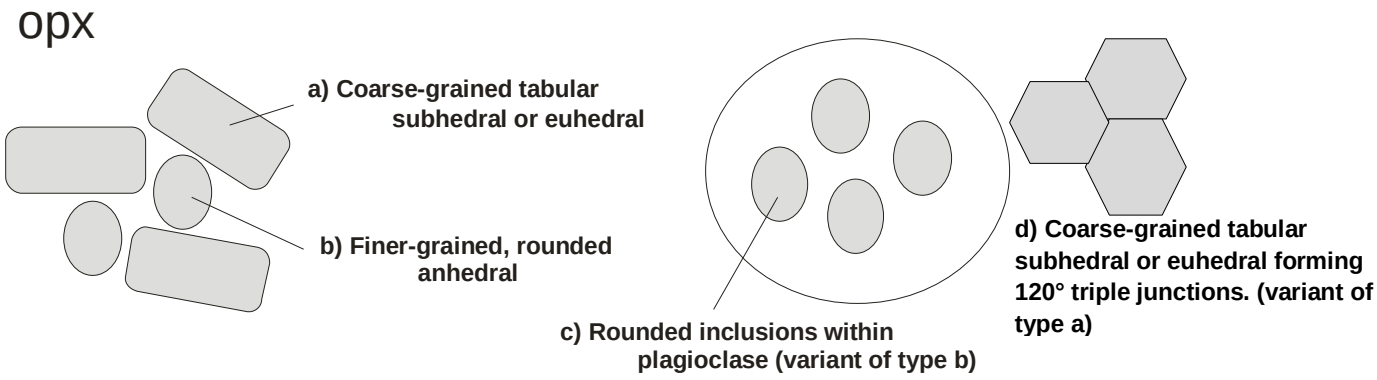

Figure 4: Simplified sketch of orthopyroxene textures found within the stratigraphy.

Plagioclase:

Plagioclase occurs as three textures, these include; inclusions, zoned tabular grains and coarse-grained recrystallized grains. The inclusions occur generally within the orthopyroxene where they appear rounded. These grains are found abundantly within areas and in other areas there are little or no plagioclase inclusions. The inclusions have very rarely been found to occur within clinopyroxene but have been found. The inclusions have also been observed in association with discontinuous rims of clinpyroxene. The zoned tabular grains have been observed as subhedral to anhedral. None of the inclusions have been observed to be zoned. This zoning generally occurs within the larger plagioclase grains within the units and occurs throughout the units with no defined zones are areas in which they do or do not occur as with the inclusions. The coarse-grained grains, like the zoned grains, appear to occur interstitially. The recrystallized grains have been interpreted as recrystallized due to the lack of zoning in the grains. The zoning will have been overprinted when the plagioclase was recrystallized. The zoned grains and coarse-grained recrystallized grains have been grouped together within the study due to the interstitial nature of the grains and because the zoned and recrystallized grains cannot be distinguished within the electron microprobe. This grouping together has also been done due to no compositional

zoning correlating to grain textures. This means that there is no systematic difference between rims and cores within the zoned plagioclase. The large range in plagioclase composition therefore does not correlate to early and late crystallisation allowing for both zoned plagioclase and recrystallized plagioclase to be grouped together. However to allow for compositional variation to be observed across grains where zoning occurs several points have been taken across the grain from rim to rim. The textures described above can be seen illustrated in figure 5.

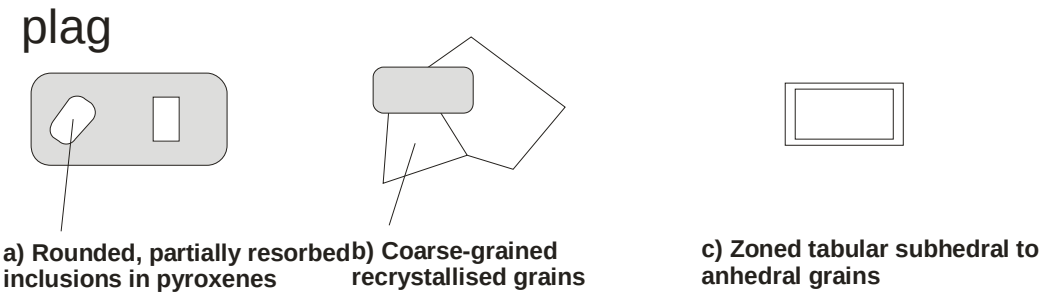

Figure 5: Simplified sketch of plagioclase textures found to occur within the stratigraphy.

Clinpyroxene:

The clinopyroxene within the samples has been observed to form in several different textures. These textures include; exsolution lamellae (a), discontinuous rims (b), intergranular necking (c), oikocrystic (d) and tabular subhedral grains (e). The exsolution lamellae often occur in association with discontinuous rims. Both occur in association with orthopyroxene where the clinopyroxene appears to have exsolved from. The lamellae form thin, vein like structures in appearance within orthopyroxene grains and can often be observed to have formed within the discontinuous rims. These lamellae are differentiated from the orthopyroxene grain in which they're hosted by their high birefringence colours, in comparison to the orthopyroxene, and by their lighter colour within the electron microprobe. The discontinuous rims are found to occur on the edges of orthopyroxene grains and between orthopyroxene grains and plagioclase inclusions. These rims vary in size and are described as discontinuous as they do not continue around the orthopyroxene grain as a reaction rim does but rather form sites. The intergranular necking is found to occur between orthopyroxene grains and sometimes between chromite grains within the UG2. The intergranular necking occurs where clinopyroxene has filled pore spaces between grains which have formed prior to the clinopyroxene. The oikocrystic clinopyroxene are extra coarse-grained and contain inclusions. These inclusions are generally plagioclase but oikocrysts have been found within the UG2 chromitite where the inclusions are chromite grains. The tabular subhedral grains are the most abundant of the textures and are found to

occur throughout the stratigraphy. These grains are subhedral and fine to coarse-grained. These differ from the oikocrysts as they do not contain inclusions. The textures have been sketched simply in the below figure 6.

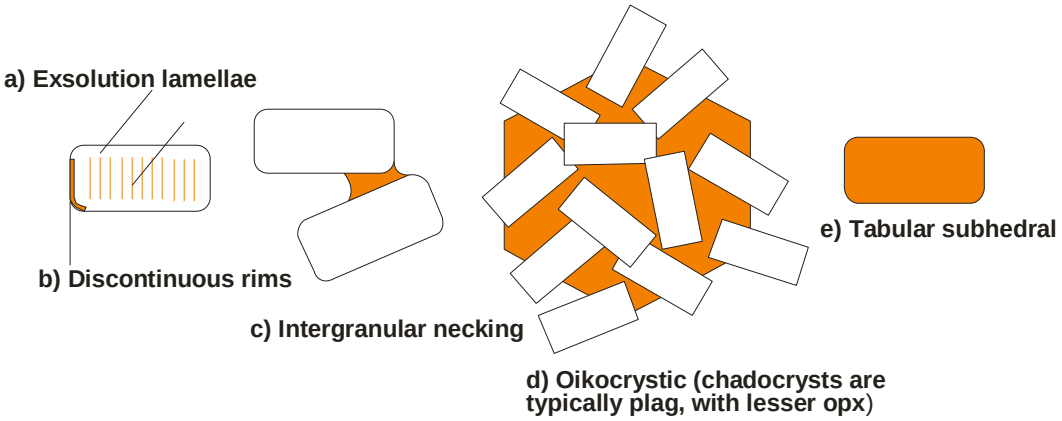

Figure 6: Simplified sketch of clinopyroxene textures found to occur within the stratigraphy.

Chromite:

The chromite has been observed to occur in three different textures. These textures include; sub-coalescent, coalescent and annealed. The sub-coalescent and coalescent textures appear very similar. These textures only differ in amount of pore space and the average grain shape. The pore space differs only slightly between the two textures with the sub-coalescent texture having slightly more interstitial pore space than the coalescent texture. The average grain shape for the sub-coalescent texture shows a generally more rounded subhedral grain shape whereas the coalescent texture shows more angular, subhedral grain shape as well as a tendency for grains to produce chains. These chains consist of several grains which show no pore space between them. These chains have no preferred orientation and no preferred areas in which they form. The annealed texture generally occurs as a zone within either of the two textures described above. These zones of annealed texture are differentiated from the surrounding texture as they appear as a large grain or mass of chromite. When observing this texture closely it can be observed to be comprised of several grains which have been recrystallized and joined together to create a relatively large mass of chromite.

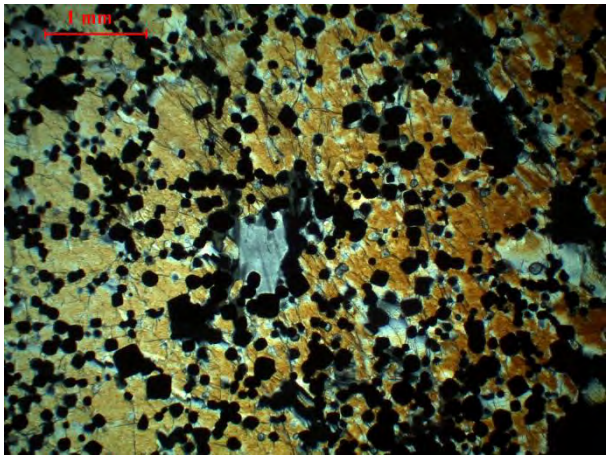

Figure 7: Chromite exhibiting sub-coalescent texture taken from slide FTW.

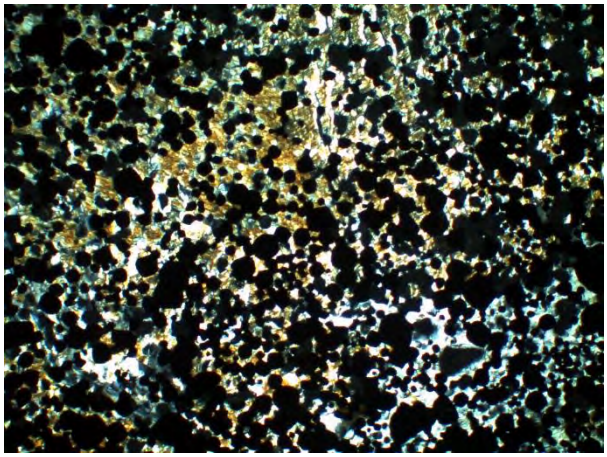

Figure 8: Chromite exhibiting coalescent texture taken from slide C2.

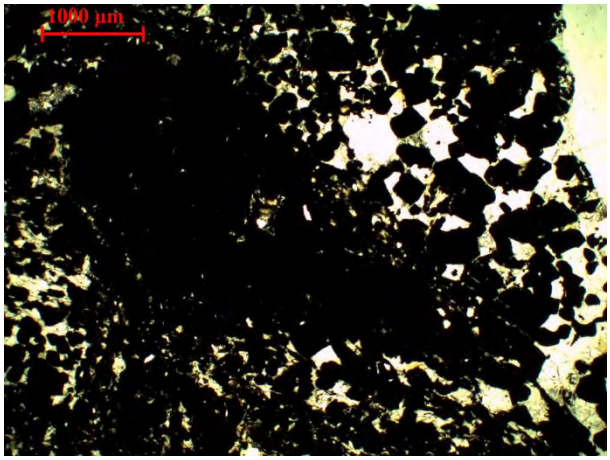

Figure 9: Chromite exhibiting annealed texture taken from slide U2.

Biotite:

Biotite appears to only be found as small lath-shaped grains which occur interstitially, generally in association with chromite. These laths are thin and rectangular in shape and form with no preferred orientation. Figure 10 below shows a good example of biotite within the samples.

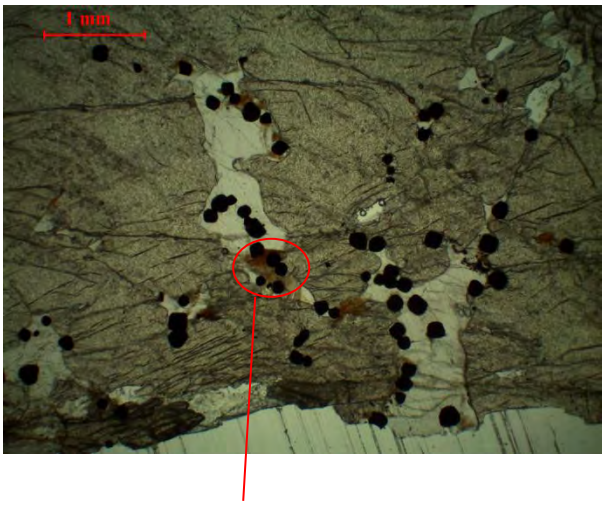

Figure 10: Example of biotite texture found within the stratigraphy taken from slide P4.

4.3 Hangingwall

The hanging wall of the UG2 gradationally changes up stratigraphy from pyroxenite to norite as well as showing grain size fining upwards. There is also a chromitite stringer present within the hanging wall just above the UG2 as described in the core log WH-1.

Mineral	Modal Abundance
Orthopyroxene	60-70%
Plagioclase	20-40%
Clinopyroxene	15-25%
Chromite	3%

Orthopyroxene:

The orthopyroxene in the hanging wall is found as course-grained tabular grains which are euhedral to anhedral in shape. The orthopyroxene has often been observed with grain boundaries of adjacent grains forming triple junctions (figure 11a) which suggests that recrystallization has occured. Some of the tabular grains have rounded grain boundaries with the interstitial plagioclase. The orthopyroxene makes up between 60% and 70% of the hanging wall rocks and ranges in grain size from 0.5mm to 1mm.

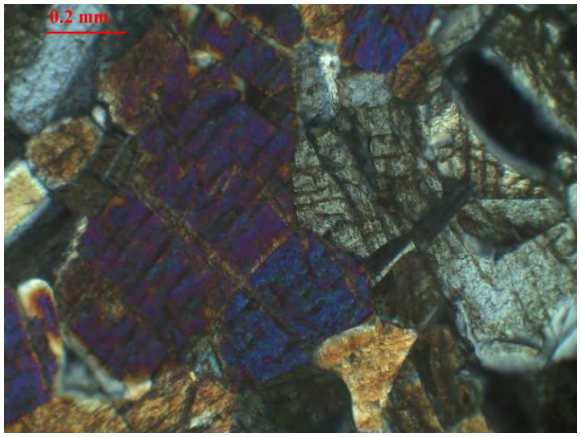

Figure 11: Photomicrograph taken from slide P2 of clinopyroxene forming a triple junction with orthopyroxene.

Plagioclase:

Plagioclase occurs mainly as a zoned or recrystallized plagioclase which occurs interstitially, filling the space between orthopyroxene and clinopyroxene grains. Zoned plagioclase is subhedral to anhedral in shape (Figure12b). The plagioclase also occurs as inclusions (Figure12a) within orthopyroxene grains which are rounded in shape suggesting resorption prior to inclusion within the host orthopyroxene. These inclusions vary in size from approximately 0.1mm to 0.5mm. Inclusions also vary in shape from ovoid to spheroidal. The inclusions unlike the zoned plagioclase do not show zoning. Plagioclase makes up 20% to 40% of the hanging wall rocks.

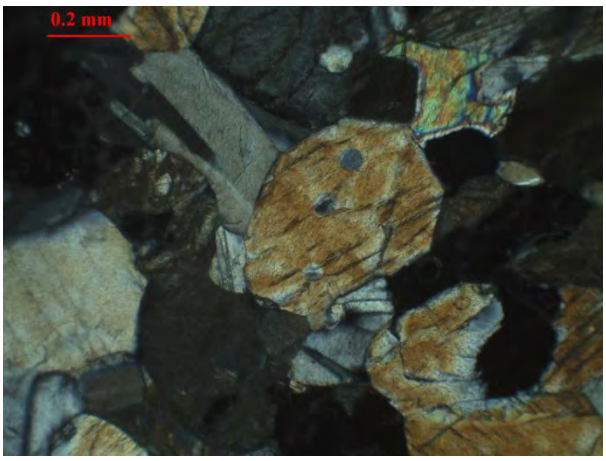

Figure 12a: Photomicrograph taken from slide P1 of plagioclase chadacrysts within orthopyroxene.

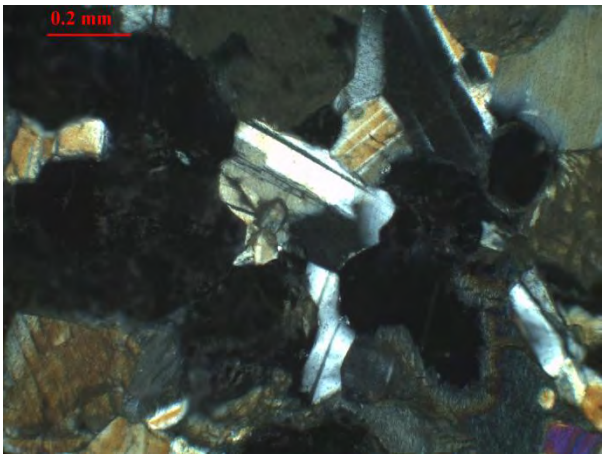

Figure 12b: Photomicrograph taken from slide P1 of zoning withinterstitial plagioclase.

Clinopyroxene:

Clinopyroxene is found in three different textures. These are tabular rims, discontinuous rims on orthopyroxene and as exsolution sites or lamellae within plagioclase and orthopyroxene. The discontinuous rims (figure 13a and 13c) occur at the boundaries of the orthopyroxene but do not continue around the whole grain. The rims are also seen in association with some of the plagioclase inclusions where the rims again do not continue around the whole inclusion but rather concentrate in one place. The exsolution lamellae of clinopyoxene are not found abundantly and occur within plagioclase (figure13c) and within orthopyroxene. These inclusions are small, <0.1mm-0.2mm, and are spheroid in shape. The rounded boundaries of the inclusions suggest resorbtion of the clinopyroxene has taken place. Tabular grains of clinopyroxene do not occur abundantly within the hangingwall but are present (figure 13a) The clinopyroxene in the hanging wall makes up between 15% and 25% and ranges in grain size from <0.1mm-0.8mm.

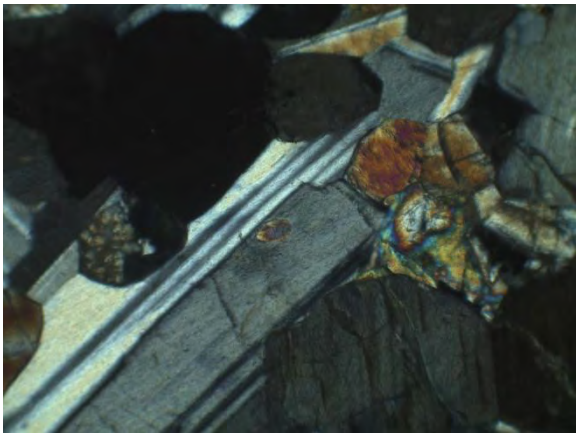

Figure 13a: Photomicrograph taken from slide P2 of clinopyroxene reaction rim in association with orthopyroxene oikocryst and clinopyroxene inclusion within plagioclase.

Figure 13b: Photomicrograph taken from slide P3 of plagioclase chadacryst within coarse-grained tabular orthopyroxene with associated clinopyroxene reaction rim.

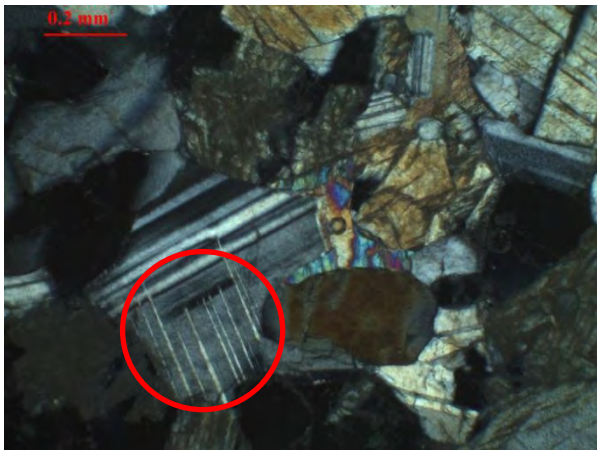

Figure 13c: Photomicrograph taken from slide P1 of clinopyroxene reaction rim around plagioclase and exsolution lamellae (circled in red).

Chromite:

Chromitite in the hanging wall is found as both disseminated grains often as inclusions within orthopyroxene and as a 2mm thick stringer. The chromitite stringer occurs just above the hanging wall- UG2 contact. Chromite within the hanging wall occurs as subhedral to anhedral grains that are generally included within orthopyroxene grains. Chromite makes up only about 3% of the hanging wall rock with concentration of chromite increasing downwrds towards the UG2- hanging wall contact. Chromite in the stinger however is about 85%-90% and shows sharp contacts with the surrounding pyroxenite.

4.4 Pegmatoid

The pegmatoid layer (slide P4) is present within the UG2 chromitite as indicated within the core log WH-1 in Appendix A. This layer is a very coarse grained pyroxenite with both orthopyroxene and clinopyroxene forming coarse-grained pegmatoidal oikocrysts and plagioclase forming the interstitial material. This pegmatoidal layer is not found to occur within the UG2 layer in the Eastern Bushveld core but rather occurs above the UG2 as is a much thicker layer.

Mineral	Modal Abundance
Orthopyroxene	60%
Plagiolcase	15%
Clinopyroxene	20%
Chromite	3%
Biotite	2%

Orthopyroxene:

The orthopyroxene occurs as euhedral to subhedral coarse-grained tabular grains. These have not been observed forming triple junctions like the tabular grains witin the hanging wall. The lack of triple junctions may only be a function of where the slide was selected from not containing triple junctions or when the slide was cut it did not cut through any triple junctions. The lack of triple junctions may also suggest that recrystallization has not taken place as in the hanging wall. Orthopyroxene makes up 60% of the pegmatite layer and ranges in grain size from 1cm to 2cm.

Plagioclase:

The plagioclase occurs both interstitially and as inclusions as in the hanging wall. Inclusions in the pegmatite are similar in shape and size to the inclusions found within the hanging wall. The inclusions are less abundant however and occur within clinopyroxene as well as orthopyroxene. The zoned and recrystallised plagioclase is the same in appearance to that of the hanging wall. The plagioclase as in the hangingwall is subhedral where it occurs as inclusions (figure 14a) and is anhedral where it occurs as zoned and recrystallized grains (figure 14b). Distinct grains are difficult to make out due to the lack of grain boundaries between plagioclase grains. Plagioclase makes up 15% of the pegmatite layer.

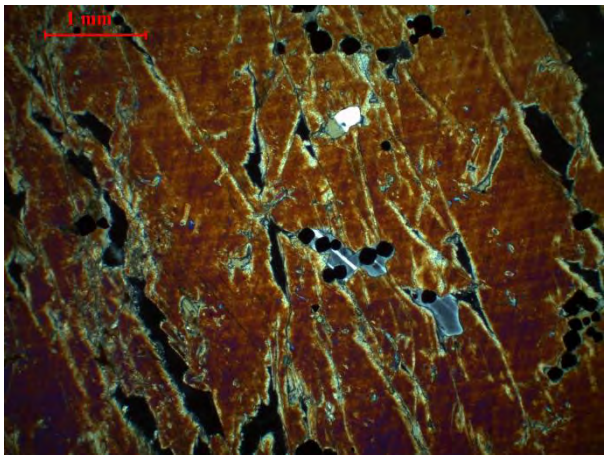

Figure 14a: Photomicrograph from slide P4 showing a large clinopyroxene oikocrysts with plagioclase chadacrysts and disseminated chromite inclusions.

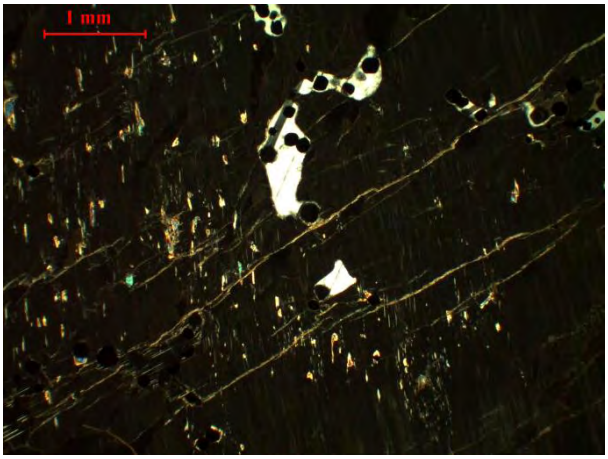

Figure 14b: Photomicrograph from slide P4 of orthopyroxene oikocryst with plagioclase chadacrysts and chromite inclusions. Shows veining and reaction sites to clinopyroxene.

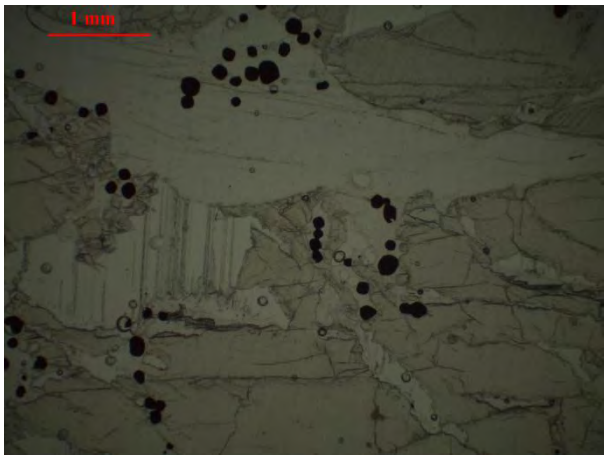

Figure 14c: Photomicrograph from slide P4 showing interstitial plagioclase with orthopyroxene oikocrysts and disseminated chromite grains forming strings of grains.

Clinopyroxene:

Clinopyroxene is found as three different textures in the pegmatoid. The first is as oikocrysts which are defined by their large size and by the inclusion of other minerals. The oikocrysts range in size from 1cm to 2cm and are euhedral to subhedral in shape. The second texture is the discontinuous rims which, like the hanging wall, do not engulf the whole grain but rather occur in one site on the orthopyroxene boundary and appear to have resorbed part of the associated orthopyroxene. The rims are also found in association with some of the inclusions as in the hangingwall. The third texture that has been observed is exsolution lamellae within the orthopyroxene grains which are not in association with inclusions of plagioclase and are vein like in appearence. Clinopyroxene makes up 20% of the pegmatite with oikocrysts being more prominent than in the hanging wall.

Chromite:

The chromite is present as both disseminated grains and stringers less than 1mm thick. The stringers however are not as well defined as the stinger found within the hanging wall and seem to have a more diffuse contact with the surrounding pegmatoid. The chromite does however form two of these less well defined stringers. The disseminated grains of chromite are found included in all of the major minerals (orthopyroxene, plagioclase and clinopyroxene) as well as between grain boundaries. The disseminated grains also form strings of grains which were not seen in the hanging wall. There is no preferred orientation to these strings of grains. The chromite is subhedral to anhedral and shows slightly rounded boundaries where they are included within other minerals. The interstitial chromite grains

between grain boundaries tend to be more euhedral grains. The grains are between <0.1mm- 0.3mm with the larger grains generally forming the strings. The chromite, similar the hanging wall, only makes up about 3% of the pegmatoid however, it seems to be better distributed throughout the layer.

Biotite:

Biotite is found within the pegmatoid unlike the hanging wall and tends to be associated with chromite grains. The biotite is generally lath shaped and found to occur as inclusions within other minerals however, there is no preference to any of the other minerals and is found in contact or within all the other minerals (figure 15a). The biotite is distinct from the other minerals as it is brown in both PPL and XPL. The biotite is lath shaped and ranges between <0.1mm- 0.2mm. The size of the grain shows no correlation to the size of the chromite. The biotite only makes up about 2% of the pegmatoidal layer.

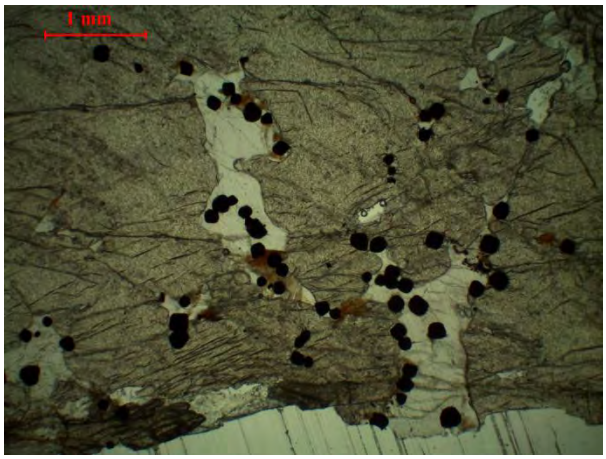

Figure 15a: Photomicrograph from slide P4 showing orthopyroxene oikocryst with plagioclase chadacrysts and disseminated chromite. Shows biotite in association with the chromite.

4.5 UG2 Chromitite

The chromitite layer present in both of the cores is the UG2. The layer is homogeneous and shows no variation in grain size or composition over the whole layer when observed in hand specimen as described within the core logs in Appendix A. The thickness of the layer varies between the two cores from about 50cm in the Eastern Bushveld core to 57cm in the WH-1 core. The WH-1 core however is a total thickness as it is split in two by the pegmatoid as described above.

Mineral	Modal Abundance
Orthopyroxene	10-15%
Plagiolcase	5-15%
Clinopyroxene	10-15%
Chromite	80-90%
Biotite	2-3%

Orthopyroxene:

The orthopyroxene in the UG2 appears interstitial (Figure 16a) to the chromite due to the grains not being euhedral and grain boundaries not being observed. This means that the orthopyroxene appears to only fill the pore spaces between the chromite within thin section. However within the core and within the slides, such as slide C1, tabular grains of orthopyroxene can be seen. These coarse-grained tabular orthopyroxenes are easily observed within hand specimen and appear as large grains which include chromite (Figure 16b). The grains are subhedral to anhedral in shape and range in grain size form 1mm to 2mm. The orthopyroxene in the UG2 makes up between 10% and 15% of the rock.

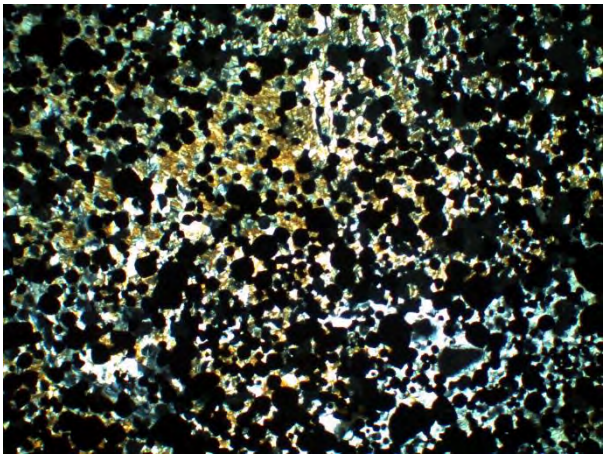

Figure 16a: Photomicrograph taken from slide C2 showing coalescent chromite texture with orthopyroxene.

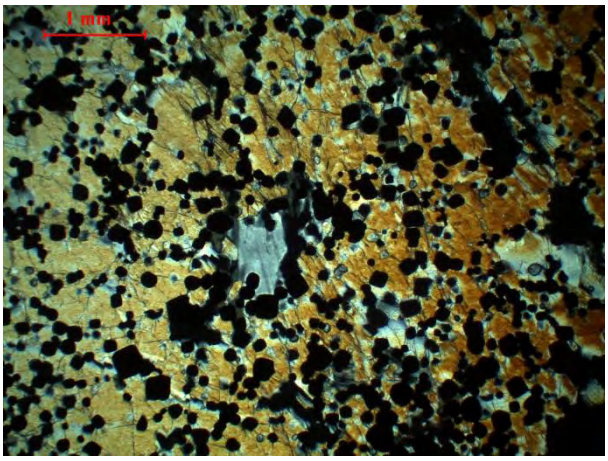

Figure 16b: Photomicrograph taken from slide Ftw showing sub-coalescent chromite texture with interstitial plagioclase and orthopyroxene.

Plagioclase:

The plagioclase is interstitial within the UG2 and appears as zoned (figure 17a) and recrystallized grains (figure17b). The recrystallized grains have been considered to be

recrystallized because of the lack of zoning. Recrystallization has overprinted the zoning within the plagioclase grains thus making the grains homogenous. Some of the slides show the interstitial material changes from pyroxenes to plagioclase. The plagioclase shows zoning as in the hangingwall and pegmatoid. The plagioclase only occurs as interstitial grains and no chadacrysts are found to occur within the UG2 layer. The plagioclase is anhedral in shape and makes up between 5% and 15% of the layer with higher concentrations of the mineral being found lower in the unit.

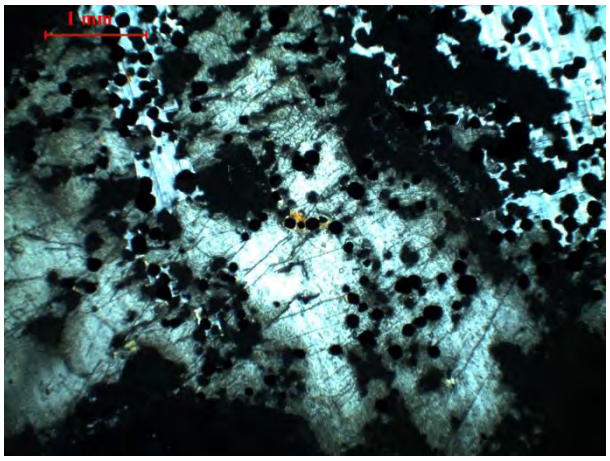

Figure 17a: Photomicrograph taken from slide C1 showing large areas of plagioclase which may be considered oikocrysts.

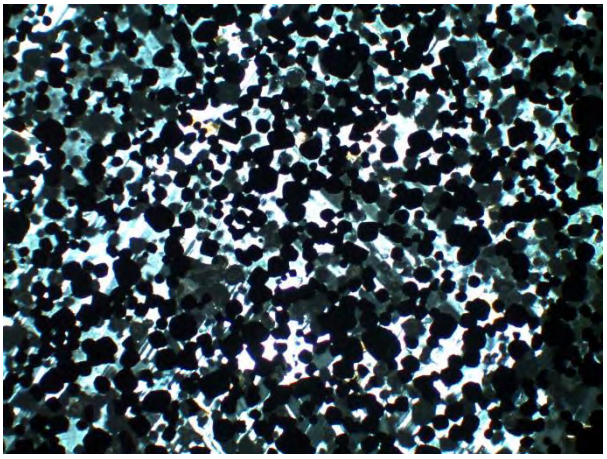

Figure 17b: Photomicrograph taken from slide Ftw showing plagioclase interstitial to sub-coalescent chromite.

Clinopyroxene:

The clinopyroxene in the UG2 forms three textures oikocrysts (figure 18a), discontinuous rims (figure 18d), as exsolution lamellae (figure 18c) and interstitially (figure 18b). The oikocrysts are very coarse-grained and have chromite and other minerals included within them. The reaction rims occur with orthopyroxene and plagioclase and appear to have formed in association with the chromite. The interstitial clinopyroxene does not have any oikocrystic characteristics and appears to have formed after the chromite. The clinopyroxene makes up between 10% and 15%, ranges in grain size from <0.1mm- 2mm, and is subhedral to anhedral in shape.

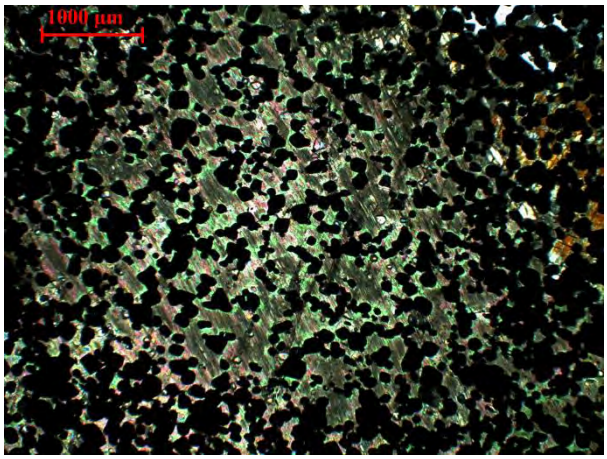

Figure 18a: Photomicrograph taken from slide C1 showing clinopyroxene oikocryst with sub-coalescent to coalescent chromite.

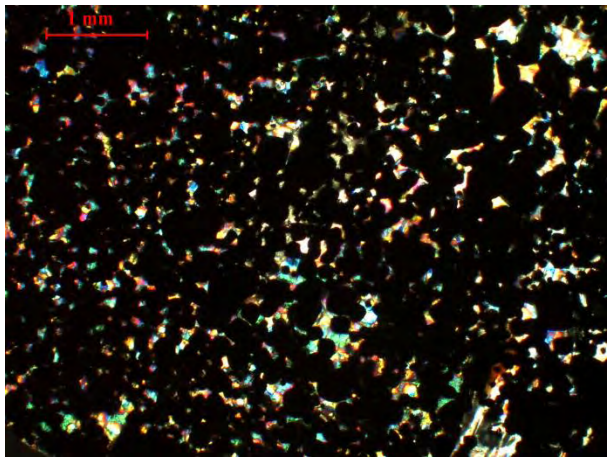

Figure 18b: Photomicrograph taken from slide C2 showing coalescent chromite with interstitial clinopyroxene.

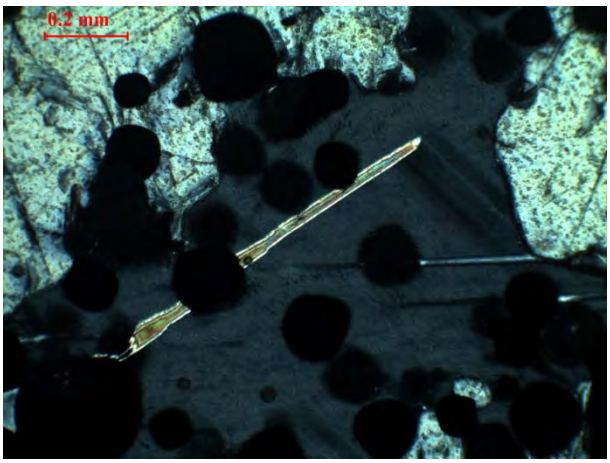

Figure 18c: Photomicrograph taken from slide C1 showing exsolved clinopyroxene within interstitial plagioclase.

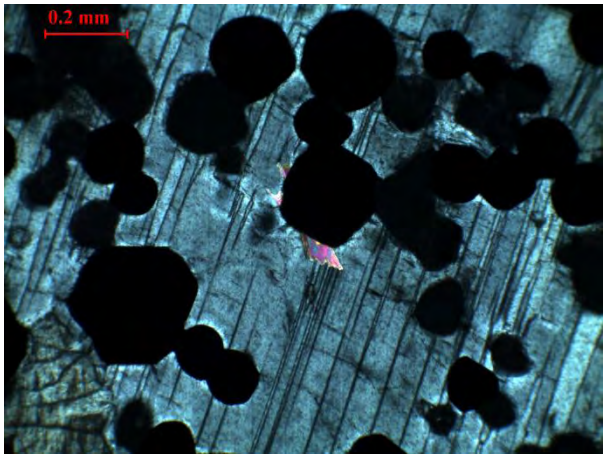

Figure 18d: Photomicrograph taken from slide C1 showing clinopyroxene reaction rim in association with chromite included within plagioclase.

Chromite:

The chromite it the UG2 shows three main textures and in some cases follows structures within the unit. The first texture is the annealed texture (figure 19b) which is large chromite grains (1mm-2mm) which are euhedral to subhedral in shape. These chromite grains have well defined grain boundaries and form clusters of grains. This texture only occurs in small zones within slides and does not cover whole slide or an area any larger the about 1cm. The annealed zones are generally found in association with fracture- like structures. This texture is a process of recrystallization and suggests that recrystallization has taken place and has been more prominent in areas where fracturing has taken place. The second texture is the coalescent texture (figure 19a). This texture is smaller in grain size (0.1mm-0.5mm) than the

annealed texture and grains are more subhedral but range still from euhedral to subhedral. This texture also has more interstitial pore space and covers large areas. The third texture found is the sub-coalescent texture (figure 19c) which is similar in appearance to the coalescent texture however, the sub-coalescent texture has more pore space present between grains and grains are subhedral to anhedral. Grain size however is the same (0.1mm-0.5mm) and grains appear as disseminated, single grains and as strings and clusters of grains. Chromite in the UG2 layer makes up between 80% and 90% of the unit.

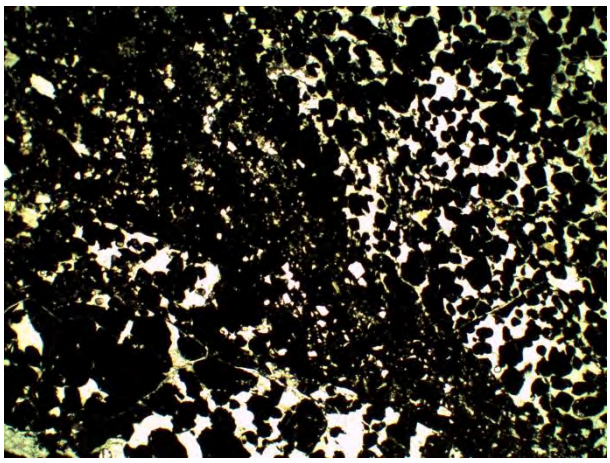

Figure 19a: Photomicrograph taken from slide U2 showing coalescent chromite with annealed chromite following a fracture structure.

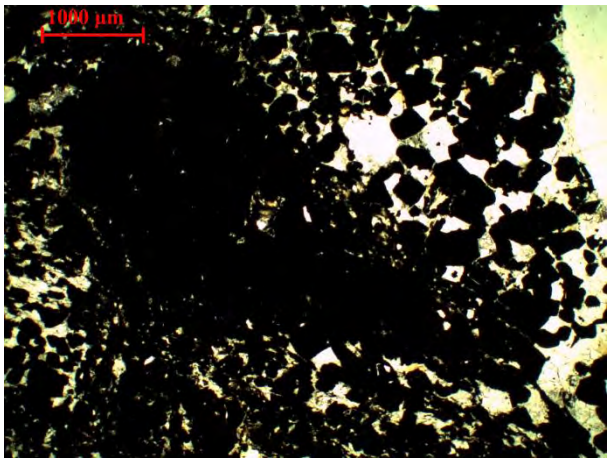

Figure 19b: Photomicrograph taken from slide U2 showing large zone of annealed chromite.

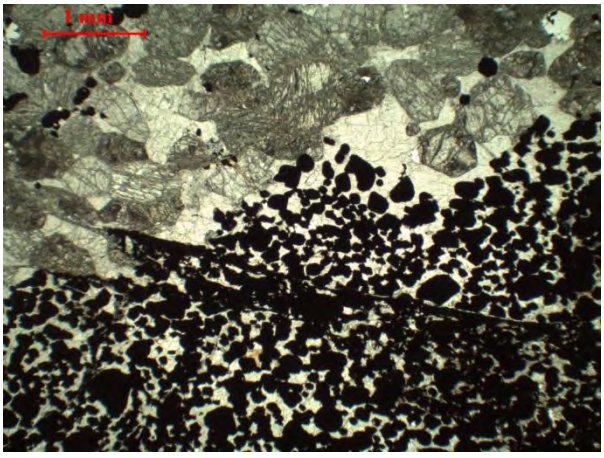

Figure 19c: Photomicrograph taken from slide U2 showing coalescent chromite at the UG2 footwall contact. Chromite can also be observed following fracture structures.

Biotite:

Biotite in the UG2 chromitite is similar to biotite within the Pegmatoid. The biotite is between 0.1mm and 0.2mm and is lath shaped (figure 20b). The biotite is interstitial to the chromite (figure 20a) and is generally found in association with chromite grains. Rarely is it found without an associated chromite grain. Biotite makes up 2%-3% of the unit.

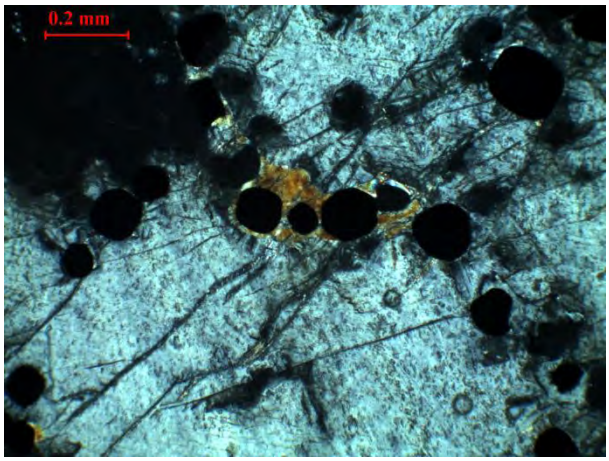

Figure 20a: Photomicrograph taken from slide C1 showing biotite in association with chromite.

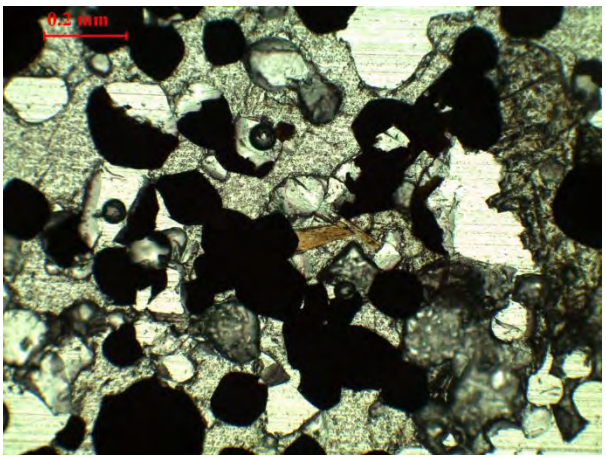

Figure 20b: Photomicrograph taken from slide C1 showing lath shaped biotite in association with chromite.

4.6 Footwall

The footwall is the same in composition as the hanging wall changing gradationally from norite to pyroxenite down stratigraphy. Chromite is also present within the footwall and is found to form a layer/seamlet of chromitite separated from the UG2.

Mineral	Modal Abundance
Orthopyroxene	50%
Plagiolcase	30-40%
Clinopyroxene	15-25%
Chromite	3% (makes up 80-90% where the seamlet occurs.)
Biotite	3%

Orthopyroxene:

The orthopyroxene in the hanging wall is found as coarse-grained tabular grains which are subhedral in shape. Grains are found to form triple junctions as in the hangingwall (figure 21a) and again suggest recrystallization. Another texture is found in the hanging wall in slide U5 where the orthopyroxene is found within a typical norite (figure 21b and 21d) composition but is rounded and appears to be resorbed by the plagioclase and clinopyroxene. The second texture found in the same slide is a cataclastic/crushed texture (figure 21c) where the orthopyroxene is small and angular and some grains appear to be sheared. The orthopyroxene makes up 50% of the footwall rocks and ranges in grain size of 0.1mm- 2mm.

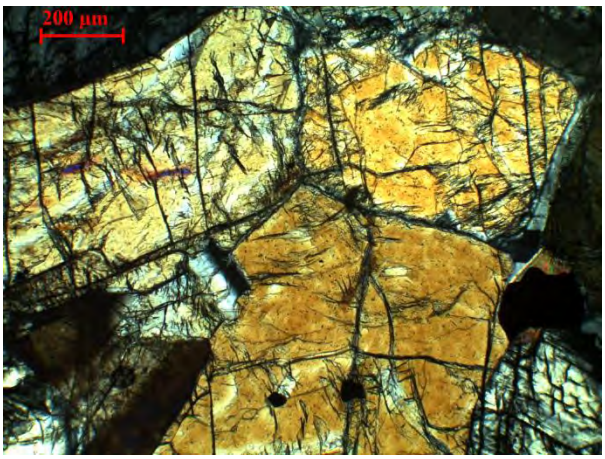

Figure 21a: Photomicrograph taken from slide U5 showing orthopyroxene forming a triple junction. Clinopyroxene is also observed as an inclusion within the orthopyroxene.

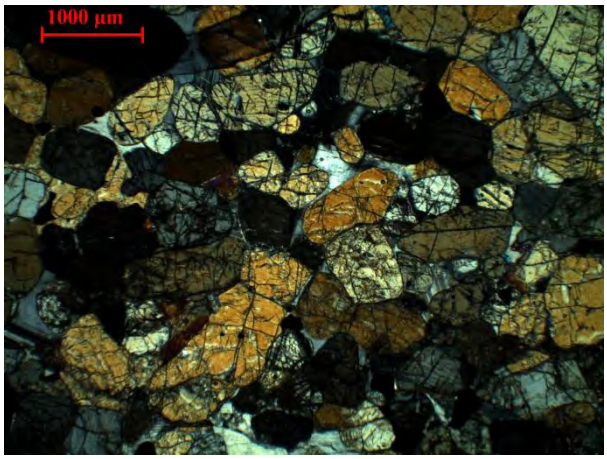

Figure 21b: Photomicrograph taken from slide U5 showing subhedral orthopyroxene oikocrysts with rounded boundaries. Plagioclase chadacrysts included within the orthopyroxene oikocrysts.

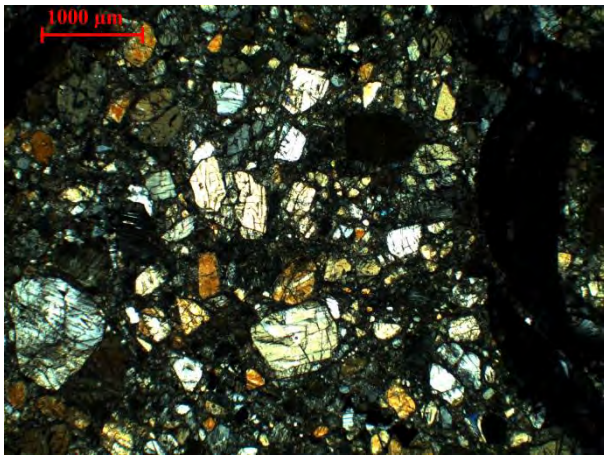

Figure 21c: Photomicrograph taken form slide U5 showing cataclastic orthopyroxene and sheared orthopyroxene oikocryst.

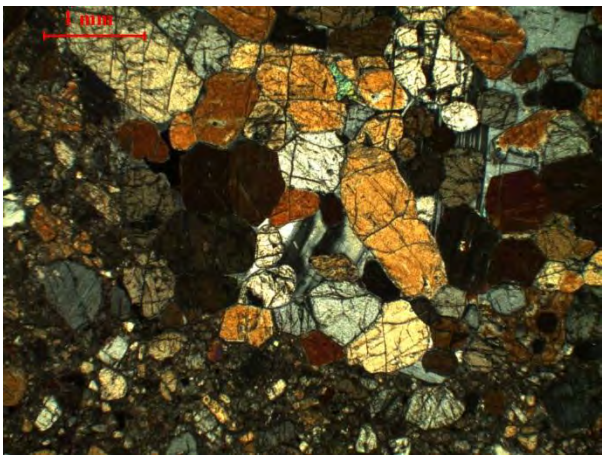

Figure 21d: Photomicrograph taken from slide U5 showing orthopyroxene oikocrysts within a norite zone.

Plagioclase:

Plagioclase in the footwall closely resembles the plagioclase found within the hangingwall, as it is found occurring interstitially and as inclusions within pyroxene grains. The plagioclase found within the norite zones (figure 22a) of slide U5 shows a liquid interaction with clinopyroxene (figure 23b) as well as having orthopyroxene grains included within it. This suggests that the plagioclase and clinopyroxene were in a liquidus state at the same time. Inclusions are also present within both the orthopyroxene and clinopyroxene and are the same shape and size as chadacrysts within the hanging wall. The plagioclase makes up between 30% and 40% and varies in grain size from <0.1mm-1mm.

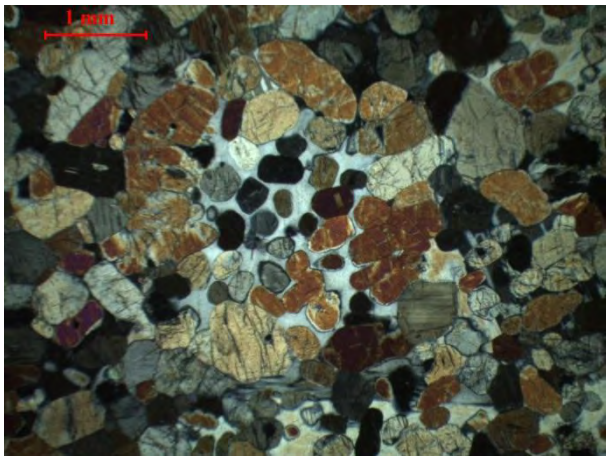

Figure 22a: Photomicrograph taken from slide U5 showing interstitial plagioclase within a norite zone. Orthopyroxene is rounded showing resorbtion by the plagioclase.

Clinopyroxene:

The clinopyroxene shows the same three textures as in the hanging wall. Triple junctions are found forming between tabular subhedral grains and as in the orthopyroxene suggest that recrystallization has taken place. There is another texture found within the footwall, clinopyroxene intergranular necking, which shows a fluid boundary (Figure 23b) with the plagioclase. This texture is found in only one of the norite zones (figure 23a) of slide U5. The clinopyroxene makes up between 15% and 25% of the footwall and ranges in grain size from 0.1mm-2mm.

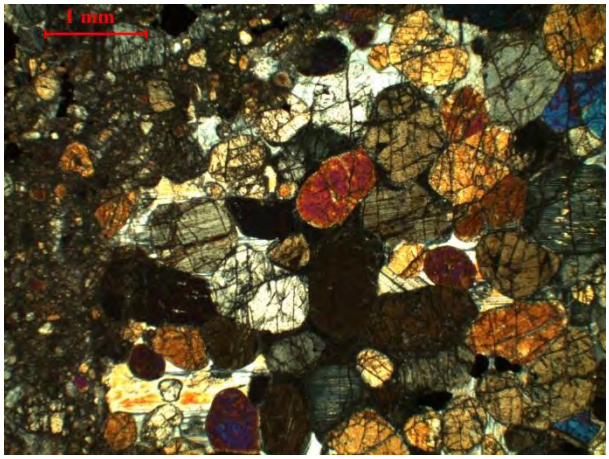

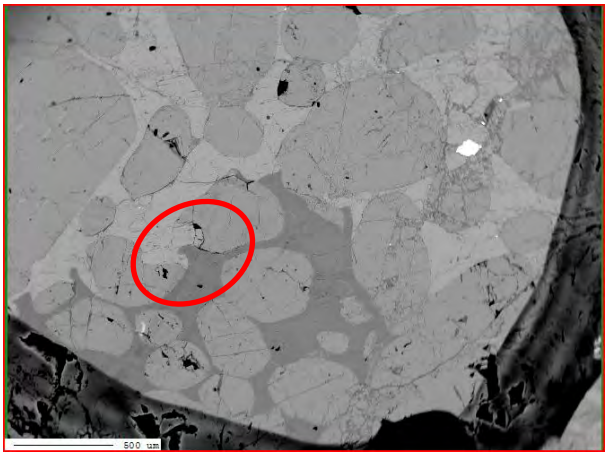

Figure 23a: Photomicrograph taken from slide U5 showing rounded clinopyroxene oikocrysts within a norite zone.

Figure 23b: Image taken using the electron microprobe of slide U5 showing clinopyroxene oikocrysts with a fluid boundary (circled in red) with plagioclase and shows orthopyroxene oikocrysts resorbed by the plagioclase and the clinopyroxene.

Chromite:

The chromite within the footwall forms a seamlet that is 3cm thick and is present 4cm below the UG2. This seamlet shows a coalescent texture and as in the UG2 there are also zones of annealed texture. Chromite also occurs within the footwall rocks as disseminated grains (figure 24). The chromite varies in shape from euhedral to subhedral and size from <0.1mm-1.5mm. The chromite makes up between 70% and 3% of the footwall.

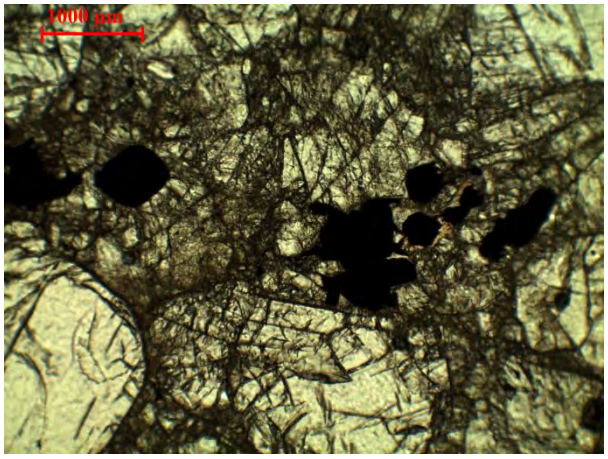

Figure 24: Photomicrograph taken from slide U2 showing disseminated chromite grains within orthopyroxene on the footwall.

Biotite:

Biotite occurs within the footwall similar to the pegmatoid. The biotite is lath shaped and interstitial (figure 25) and ranges from <0.1mm-0.5mm. The biotite in the footwall however, does not occur in association with chromite as in the pegmatoid and shows no preference to any of the minerals in the footwall. The biotite is not found included within any of the minerals as in the pegmatoid and may be due to not being associated with chromite. The biotite makes up 3% of the footwall.

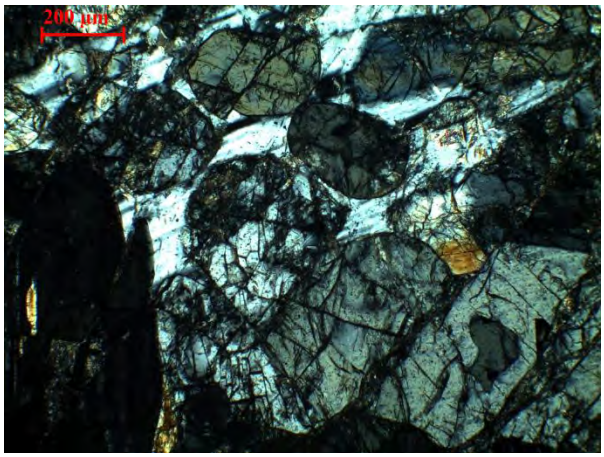

Figure 25: Photomicrograph taken from slide U5 showing resorbed orthopyroxene oikocrysts within interstitial plagioclase and biotite.

5. Geochemistry

The aim of the geochemistry section is illustrate the mineral data obtained from the electron microprobe and in turn describe what the data shows. The electron microprobe data can be found in appendices 8.3 a, b and c. This is complimented with appendix 8.4 which contains the photomicrographs taken by the electron microprobe during sampling. The photomicrographs show the points where samples were taken. The observaions made in the geochemistry section will be summarised and discussed within the discussion at the end.

5.1 Hangingwall

Orthopyroxene:

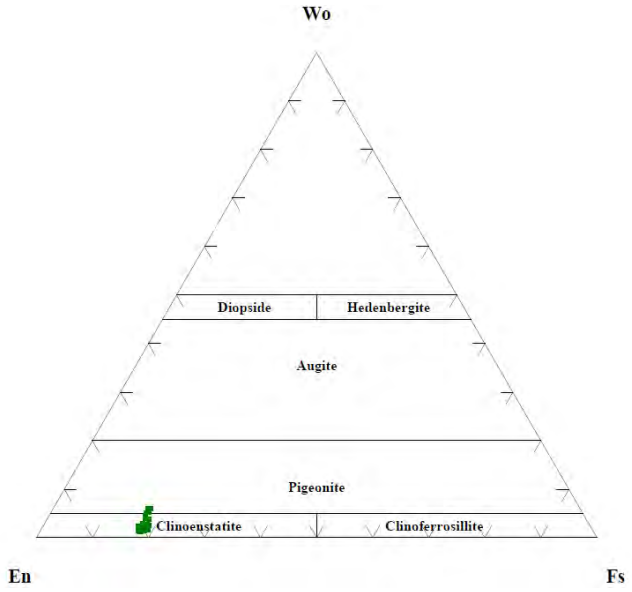

	WO	EN	FS
Minimum	1.217	76.594	16.954
Maximum	5.995	81.095	19.137
Mean	2.526	79.492	17.981
Std. Dev.	1.226	1.037	0.524
Number Of Cases	43	43	43

Figure 26a: Ternary diagram plotting the composition of coarse-grained tabular orthopyroxene grains accompanied by a summarised table of values.

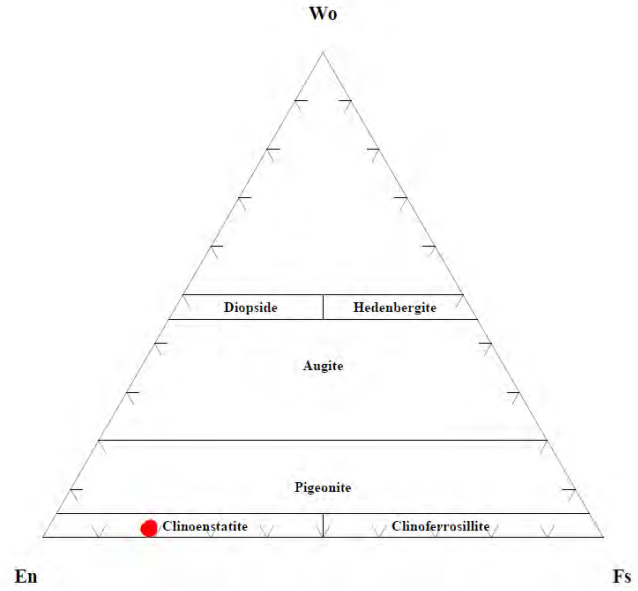

	WO	EN	FS
Minimum	1.506	79.554	17.807
Maximum	2.337	80.454	18.467
Mean	1.791	80.058	18.151
Std. Dev.	0.377	0.395	0.274
Number Of Cases	4	4	4

Figure 26b: Ternary diagram plotting the composition of finer-grained rounded orthopyroxene grains accompanied by a summarised table of values.

The above figures show the compositions of orthopyroxenes within the hangingwall. Each figure shows the composition of a different orthopyroxene texture which were described within the petrology section. The finer-grained, rounded orthopyroxene overlap in composition with the coarse-grained, tabular grains of orthopyroxene. The coarse-grained, tabular grains show a greater range of composition than the finer-grained, rounded orthopyroxenes. This may due to having a larger amount of samples of the tabular grains than the finer-grained rounded grains, and a greater range may be seen in the finer-grained rounded grains if the amount of samples is increased. The finer-grained, rounded grains show a very low Wo content but a comparable En content to the coarse-grained, tabular grains. This range is illustrated in the associated tables provided with the figures.

Plagioclase:

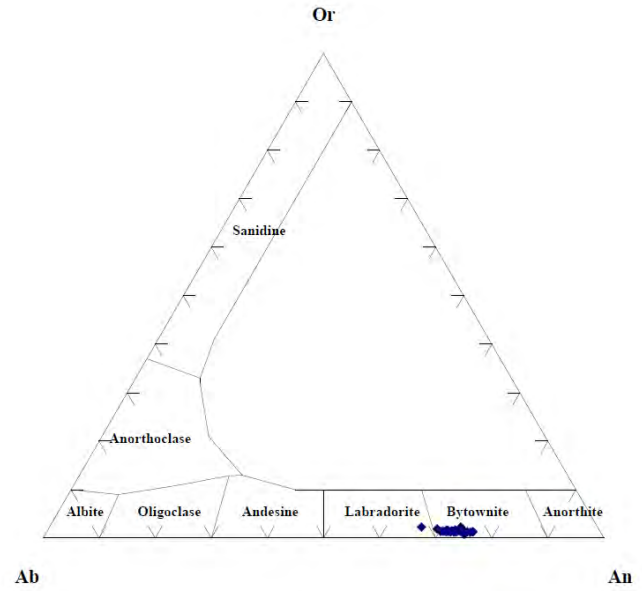

	Ab	An	Or
Minimum	22.7	66.3	0.8
Maximum	31.4	76	2.3
Mean	25.9	72.7	1.4
Std. Dev.	2	2.1	0.3
Number Of Cases	29	29	29

Figure 27a: Ternary diagram plotting the composition of plagioclase inclusions accompanied by a summarised table of values.

	Ab	An	Or
Minimum	21.7	69	0.9
Maximum	29.4	77.4	1.7
Mean	26.1	72.6	1.4
Std. Dev.	1.2	1.3	0.1
Number Of Cases	37	37	37

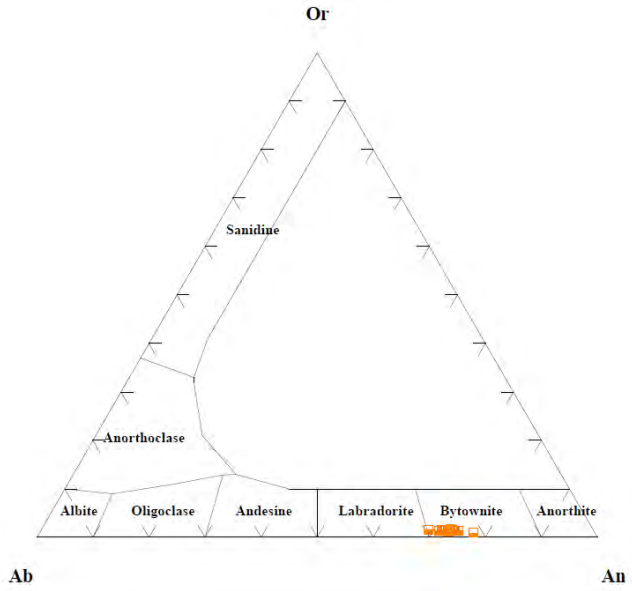

Figure 27b: Ternary diagram plotting the composition of zoned and recrystallized plagioclase grains accompanied by a summarised table of values

The two above figures show compositions of plagioclase of different textures found within the hangingwall. Both figures show high ranges of An for both textures and show that the compositions of both textures overlap. Both figures show a similar range in composition however in figure the plagioclase inclusions show a range of compositions slightly lower than that of the zoned and recrystallized plagioclase grains. The zoned and recrystallized plagioclase have not been split into rims and cores due to only cores being sampled for reasons stated within the petrology.

Clinopyroxene:

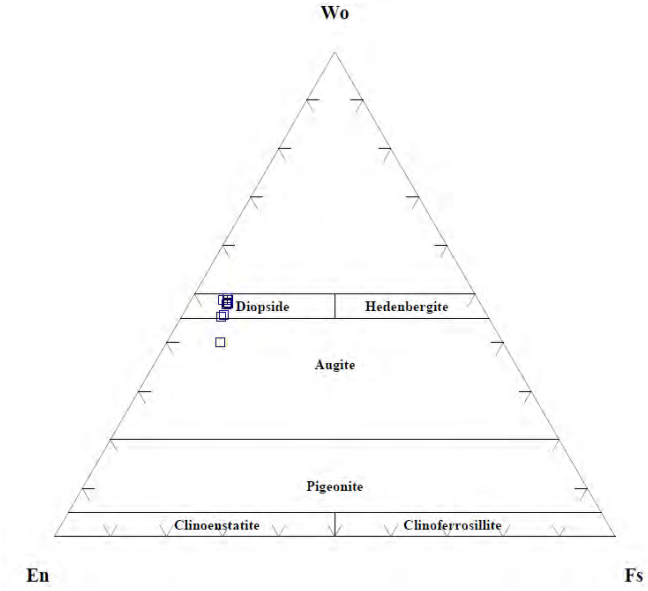

	WO	EN	FS
Minimum	40.037	44.575	5.662
Maximum	49.192	50.445	9.518
Mean	46.894	46.114	6.992
Std. Dev.	2.919	1.938	1.073
Number Of Cases	9	9	9

Figure 28a: Ternary diagram plotting the composition of tabular clinopyroxene grains accompanied by a summarised table of values.

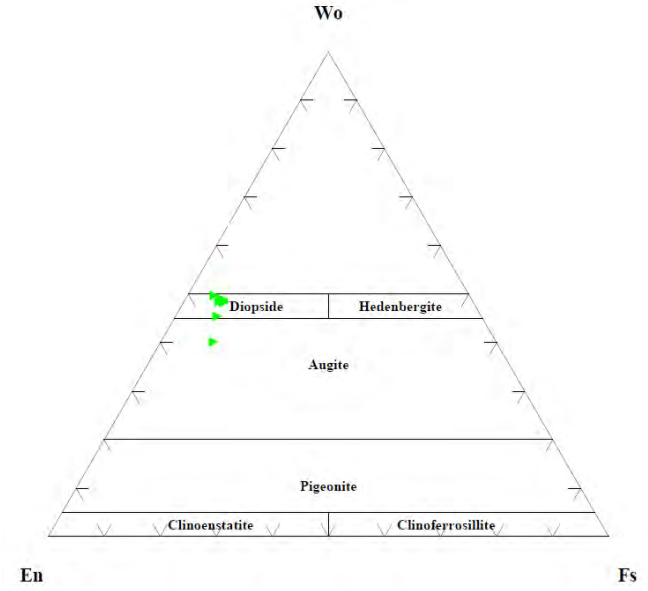

	WO	EN	FS
Minimum	40.167	44.267	4.744
Maximum	49.761	50.429	9.403
Mean	47.543	45.503	6.954
Std. Dev.	2.819	1.937	1.155
Number Of Cases	10	10	10

Figure 28b: Ternary diagram plotting the composition of intergranular necking clinopyroxene accompanied by a summarised table of values.

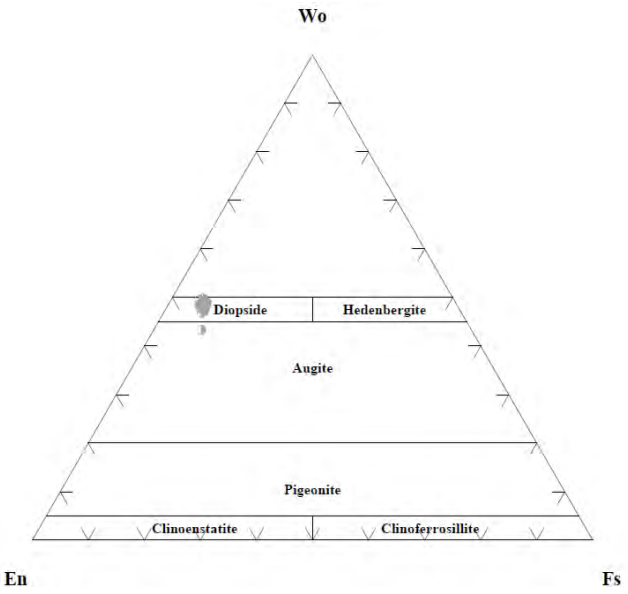

	WO	EN	FS
Minimum	43.335	44.331	5.038
Maximum	49.809	48.171	8.495
Mean	48.129	45.523	6.348
Std. Dev.	1.112	0.685	0.659
Number Of Cases	30	30	30

Figure 28c:Ternary diagram plotting the composition of discontinuous rim clinopyroxene accompanied by a summarised table of values.

The figures above show the compositions for clinopyroxene textures found within the hangingwall. The three textures overlap in their compositional ranges; however the compositions of the intergranular necking clinopyroxenes and tabular clinopyroxenes show a greater range in compositions than the discontinuous rims. The discontinuous rims compositions all plot within a short range with a generally higher Wo content than the other two textures. There is also outlier samples for all the textures which plot below the mode composition, these outliers may be anomalies within their respective textures or the probe may have probed the mineral behind the intended grains and slightly affected the composition.

5.2 Pegmatoid

Orthopyroxene:

The orthopyroxene within the pegmatoid, as discussed within the petrology section, exhibits only one texture which is oikocrystic. Figure 29 above shows that the samples taken from the pegmatoid have a relatively large range in Wo content, consistent with the hangingwall orthopyroxene, and a relatively narrow range in En content. The orthopyroxene within the pegmatoid show an overlapping of compositions with the orthopyroxene within the hangingwall, even though this texture was not observed to occur within hangingwall.

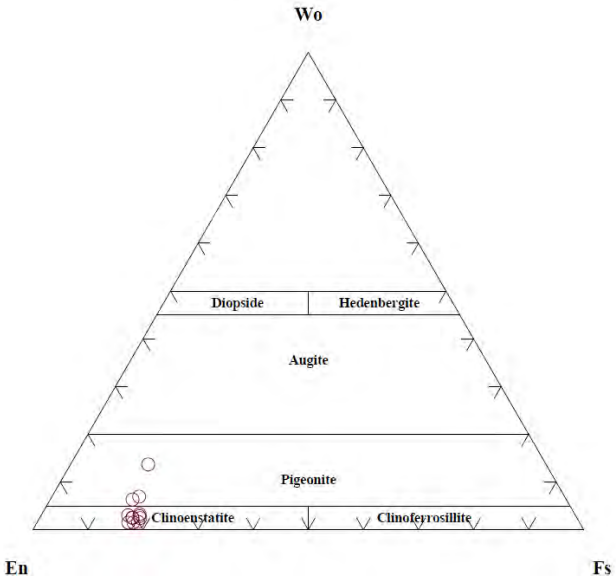

	WO	EN	FS
Minimum	1.488	72.21	14.112
Maximum	13.678	81.911	18.285
Mean	4.015	79.261	16.724
Std. Dev.	3.508	2.568	1.336
Number Of Cases	12	12	12

Figure 29: Ternary diagram plotting compositions of oikocrystic orthopyroxene accompanied by a summarised table of values.

Plagioclase:

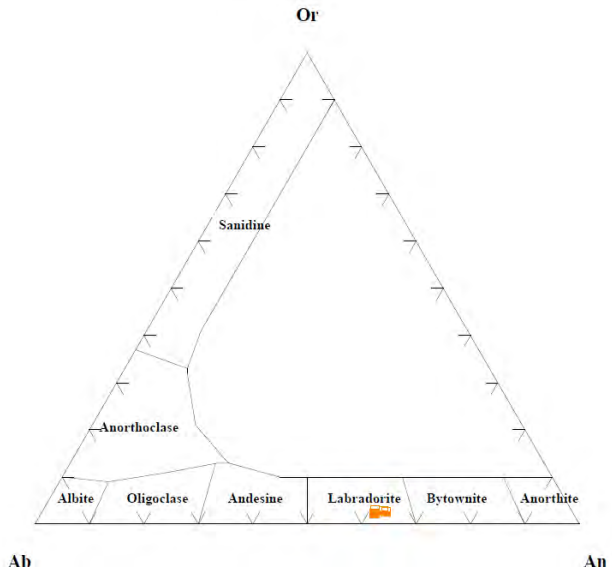

	Ab	An	Or
Minimum	34.1	61	2.2
Maximum	36.5	63.2	3
Mean	35.3	62	2.7
Std. Dev.	1.1	1	0.3
Number Of Cases	4	4	4

Figure 30: Ternary diagram plotting compositions of zoned and recrystallised plagioclase accompanied by a summarised table of values.

The plagioclase, as with the orthopyroxene, only exhibits a single texture within the pegmatoid as described within the above petrology section. Figure 30 shows the

compositions of the zoned and recrystallized plagioclase grains sampled within the pegmatoid. The samples are few and show that compositions with the plagioclase grains of the pegmatoid differ in An content by +/- 10 to plagioclase of the same texture within the hangingwall. The amount of samples is few within this unit due to the slide having little plagioclase within it and because the polishing process which prepared the slide damaged some of the plagioclase meaning that samples could not be taken from some of the grains.

Clinopyroxene:

Clinopyroxene was sampled within the pegmatoid but the analyses that were produced were unusable due to the data being incomplete or wrong. This may have been due to a problem with the electron microprobe or because the probe sampled through the clinopyroxenes into the minerals behind which will have altered the analysis.

5.3 UG2 chromitite

Orthopyroxene:

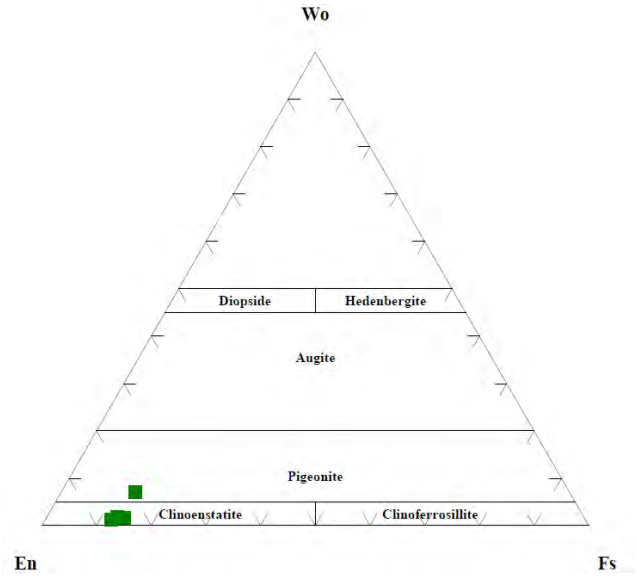

	WO	EN	FS
Minimum	1.287	79.338	12.054
Maximum	7.078	86.659	14.198
Mean	2.669	84.07	13.26
Std. Dev.	2.47	2.799	0.811
Number Of Cases	5	5	5

Figure 31: Ternary diagram plotting compositions of coarse-grained tabular grains of orthopyroxene accompanied by a summarised table of values.

Orthopyroxene within the UG2 chromitite shows an overlapping in compositions with the above units as shown in figure 31. However the compositions within the UG2 due show more of a range in En content and less of a range in Wo content (except for a single outlier).

Plagioclase:

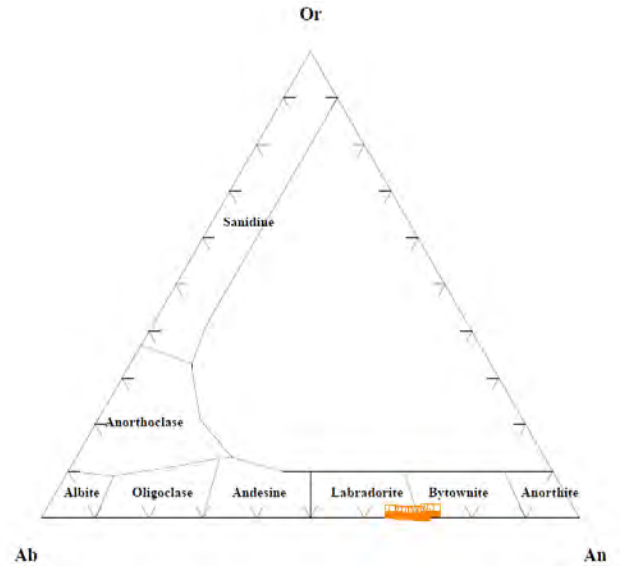

	Ab	An	Or
Minimum	26.3	64.3	0.7
Maximum	34.3	72.1	1.6
Mean	30.4	68.4	1.2
Std. Dev.	2.4	2.4	0.3
Number Of Cases	12	12	12

Figure 32: Ternary diagram plotting compositions of zoned and recrystallised plagioclase accompanied by a summarised table of values.

The plagioclase within the UG2 chromitite layer exhibits only one textural type as discussed within the above petrology section. Figure 32 shows the compositions of the zoned and recrystallized grains which overlap with the compositions of plagioclase within the previous units. The figure also shows a relatively large range in An content. This range exceeds that found within the hangingwall plagioclase with the same texture as the plagioclase within the UG2 show some samples have lower An content than those within the hangingwall.

Chromite:

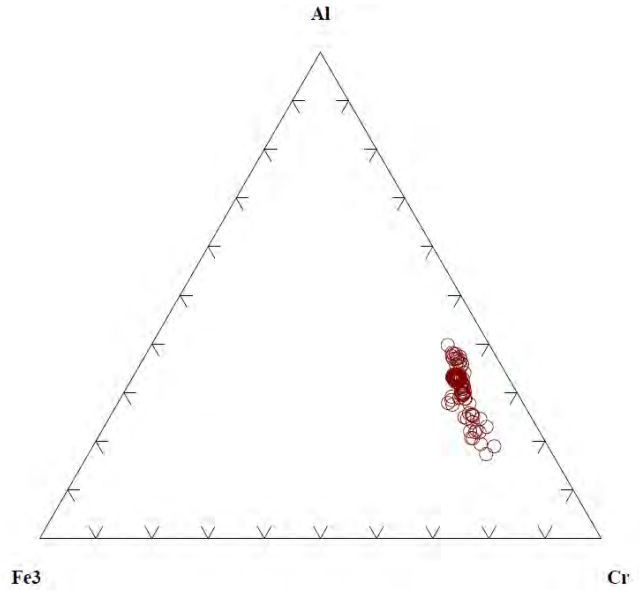

Figure 33: Ternary diagram plotting the compositions of chromite grains within the UG2 chromitite.

The chromite within the UG2 shows a large range in Cr and Al content with little variation in the Fe3 content, as observed within figure. These samples have not been separated into textural differences due to grains being of similar shape and size. The textures, as described within the petrology section, are more of an overall texture within the unit rather than textures specific to individual grains and affect the amount of pore space present within the layer. Figure 33 above shows that the composition of chromite varies greatly within a single unit where some grains are more Cr rich and others are more Al rich. The Cr content ranges from approximately 80 to 55 with Al ranging from 20 to 45 and the Fe3 only has a small range of 5 to 20. The average composition is approximately Cr 65: Al 35: Fe3 15.

5.4 Footwall

Orthopyroxene:

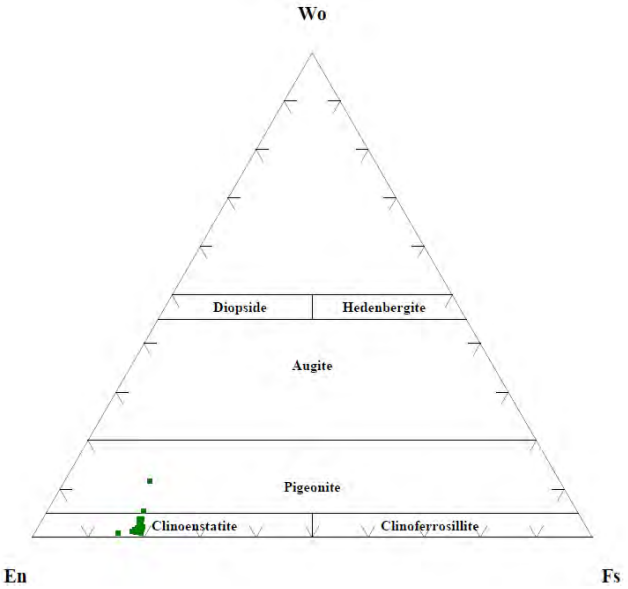

	WO	EN	FS
Minimum	0.879	73.204	14.929
Maximum	11.592	84.192	18.991
Mean	2.418	79.697	17.885
Std. Dev.	2.026	1.693	0.911
Number Of Cases	29	29	29

Figure 34a: Ternary diagram plotting the compositions of coarse-grained tabular grains of orthopyroxene accompanied by a summarised table of values.

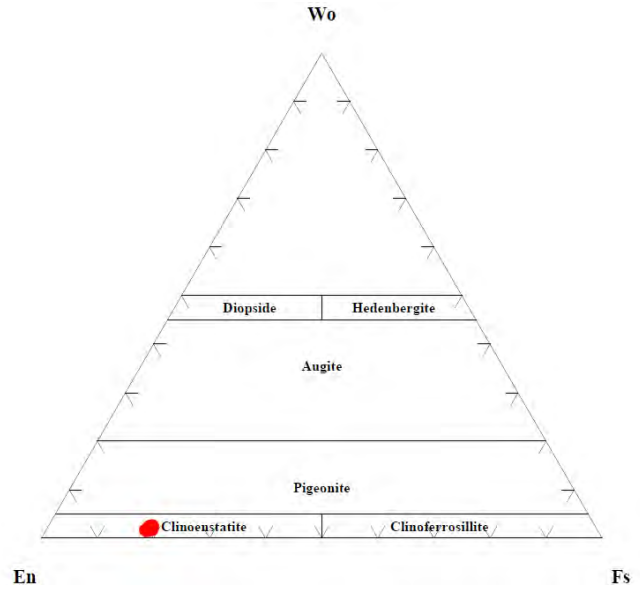

	WO	EN	FS
Minimum	1.569	78.915	17.821
Maximum	2.504	80.499	18.813
Mean	2.031	79.67	18.299
Std. Dev.	0.369	0.551	0.315
Number Of Cases	8	8	8

Figure 34b: Ternary diagram plotting the compositions of rounded orthopyroxene grains accompanied by a summarised table of values.

The footwall orthopyroxene exhibits the same textural types as the hangingwall and compositions which overlap those of the hangingwall as illustrated in the above figures. The rounded orthopyroxene grains observed in figure 34b show again concentrated compositions with little range in En or Wo content. The coarse-grained, tabular grains of orthopyroxene (figure 34a) again show a large range in Wo content. These samples as with previous units show an outlier with a large Wo content relative to the rest of the samples. The coarse-grained, tabular samples show a similar range in En to those found within the UG2 chromitite layer, which is again larger in their range than those found within the hangingwall. The samples within the figures show not only overlapping in composition between the same textures of other units but also overlapping of compositions between different textures within and between units.

Plagioclase:

Plagioclase within the footwall again exhibits the same textural types as the hangingwall. The zoned and recrystallized plagioclase, in figure 35a, shows a similar range in An content to the plagioclase of the UG2 chromitite. This means the An content range for the zoned and recrystallized plagioclase has a greater range than that of the hangingwall. However the bulk of the compositions overlap between the same textures of all the units. The plagioclase inclusions in figure show a small range in An and do not overlap in composition with the inclusions found within the hangingwall. The compositions of the inclusions found within the footwall show a higher An content than those of the hanging wall. This high An content and small range mean that these inclusions are compositionally different to the plagioclase

found within the hangingwall as they do not overlap with plagioclase of the same texture or with the zoned and recrystallized texture.

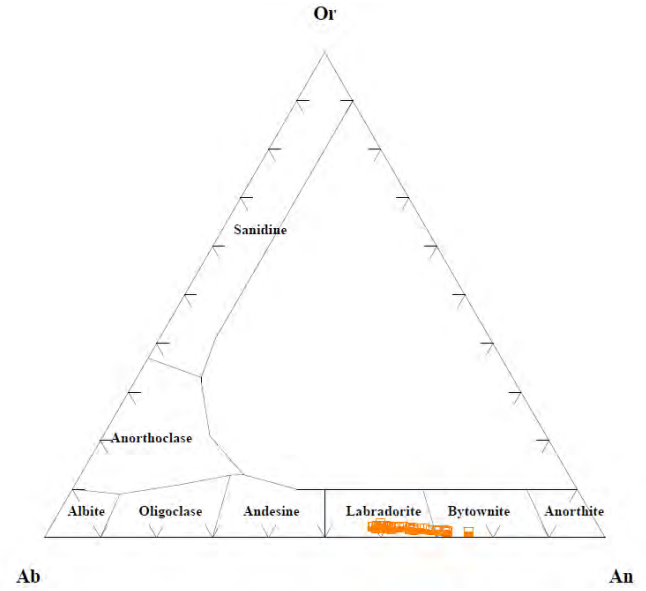

	Ab	An	Or
Minimum	23.8	57.5	1.1
Maximum	40.3	75.1	2.9
Mean	34.4	63.7	1.9
Std. Dev.	4.8	5.1	0.4
Number Of Cases	35	35	35

Figure 35a: Ternary diagram plotting the compositions of zoned and recrystallized plagioclase grains accompanied by a summarised table of values.

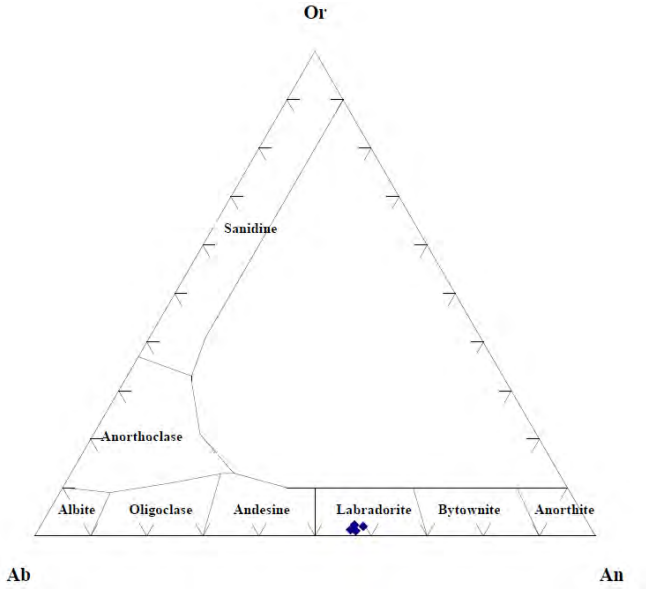

	Ab	An	Or
Minimum	40.4	55.7	1.1
Maximum	43	57.6	2.3
Mean	41.8	56.5	1.7
Std. Dev.	1.1	0.9	0.6
Number Of Cases	4	4	4

Figure 35b: Ternary diagram plotting the compositions of plagioclase inclusions accompanied by a summarised table of values.

Clinopyroxene:

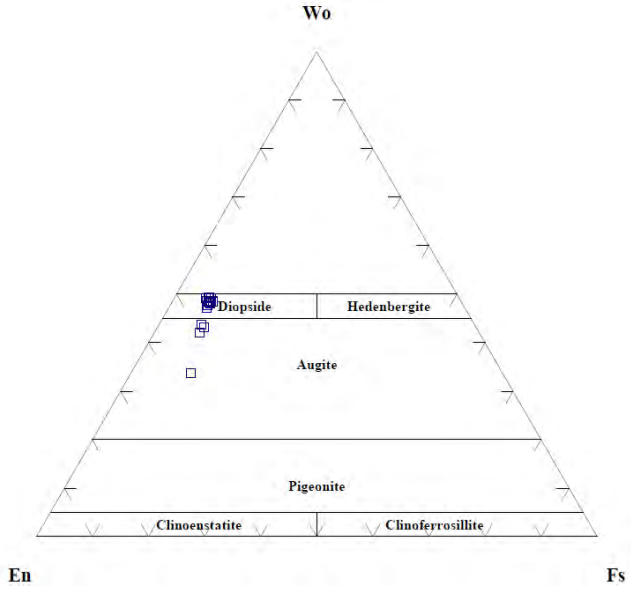

	WO	EN	FS
Minimum	33.739	44.249	5.707
Maximum	49.355	55.59	10.672
Mean	47.104	45.913	6.983
Std. Dev.	3.605	2.644	1.037
Number Of Cases	22	22	22

Figure 36a: Ternary diagram plotting the compositions of tabular clinopyroxene grains accompanied by a summarised table of values.

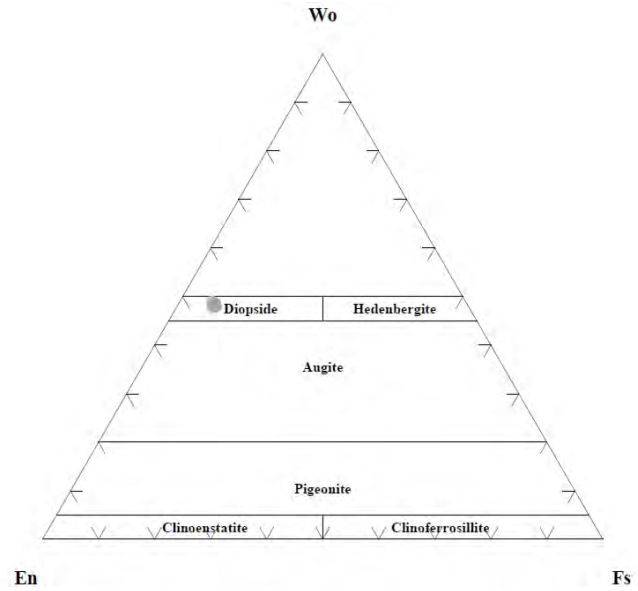

	WO	EN	FS
Minimum	47.63	44.649	5.691
Maximum	49.205	45.907	7.204
Mean	48.319	45.309	6.372
Std. Dev.	0.451	0.312	0.395
Number Of Cases	20	20	20

Figure 36b: Ternary diagram plotting the compositions of discontinuous rim clinopyroxenes accompanied by a summarised table of values.

The Clinopyroxene exhibits only two textures within the footwall. Figures 36a and 36b show the compositions for tabular clinopyroxene and discontinuous rims of clinopyroxene respectively. The tabular clinopyroxene shows a similar range in Wo and En content to the tabular clinopyroxene of the hangingwall, with the exception of the outer most outlier which has a low Wo content. The compositions of the tabular clinopyroxene overlap with the compositions of the tabular clinopyroxene of the hangingwall. The discontinuous rims of clinopyroxene within the footwall, as with the tabular clinopyroxene, overlap in composition with the clinopyroxene of the same texture within the hangingwall. The range again is small in both En and Wo content and shows less of a range than the tabular samples. The clinopyroxene of the footwall not only overlaps in composition within the same textures between units but between textures within and between units.

Chromite:

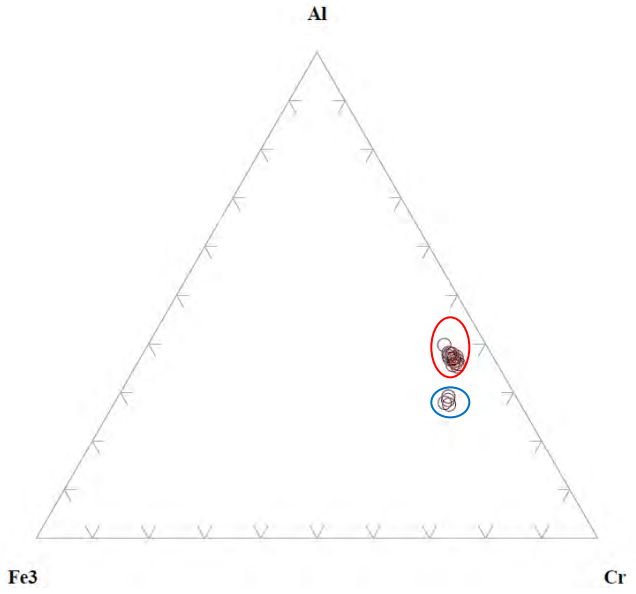

Figure 37: Ternary diagram plotting the composition of chromite grains within the footwall. Group 1 is marked in blue and group 2 is marked in red. Group 1 represents disseminated grains and group 2 represents samples from the seamlet.

The chromite within the footwall was sampled from some disseminated grains found to occur within the unit but mainly from the seamlet found beneath the UG2. Figure 37 shows two distinct groups of chromite. The first group is more Cr rich than the other ranging from 68 to 70 Cr, 30 to 32 Al and 18 to 20 Fe3. The second group ranges in Cr from 77 to 65, Al 35 to 23 and Fe3 8 to 10. The second group compositions overlap with the bulk of the samples from the UG2. The first group overlaps to an extent with the UG2 chromites. This grouping may be due to having fewer samples than the UG2, if more samples are taken the area between the two groups may be filled as in figure. This may also be due to a genuine difference in compositions between chromite within the seamlet (group 2) and disseminated grains (group 1).

6. Discussion

6.1 Textural analysis

Many of the textures observed in this study have been described and studied in some detail in previous publications. The plagioclase inclusions have been extensively described by Eales et al. (1991). and occur as plagioclase inclusions within cumulate pyroxenes ranging in size from 0.02mm-0.25mm and range in shape from, spheroid to irregular. These characteristics described by Eales et al. (1991) are similar to the inclusions found within this study. This would therefore suggest that the inclusions plagioclase inclusions found to occur with the orthopyroxenes and to a lesser extent the clinopyroxenes are chadacrysts. There is however one characteristic not shared with the chadacrysts that Eales et al. (1991) found, and that is zoning of the plagioclase chadacrysts. This characteristic has not been observed within the slides. This does not mean it is not present at all but is a rarity within in these samples. Eales et al. (1991) suggests that these chadacrysts may be aberrations within the typical crystal sequence but does not suggest why this would occur. If these were to be aberrations within the normal crystallisation sequence there would have to be a trigger for it to occur. One possibility is that there was a mixing of magmas. This mixing would have occurred between to normal parent magma and a secondary magma that was introduced into the magma chamber from another source. The second notable texture is found to occur within the hangingwall and footwall. This is the triple junctions which occur between the orthopyroxenes. These 120° triple junctions suggest that at some point the units have undergone recrystallization. The chadacrysts of plagioclase within the pyroxenes may also be evidence of recrystallization as suggested by Mondal and Mathez (2007). Mondal and Mathez (2007) suggest that the included plagioclase grains within the pyroxenes may be due to the pyroxenes undergoing 'post-accumulation enlargement'. This may also explain why the chadacrysts mainly exhibit round boundaries. The rounded nature of the chadacrysts may due to resorption of the plagioclase grains within their host liquid and then later incorporated within an interstitial melt which crystallised pyroxene thus including the chadacrysts within the pyroxenes. The other textures found within Mondal and Mathez (2007) however have not been observed e.g. the sub-parallel orientation of lath shaped plagioclase grains or the slender 3mm pyroxenes which show a similar orientation. The textures found within the silicate rocks show no preference in orientation in any of the units which in its self does not suggest anything. This lack of orientated minerals may be due to the magma not flowing in a single direction or crystals be churned up fairly regularly not allowing for and orientation of minerals to form. The pegmatoid does not appear to include the chadacrysts or the 120° triple junctions. Given that there large oikocrysts of orthopyroxene and clinopyroxene it would be expected that these textures would be observed within the slides and hand specimens. This however is not the case and would suggest that this layer has not undergone any recrystallization or possible magma mixing. This would therefore suggest that the pegmatoid layer formed later than the hangingwall or footwall which has evidence of undergoing recrystallization and possible magma mixing. If

the pegmatoid formed later and is found to occur within the UG2 layer it would suggest that the layer was injected into the UG2 chromitite while it was still forming. This may also suggest that the pegmatoid or the UG2 chromitite may be responsible for the recrystallization. The UG2 however also shows evidence of recrystalisation in the presence of the annealed texture. The annealed texture as described by Eales suggests that the chromite has undergone extensive recrystallization. The zoned plagioclase is evidence that recrystallization has not taken place as the zoning would not be present if it had. This is due to the grains being recrystallised and any textural characteristics being over printed. This would suggest that the plagioclase that has been recrystallized was present before recrystallization took place and that zoned plagioclase formed later, after the recrystallization. This earlier plagioclase which has been recrystallized may have originated in the same liquid in which the chadacrysts originated and may also explain why the chadcrysts are not zoned. The cataclastic texture found within the slide U5 has only been found to occur within this slide. This is also true for the rounded zones of norite found to occur within the cataclastic zone. This texture may be due a localised fault running through the area in which the core was taken from. The presence of the norite zones may be remnants of the original rock or may have formed due to the presence of liquid. Evidence for the presence of liquid would be the liquid boundary found to occur between the plagioclase and clinopyroxene within one of these zones in figure. These to textures were only observed under microscope and within the electron microprobe and were not observed in hand specimen. The discontinuous rims and exsolution lamellae suggest that at some point there has been disequilibrium within the crystal mush. This is due to the discontinuous rims appearing similar to reaction rims or sites. These discontinuous rims may have formed from exsolved clinopyroxene which originated from the orthopyroxene exsolved out of the crystals via the lamellae or may have formed in situ within the grain boundaries. Both of these textures would however suggest disequilibrium as they would not form if the orthopyroxene was in equilibrium within the crystal mush. This may have been due to contamination within the mush or the infiltration of silicate fluids through the mush as suggested by Chutas et al. (2012).

6.2 Controls on geochemical variation

The analyses produced in this study show compositional variation within the plagioclase and chromite, little to no variation occurs within the pyroxenes. The compositional variation of the plagioclase is found to occur within each unit with samples showing ranges on An content. The compositions as a whole do overlap to an extent and show that the textures do not control the composition as compositions of different textures as well as the same textures overlap between units. This however is not the case in the plagioclase inclusions within the footwall, where the samples show low An content and plot at the extreme of the labradorite field. This compositional change from the norm would suggest that the plagioclase inclusions have formed from a different parent magma to the zoned and recrystallized plagioclase found interstitially.

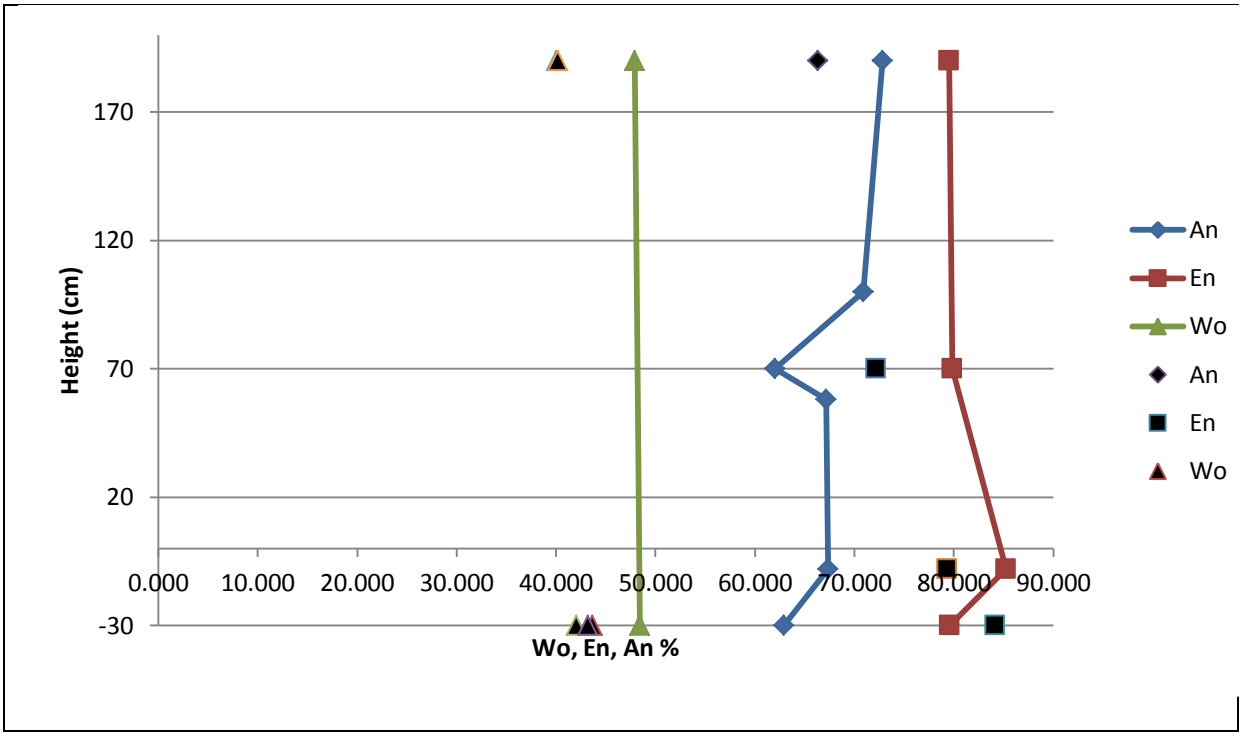

Figure 38: scatter graph showing compositions of orthopyroxene, clinopyroxene and plagioclase with respect to height in the stratigraphy. Points marked in black represent data that is outside the average which in plotted in each components respective colour.

Figure 38 above illustrates the change in average An values for plagioclase, En values for orthopyroxene and Wo values for clinopyroxene. The averages were used in order to provide a better comparison. Where more than one value is plotted the average has been plotted as well as any data which falls outside the average. This figure is to compare the variations mineral compositions between units and between minerals in order to see if compositional variation occurs over a whole unit or if just one mineral is affected. The figure shows that both the orthopyroxene and plagioclase shows variation between units. It also shows that the compositional variation is apparent in more than one mineral group. This suggests that when each unit was emplaced the parent magma may have changed compositions slightly or that there has been periods of disequilibrium that have taken place during the crystal mush stage of the original parent magma. This theory has been suggested by Chutas et al. (2011) where Sr and Pb isotope data was used to suggest disequilibrium taking place via liquids moving through the crystal mush. The pyroxenes as observed in the geochemistry section and the above figure show little variation in composition with the bulk of samples across the stratigraphy overlapping in textures and between units. There is however one or two exceptions which have been pointed out and may be due to enrichment or the probe analysing minerals behind or next to the intended site.

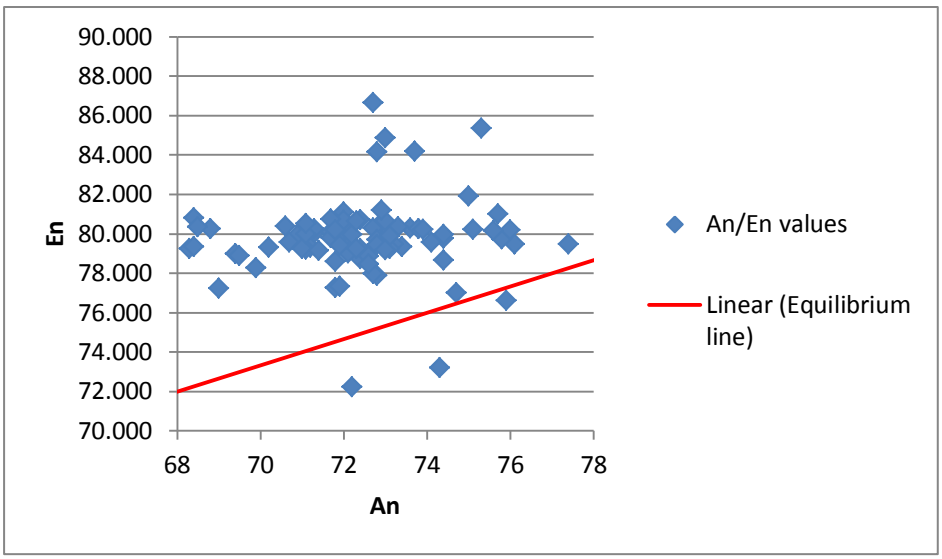

Figure 39: Scatter graph showing orthopyroxene En values plotted against plagioclase An values. Line of equilibrium taken from Ashwal et al. (2005).

Figure 39 above shows the An values from the plagioclase grains and En from the orthopyroxene grains from the whole stratigraphy. The plagioclase values have come from the cores of the plagioclase grains meaning that no relationship can be observed between rim and core compositions. This is due to no systematic difference in composition being observed between cores and rims. This figure illustrates where the values should plot along the line of equilibrium (red line) if the rocks were of equal amounts of plagioclase and pyroxene (norites).This is not the case, however as the rocks dealt with in this study are pyroxenites. The variation in An content may be due to trapped liquids crystallising new plagioclase or the infiltration of liquid into the older cumulate which then crystallises plagioclase (figure 40). Due to only taking data from plagioclase cores distinguishing between late crystallisation of trapped liquids and the infiltration of later evolved liquid is not possible. This new plagioclase from either of these two modes becomes increasingly more sodic in composition due to the original plagioclase in the cumulate becoming less and thus plotting further from the line of equilibrium. This means that the new plagioclase is less able equilibrate to the original plagioclase and hence more extreme or “fractional” the late plagioclase compositions become, as illustrated within figure 39.

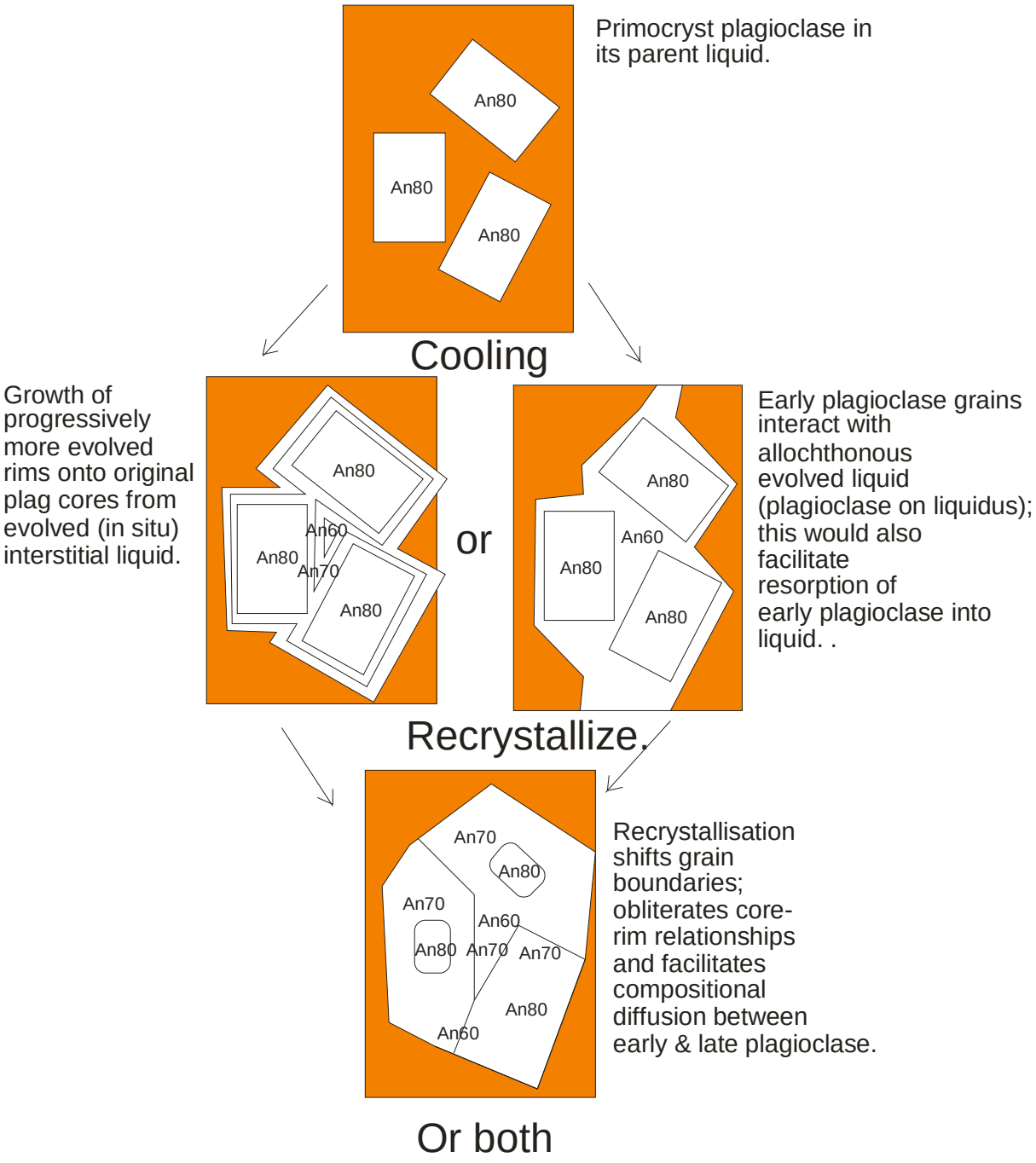

Figure 40: Simple sketch illustrating the two processes by which plagioclase compositions may become more "fractional".

These processes however do not rule out disequilibrium and Chutas et al. (2011) suggest that disequilibrium can easily take place in large igneous complexes such as the Bushveld where prolonged cooling and crystallisation time allow for the infiltration of minor contaminants. This is particularly true if there is active recrystallization driven by mineral aging, compaction or exsolution.

Chromite analyses also show variation within their respective units and between the UG2 chromitite and the footwall. The variation within both units is most notably in the Cr and Al content with the Fe3 content changing very little. The most notable variation is that in the footwall where two distinct compositional groups are found. These groups are the disseminated grains within the silicates and the seamlet found to occur within the footwall below the UG2. The seamlet compositions overlap with the bulk of the UG2 chromitite sample compositions and would suggest that the seamlet may in fact be part of the UG2 which had been separated by pyroxenite. This separation may have taken place by a reversal to conditions prior to the emplacement of the chromite. The disseminated grains may have a different composition due to the grains possibly forming prior to the chromitite layer or at the start of chromite production where conditions had just changed or a new magma had been injected into the original parent magma causing the production of chromite.

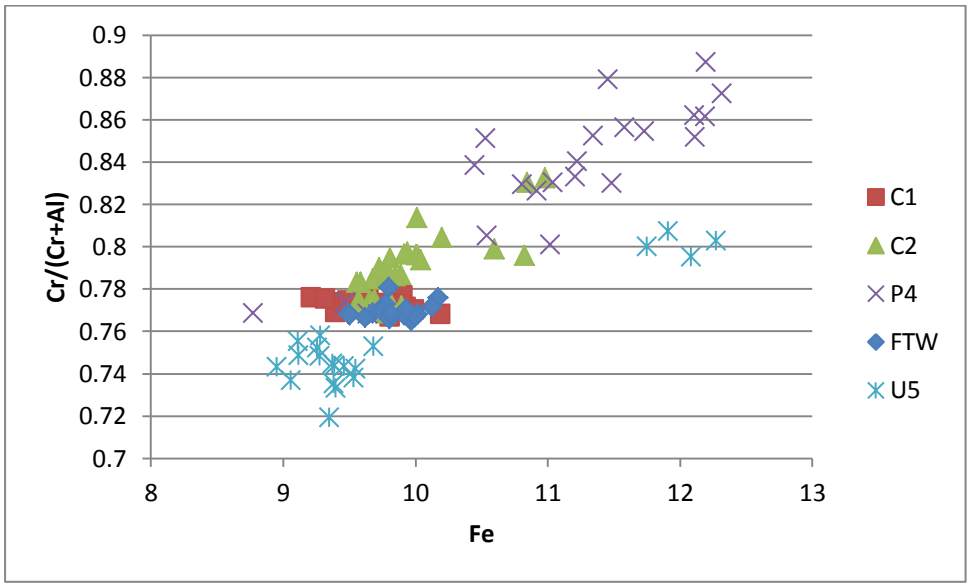

Figure 41a: Scatter graph plotting Cr# against Fe #.

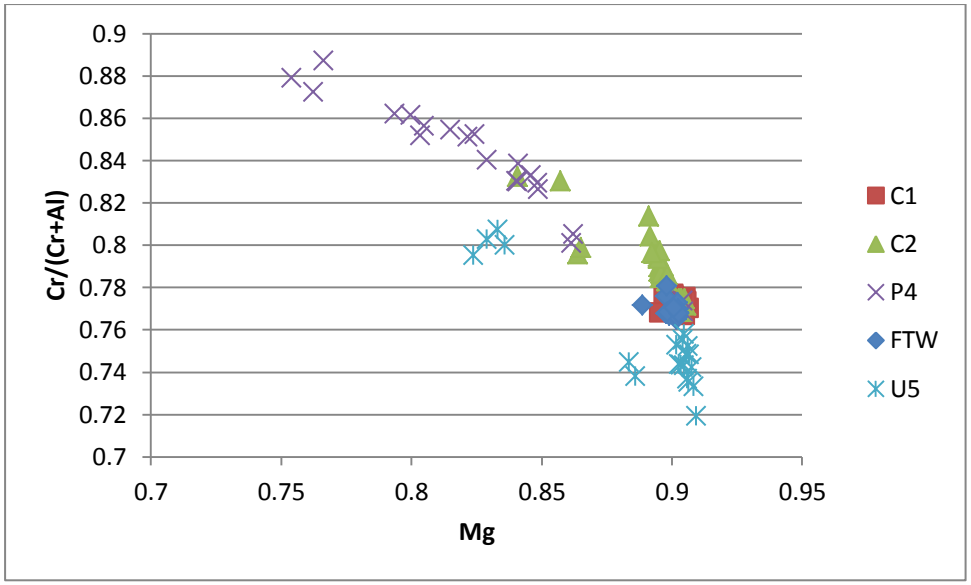

Figure 41b: Scatter graph plotting Cr# against Mg#.

The two figures above (figures 40a and 40b) show the composition of chromite per slide and how it varies. Some of the compositions overlap but most of the samples do not share the same composition in terms or Fe or Mg. This variation is not observed in the ternary figures due the diagrams not plotting the two components. This variation in compositions would suggest that throughout the footwall and UG2 chromitite the chromite has been enriched by Fe and Mg in varying quantities which may be a product of disequilibrium as discussed above or may be due to the mixing of two magmas to produce the chromite. The production of chrome during the mixing of the magmas would use up components such as Fe and Mg and as one was depleted the other would take its place thus meaning that later chromite would have a different composition to earlier chromite.

Variation in composition does not appear to be texturally controlled the minerals overlap in all instances but one which may suggest that in the case of plagioclase inclusions within the footwall texture does control the composition. This however does not appear true for the rest of the stratigraphy but compositional ranges do appear to vary between units and would suggest that composition may be a control of stratigraphy. The evidence provided suggests that lower An content occurs within the plagioclase in the footwall of the UG2 and the pegmatoid. These two layers have An contents of between 55% and 70% and in comparison the UG2 and the hanging wall have compositions of 70% and 80%. There is however a part of the UG2 that shows lower An content and this may be due to this part of the UG2 being formed by a different pulse of magma from a different source or the magma composition changing for a short period of time and then reverting the original composition. This may also be due to a period of disequilibrium where minerals have either been enriched or depleted.

The compositional variation within the chromite as with the plagioclase shows no textural controls however composition seems to vary from sample to sample within the same stratigraphic unit. The overall variation in composition shows varying concentrations of Cr and Al. The Cr content ranges between 55% and 80% over the whole stratigraphy, this includes the UG2 and the chromite found within the other units. The Cr# vs Fe# and Mg# graphs reinforce the variation in composition and better identify variation within samples and between units. The Cr# vs Mg# shows the most compositional variation between units and shows that samples taken from within the UG2 show a large compositional variation within between UG2 samples. These UG2 samples show completely different Mg and Cr compositions and suggest that the UG2 was not formed by the same magma pulse but rather two or more different pulses. The chromite within the footwall is compositionally similar to the lower of the two samples taken from UG2. This may be due to crystals settling out of the chrome rich layer during formation. The chromite in the pegmatoid shows the most variation within a single sample and shows composition spread right across from Mg rich to Cr rich. This may due the pegmatoid interrupting the production of chromite and scavenging chromite from the layers both above and below the pegmatoid. The Cr# vs Fe# suggests that the UG2 composition is the same as the UG2 sample data overlaps and shows the same composition along with the footwall. This again suggests that the chromite in the footwall has been scavenged from the above UG2. The Pegmatoid again shows a large range in compositional variation and again suggests that the chromite may have be scavenged from above and below the unit however, the composition of the UG2 does not vary like in the previous graph and suggests that the chromite within the pegmatoid may show variation due to enrichment and recrystallization when it was scavenged by the pegmatoid.

The pyroxenes show no real systematic compositional variation apart from between orthopyroxene and clinopyroxene. As with the plagioclase it was expected that with so much textural variation compositional variations and groups could be found forming in the data but again this has not been observed. Each texture has the same composition as the other textures for their respective minerals. There is some anomalous data that appears on the ternary graphs but this can be attributed to the sites that were picked for sampling being too thin or too close to a fracture or crystal boundary. This means that when the electron microprobe sampled the site the beam went through the intended mineral and into the mineral behind it giving a false reading and altering the data. The little variation that does occur within the clinopyroxene shows variation Wo content and ranges between 40% and 50% with a single outlier at 35%. This however is not a consequence of texture as explained above and does not help to explain why reaction rims or oikocrysts all within the same sample and unit. The orthopyroxene shows variation in En content and ranges between 80% and 90% with the majority of grains around the 80% region. These compositional ranges are observed to be the ranges for individual samples and for the whole stratigraphy showing no variation between any of the units suggesting that the silicate rich magma that produced the hanging wall, pegmatoid and footwall was chemically

and compositionally the same separated only by a period of time in which chrome rich layers were formed.

All these observations suggest that there is a resident magma which is represented by the hanging wall and the footwall. The crystallization of the resident magma is halted by the pulse of a new magma or mixed with a chemically different magma to form the UG2 chromite layer. This period of new magma then resides and the resident magma crystallizes again and forms the hanging wall. This explains how the hanging and footwall have similar compositions and how disequilibrium textures may have formed. The two models for which the data best represents are the mixing model by Irvine 1977 and the magma injection model by Eales 2000. The Irvine model put forward in 1977 suggests that the mixing of a primitive magma and a more evolved magma would produce a chromite saturated layer. The mixing of the two magmas may also explain the disequilibrium found within the layers a one of the magmas may be already starting to crystalize when the new magma is mixed into the chamber. The Eales model however, suggests that there is a second sub-chamber below the main Bushveld chamber where magma is already crystallizing in crystal mushes. This secondary chamber periodically injects crystal charged magmas into the main chamber where the crystal mush interacts with the resident liquid. This also explains the occurrence of disequilibrium textures and may explain why in a certain area there is a pegmatoid and in other areas there isn't. The occurrence of the pegmatoid may be due to several feeder dykes from the sub-chamber and the crystal charged magma may not be injected through all of them. The injections may be chromite rich in composition accounting for the chromite but may also be similar in composition which would account for the disequilibrium of orthopyroxene and plagioclase. The best model to explain the data and petrological observations would be a model that incorporates both these models where a more evolved crystal charged magma is injected from the sub-chamber into the primitive resident magma or vice versa. This would allow for the mixing of similar magmas and occasionally the sub-chamber injecting a chemically different crystal charged magma which when mixed with the resident magma produces chrome saturated layers such as the UG2.

7. References

Adetunji, J., Everitt, S., Rollinson, H. (2013). New Mössbauer measurements of $Fe^{3+}/\sum Fe$ ratios in chromites from the early Proterozoic Bushveld Complex, South Africa, Precambrian Research, 228, 194-205.

Armstrong, R.A., Compston, W., Retief, E.A., Williams, I.S. and Welke, H.J. (2000). Zircon ion microprobe studies bearing on the age and evolution of the Witwatersrand triad. Precambrian Research, 53, 243-266.

Ashwal L. D, Webb S. J, Knoper M. W. (2005). Magmatic stratigraphy in the Bushveld Northern Lobe: continuous geophysical and mineralogical data from the 2950 m Bellevue drillcore. South African Journal of Geology. 108 (1), p199-232.

Cameron, E. N. (1977), Chromite in the central sector of the Eastern Bushveld Complex, South Africa: Am. Mineralogist, v.62, p. 1082-1096.

Cameron, E. N. (1980). Evolution of the Lower Critical Zone, Central Sector, Eastern Bushveld Complex, and Its Chromite Deposits.Economic Geology. 75 , p845-871.

Chutas N. I, Bates E, Prevec S. A, Coleman D. S, Boudreau A. E. (2011). Sr and Pb isotopic disequilibrium between coexisting plagioclase and orthopyroxene in the Bushveld Complex, South Africa: microdrilling and progressive leaching evidence for sub-liquidus contamination.Contrib mineral Petrol.

Eales H. V. (2000). Implications of the chromium budget of the Western Limb of the Bushveld Complex. South African Journal of Geology. 103 (2), p141-150.

Eales, H. V., & Cawthorn, R. G. (1996). The Bushveld Complex. *Developments in Petrology*, *15*, 181-229.

Eales, H.V. and Costin, G. (2012) Crustally contaminated komatiite: primary source of the chromitites and Marginal, Lower, and Critical Zone magmas in a staging chamber beneath the Bushveld Complex. Economic Geology, 107, 645-665.

Eales.H.V, Maier.W.D, Teigler.B. (1991). Corroded plagioclase feldspar inclusions in orthopyroxene and olivine of the Lower and Critical Zones, Western Bushveld Complex. *Mineralogical magazine*. 55 (0), p479-486.

Harmer, R.E. and Sharpe, M.R. (1986). Field relations and strontium isotope systematics of the marginal rocks of the eastern Bushveld Complex. Econ. Geol. 80, 813-837

Harmer, R. E. (2000). New precise dates on the acid phase of the Bushveld and their implications. In *Workshop on the Bushveld Complex, 18 th–21 st November 2000. University of the Witwatersrand, Johannesburg, South Africa*.

Hunter, R.H. (1996). Texture Development in Cumulate Rocks. in , Layered Intrusions (edited by R.G. Cawthorn), p77-98.

Hunter, D. R. (1975). The Regional Geological Setting of the Bushveld Complex: (An Adjunct to the Provisional Tectonic Map of the Bushveld Complex). Johannesburg: Economic Geology Research Unit, University of the Witwatersrand, p1-5.

Hunter, D.R. and Hamilton, P.J.1987. The Bushveld Complex. In: D.H. Tarling (Editor), Evolution of the Earth's crust. Academic Press, London 107-173.

Irvine.T.N. (1977). Origin of chromitite layers in the Muskox intrusion and other stratiform intrusions: A new interpretation. *Geolgy*. 5, p273-277.

Kinnaird, J. A. (2005). The Bushveld Large Igneous Province. School of Geosciences, Witwatersrand University. P1-25.

Lipin.B.R. (1993). Pressure Increases, the Formation of Chromite Seams, and the Development of the Ultramafic Series in the Stillwater Complex, Montana. *JOURNAL OF PETROLOGY*. 34 (5), p955-976.

Maier W. D, Barnes S. J. & Groves D. I. (2012). The Bushveld Complex, South Africa: formation of platinum– palladium, chrome- and vanadium-rich layers via hydrodynamic sorting of a mobilized cumulate slurry in a large, relatively slowly cooling, subsiding magma chamber. Mineralium Deposita.

Mitchell.A.A, Scoon.R.N. (2004). The platiniferous dunite pipes in the eastern limb of the Bushveld Complex: review and comparison with unmineralized discordant ultramafic bodies. *South African Journal of Geology*. 107 (4), p505.

MONDAL S. K. AND MATHEZ E. A. (2007). Origin of the UG2 chromitite layer, Bushveld Complex. JOURNALOF PETROLOGY. 48 (3), 495-510.

Prevec.S.A., Ashwal.L.D, and Mkaza.M.S. (2005). Mineral disequilibrium in the Merensky Reef, western Bushveld Complex, South Africa: new Sm–Nd isotopic evidence. *Contributions to mineralogy and petrology*. 149 (3), p306-315.

Robb L. (2005). Introduction into Ore forming Processes. p49-53

Seabook.C.L., Cawthorn, R.G. and Kruger, F.J. (2005). The Merensky Reef, Bushveld Complex: mixing of minerals not mixing of magmas. *Economic geology*. 100 (6), p1191.

8. Appendix

8.1 Core Logs

LITHOLOGY LOG

core: BHID: WH-1

Deflection: D0

FROM (m)	TO	LITHOLOGY	STRATIGRAPHY	Top Contact	Basal Contact	GSIZE	COMMENTS	TEXTURE	COLOUR
0.00	0.33	Norite	Upper Critical Zone	Unknown (not present)	gradational	Fine		Massive	Light grey/brown
0.33	0.67	Pyroxenite	Upper Critical Zone	Gradational	unkown (not	Fine- Medium		Massive	Grey/brown
0.67	0.85	Pyroxenite	Upper Critical Zone	Unknown (not present)	Sharp	Medium	5mm-thick chromitite seamlet 3cm from the top of the unit.	Massive	Brown
0.85	1.06	UG2 Chromitite	Upper Critical Zone	Sharp	Sharp	Fine	Shows interstitial Plag/Opx	Massive	Black
1.06	1.13	Pyroxenite	Upper Critical Zone	Sharp	gradational	Medium- Coarse		Massive	Brown
1.13	1.26	Pyroxenite	Upper Critical Zone	Gradational	gradational	Very Coarse	Small chromitite seamlets throughout units, all < 4mm	Pegmatoidal	Brown
1.26	1.75	UG2 Chromitite	Upper Critical Zone	Gradational	sharp	Fine	Shows interstitial Plag/Opx	Massive	Black
1.75	1.77	Pyroxenite	Upper Critical Zone	Sharp	Sharp	Medium		Massive	Brown
1.77	1.85	UG2 Chromitite	Upper Critical Zone	Sharp	Sharp	Fine	Shows interstitial Plag/Opx	Massive	Black
1.85	1.98	Pyroxenite	Upper Critical Zone	Sharp	unkown (not	Coarse	Footwall of the UG2	Massive	Brown

LITHOLOGY LOG

BHID: Eastern Bushveld core

Deflection: D0

FROM (m)	TO	LITHOLOGY	STRATIGRAPHY	Top Contact	Basal Contact	GRAIN SIZE	COMMENTS	TEXTURE	COLOUR
0.00	0.11	Leuconorite	Upper critical zone	Not Present	Sharp	Fine-Medium	Chromitite stringer at the base of the unit 2mm thick.	Massive	White-Light grey
0.11	0.21	Pyroxenite	Upper critical zone	Sharp	Gradational	Medium-Coarse		Massive	Grey/Brown
0.21	0.26	Pyroxenite	Upper critical zone	Gradational	Gradational	Very Coarse		Pegmatoidal	Grey/Brown
0.26	3.05	Pyroxenite	Upper critical zone	Gradational	Gradational	Medium-Coarse		Massive	Grey/Brown
3.05	3.55	Pyroxenite	Upper critical zone	Gradational	Gradational	Very Coarse		Pegmatoidal	Grey/Brown
3.55	3.85	Pyroxenite	Upper critical zone	Gradational	Gradational	Medium-Coarse		Massive	Grey/Brown
3.85	5.32	Pyroxenite	Upper critical zone	Gradational	Gradational	Coarse		Massive	Grey/Brown
5.32	5.40	Pyroxenite	Upper critical zone	Gradational	Sharp	Very Coarse		Pegmatoidal	Grey/Brown
5.40	5.90	Chromitite	Upper critical zone	Sharp	Sharp	Fine	UG2 chromitite layer	Massive	Black
5.90	7.90	Pyroxenite	Upper critical zone	Sharp	Gradational	Medium-Coarse	1mm thick chromitite stringer 2cm from the base of the unit.	Massive	Grey/Brown
7.90	8.50	Norite	Upper critical zone	Gradational	Gradational	Fine-Medium		Massive	Light brown
8.50	9.12	Pyroxenite	Upper critical zone	Gradational	Not present	Medium-Coarse		Massive	Grey/Brown

8.2 Average mineral compositions versus stratigraphic position

Sample	An	Height	Standard Deviation	n	Sample	En	Height	Standard Deviation	n	Sample	Wo	Height	Standard Deviation	n
U5	62.923	-30.000	5.343	39.000	U5	79.566	-30.000	1.326	36.000	U5	43.635	-30.000		
Ftw	67.340	-8.000	1.258	5.000	U5	84.192	-30.000			U5	42.031	-30.000		
C2	67.163	58.000	1.868	8.000	Ftw	79.338	-8.000			U5	43.231	-30.000		
P4	62.000	70.000	1.010	4.000	Ftw	85.254	-8.000	1.057	4.000	U5	48.422	-30.000	0.490	38.000
C1	70.900	100.000	0.909	4.000	P4	72.210	70.000			P1	40.037	190.000		
P1	72.824	190.000	1.575	74.000	P4	79.818	70.000	1.467	8.000	P1	40.167	190.000		
P1	66.300	190.000			P1	79.542	190.000	0.998	48.000	P1	47.901	190.000	1.329	68.000

See also figure 38.

	8.3 Appendix A: PYROXENE EMP DATA															
Sample	EMP sample No.	SiO_2	TiO_2	Al_2O_3	FeO*	Cr_2O_3	MnO	MgO	CaO	Na_2O	K_2O	**Total**	WO	EN	FS	Texture
		(wt.%)	(wt.%)	(wt.%)	(wt.%)	(wt.%)	(wt.%)	(wt.%)	(wt.%)	(wt.%)	(wt.%)	(wt.%)				
P1	18_1	55.173	0.034	1.076	11.29	0.348	0.103	29.366	2.706	0.001	0.025	**100.12**	5.158	77.888	16.954	tabular
P1	18_10	52.818	0.033	1.314	4.044	0.561	0.092	16.561	24.34	0.072	0.014	**99.85**	48.091	45.528	6.38	rim
P1	18_11	53.161	0.061	1.254	3.899	0.593	0.044	16.621	24.869	0.08	0.021	**100.6**	48.693	45.28	6.027	Rim
P1	18_12	53.276	0.041	1.242	3.712	0.587	0.073	16.536	25.003	0.065	0.023	**100.56**	49.058	45.144	5.798	Rim
P1	18_13	52.859	0.026	1.325	3.87	0.611	0.024	16.549	24.466	0.066	0.039	**99.84**	48.417	45.568	6.015	Rim
P1	18_14	53.027	0.042	1.31	4.091	0.577	0.046	16.6	24.598	0.098	0.026	**100.42**	48.303	45.355	6.342	Rim
P1	18_15	53.279	0.048	1.344	3.685	0.599	0.02	16.531	24.449	0.075	0.034	**100.06**	48.566	45.689	5.745	Rim
P1	18_16	53.217	0.026	1.292	3.83	0.603	0.054	16.688	24.652	0.099	0.032	**100.49**	48.429	45.615	5.957	Rim
P1	18_17	53.193	0.029	1.222	3.732	0.632	0.107	16.826	24.345	0.073	0.03	**100.19**	47.967	46.127	5.906	Rim
P1	18_18	51.97	0.057	1.976	4.691	0.688	0.041	16.855	22.622	0.092	0.03	**99.02**	45.455	47.123	7.422	necking
P1	18_19	52.447	0.034	1.75	4.676	0.668	0.072	16.326	24.733	0.07	0.019	**100.8**	48.349	44.405	7.246	necking
P1	18_2	55.217	0.02	1.081	11.693	0.374	0.088	30.523	0.772	0	0.013	**99.78**	1.472	80.99	17.538	tabular

P1	18_20	52.92	0.067	1.638	6.038	0.643	0.065	18.147	20.04	0.069	0.021	**99.65**	40.037	50.445	9.518	tabular
P1	18_21	52.771	0.066	1.583	4.525	0.697	0.04	16.596	23.794	0.089	0.027	**100.19**	47.164	45.772	7.064	Rim
P1	18_22	54.928	0.019	1.082	12.331	0.291	0.153	30.378	0.804	0.022	0.039	**100.05**	1.522	80.026	18.452	tabular
P1	18_23	55.093	0.051	1.071	12.347	0.321	0.083	30.374	0.871	0.018	0.024	**100.25**	1.648	79.987	18.364	tabular
P1	18_24	54.936	0.031	1.272	12.232	0.329	0.104	29.745	1.176	0.001	0.02	**99.85**	2.253	79.296	18.451	tabular
P1	18_25	54.954	0.011	1.155	12.118	0.357	0.078	30.233	0.77	0	0.017	**99.69**	1.471	80.346	18.184	tabular
P1	18_26	54.956	0.028	1.209	11.801	0.369	0.098	29.649	1.2	0.006	0.026	**99.34**	2.319	79.729	17.952	tabular
P1	18_27	54.953	0.019	1.278	11.764	0.392	0.085	29.639	1.412	0	0.012	**99.55**	2.721	79.458	17.822	tabular
P1	18_28	55.379	0.028	1.202	12.132	0.357	0.119	29.759	0.819	0	0.02	**99.82**	1.581	79.952	18.467	rounded
P1	18_29	55.188	0.035	1.192	12.121	0.333	0.127	30.273	0.79	0	0.025	**100.08**	1.506	80.273	18.222	rounded
P1	18_3	54.78	0.029	1.201	11.503	0.375	0.082	28.581	3.109	0	0.013	**99.67**	5.988	76.594	17.418	tabular
P1	18_30	55.301	0.051	1.36	12.071	0.354	0.118	29.326	2.017	0.02	0.009	**100.63**	3.854	77.965	18.181	tabular
P1	18_31	52.344	0.051	1.434	4.287	0.612	0.067	16.251	24.086	0.078	0.029	**99.24**	48.079	45.136	6.785	Rim
P1	18_32	52.857	0.05	1.88	4.39	0.639	0.07	16.855	22.308	0.099	0.032	**99.18**	45.303	47.626	7.071	tabular
P1	18_33	52.497	0.046	1.779	4.47	0.7	0.024	16.193	24.087	0.08	0.019	**99.9**	48.053	44.948	6.998	unkown
P1	18_34	52.795	0.066	1.558	4.035	0.588	0.067	16.508	23.94	0.062	0.025	**99.64**	47.773	45.836	6.391	Rim

P1	18_35	52.864	0.052	1.662	4.685	0.713	0.075	17.121	22.983	0.051	0.013	**100.22**	45.492	47.153	7.356	unkown
P1	18_36	52.035	0.039	1.69	4.847	0.678	0.096	16.264	23.997	0.083	0.036	**99.76**	47.532	44.824	7.644	unkown
P1	18_37	53.068	0.041	1.602	4.171	0.7	0.052	16.372	24.235	0.081	0.018	**100.34**	48.17	45.278	6.553	unkown
P1	18_38	52.706	0.049	1.543	4.32	0.638	0.031	16.771	23.729	0.052	0.023	**99.86**	47.025	46.244	6.731	unkown
P1	18_39	52.288	0.029	1.806	4.265	0.744	0.061	16.155	24.079	0.08	0.01	**99.52**	48.221	45.015	6.763	tabular
P1	18_4	55.127	0.049	1.175	11.703	0.396	0.079	29.921	1.468	0.001	0.015	**99.93**	2.807	79.606	17.586	tabular
P1	18_40	52.747	0.051	1.662	4.363	0.687	0.015	16.696	23.451	0.067	0.009	**99.75**	46.809	46.369	6.821	Rim
P1	18_41	52.726	0.057	1.712	4.602	0.678	0.107	16.762	22.659	0.079	0.018	**99.4**	45.63	46.966	7.404	tabular
P1	18_42	52.708	0.064	1.744	4.427	0.665	0.105	16.307	24.374	0.086	0.016	**100.5**	48.168	44.839	6.993	tabular
P1	18_43	52.615	0.022	1.557	4.056	0.674	0.049	16.458	24.118	0.062	0.011	**99.62**	48.023	45.596	6.381	Rim
P1	18_44	52.781	0.062	1.596	4.434	0.679	0.091	16.403	24.134	0.067	0.028	**100.28**	47.8	45.203	6.997	Rim
P1	18_45	53.124	0.06	1.473	4.028	0.563	0.05	16.473	24.679	0.088	0.035	**100.57**	48.597	45.134	6.269	unkown
P1	18_46	53.019	0.04	1.492	4.056	0.626	0.056	16.456	24.377	0.086	0.031	**100.24**	48.287	45.355	6.359	unkown
P1	18_47	52.807	0.046	1.753	3.969	0.651	0.03	16.044	24.636	0.096	0.021	**100.05**	49.192	44.575	6.233	tabular
P1	18_48	52.603	0.04	1.617	3.526	0.68	0.087	16.091	25.018	0.053	0.019	**99.73**	49.809	44.575	5.616	Rim
P1	18_5	51.86	0.049	1.776	4.104	0.687	0.113	16.069	24.46	0.094	0.034	**99.25**	48.812	44.618	6.571	tabular

P1	18_50	54.843	0.028	1.181	11.879	0.339	0.09	29.891	0.923	0.008	0.017	**99.2**	1.78	80.202	18.018	tabular
P1	18_52	54.855	0.051	1.26	11.798	0.409	0.086	29.763	1.283	0.015	0.014	**99.53**	2.469	79.682	17.85	rounded
P1	18_54	55.121	0.039	1.156	12.037	0.342	0.126	29.814	1.219	0.011	0.016	**99.88**	2.335	79.474	18.191	tabular
P1	18_55	54.828	0.03	1.017	11.337	0.372	0.093	29.29	2.399	0.009	0.01	**99.39**	4.607	78.259	17.134	tabular
P1	18_56	55.858	0.042	0.992	11.975	0.276	0.125	30.009	0.713	0.008	0.038	**100.04**	1.373	80.431	18.196	tabular
P1	18_57	55.09	0.051	1.045	11.721	0.325	0.102	29.707	0.988	0.007	0.014	**99.05**	1.917	80.18	17.903	tabular
P1	18_6	53.176	0.056	1.322	3.68	0.552	0.008	16.631	24.825	0.077	0.013	**100.34**	48.826	45.512	5.662	tabular
P1	18_60	52.682	0.044	1.577	4.5	0.688	0.064	15.922	24.274	0.082	0.032	**99.86**	48.557	44.316	7.127	necking
P1	18_62	53.332	0.018	0.999	3.086	0.539	0.012	16.669	25.368	0.074	0.013	**100.11**	49.761	45.495	4.744	necking
P1	18_63	52.543	0.027	1.951	4.389	0.763	0.08	16.325	23.655	0.09	0.008	**99.83**	47.444	45.558	6.998	Rim
P1	18_64	52.253	0.041	1.839	4.53	0.687	0.076	16.394	24.631	0.06	0.01	**100.52**	48.261	44.694	7.046	unkown
P1	18_65	52.609	0.069	1.854	4.139	0.738	0.021	16.218	23.62	0.051	0.026	**99.35**	47.782	45.649	6.569	tabular
P1	18_67	55.158	0.022	0.885	11.877	0.334	0.102	30.05	0.644	0	0.017	**99.09**	1.243	80.707	18.05	tabular
P1	18_68	55.037	0.041	1.212	11.466	0.338	0.079	29.47	1.515	0	0.022	**99.18**	2.94	79.571	17.489	tabular
P1	18_7	53.263	0.056	1.022	3.491	0.548	0.031	16.859	24.827	0.064	0.014	**100.18**	48.648	45.964	5.387	rim
P1	18_70	52.974	0.058	1.609	4.35	0.651	0.073	16.303	24.477	0.069	0.028	**100.59**	48.36	44.817	6.822	Rim

P1	18_72	52.557	0.056	2.04	5.376	0.652	0.035	17.215	21.548	0.064	0.023	**99.57**	43.335	48.171	8.495	Rim
P1	18_73	52.348	0.049	2.037	4.251	0.784	0.045	15.907	24.44	0.066	0.019	**99.95**	48.952	44.331	6.717	Rim
P1	18_74	52.537	0.052	1.455	4.125	0.627	0.048	16.269	24.438	0.076	0.017	**99.64**	48.553	44.974	6.472	Rim
P1	18_75	53.006	0.037	1.492	3.89	0.601	0.049	16.337	24.58	0.078	0.029	**100.1**	48.783	45.114	6.103	unkown
P1	18_76	52.113	0.059	1.781	4.31	0.737	0.018	16.04	24.089	0.078	0.014	**99.24**	48.386	44.828	6.786	unkown
P1	18_8	53.313	0.05	1.036	3.208	0.478	0.063	16.529	25.139	0.068	0.02	**99.9**	49.593	45.369	5.038	Rim
P1	18_9	52.734	0.028	1.892	6.015	0.638	0.082	18.346	20.332	0.066	0.021	**100.15**	40.167	50.429	9.403	fluid necking
P1	19_1	54.599	0.025	1.115	11.496	0.397	0.057	29.317	2.099	0.008	0.024	**99.14**	4.044	78.583	17.373	tabular
P1	19_10	52.466	0.056	1.761	4.31	0.684	0.04	16.439	23.92	0.077	0.016	**99.77**	47.66	45.574	6.766	rim
P1	19_11	55.323	0.019	1.088	12.038	0.341	0.065	29.962	0.879	0	0.019	**99.73**	1.69	80.147	18.163	tabular
P1	19_12	55.339	0.046	1.201	12.477	0.356	0.066	29.959	1.133	0	0.034	**100.61**	2.154	79.235	18.611	tabular
P1	19_14	54.909	0.034	1.103	11.614	0.361	0.097	29.123	2.788	0	0.02	**100.05**	5.315	77.255	17.429	tabular
P1	19_15	52.416	0.037	1.613	4.198	0.65	0.084	16.034	24.771	0.093	0.015	**99.91**	49.126	44.244	6.63	tabular
P1	19_16	52.525	0.052	1.845	5.65	0.717	0.072	17.05	22.145	0.085	0.019	**100.16**	43.995	47.13	8.875	tabular
P1	19_19	51.745	0.083	1.923	4.162	0.691	0.049	15.827	24.436	0.093	0.015	**99.02**	49.123	44.269	6.608	tabular
P1	19_2	55.122	0.03	1.144	12.402	0.376	0.077	30.015	1.064	0	0.032	**100.26**	2.024	79.445	18.531	tabular

P1	19_20	54.612	0.044	1.06	11.887	0.409	0.069	29.872	1.081	0.017	0.019	**99.07**	2.08	79.965	17.956	tabular
P1	19_21	54.978	0.028	1.176	12.556	0.316	0.097	29.608	1.3	0	0.013	**100.07**	2.482	78.659	18.859	tabular
P1	19_22	54.906	0.065	1.208	11.532	0.393	0.116	29.688	1.072	0.019	0.029	**99.03**	2.083	80.252	17.666	tabular
P1	19_23	54.522	0.035	1.186	12.091	0.38	0.099	29.519	1.27	0.005	0.029	**99.14**	2.449	79.201	18.35	tabular
P1	19_25	53.114	0.058	1.267	4.19	0.571	0.031	16.462	24.354	0.077	0.016	**100.14**	48.174	45.308	6.518	Rim
P1	19_26	52.258	0.046	1.756	4.315	0.645	0.067	15.996	24.601	0.079	0.016	**99.78**	48.929	44.267	6.804	necking
P1	19_27	53.233	0.045	1.204	3.633	0.614	0.05	16.743	24.831	0.073	0.016	**100.44**	48.686	45.676	5.638	Rim
P1	19_28	53.312	0.037	1.124	4.113	0.523	0.034	16.879	24.525	0.102	0.028	**100.68**	47.856	45.827	6.317	Rim
P1	19_29	52.897	0.039	1.41	5.187	0.573	0.052	17.141	22.632	0.054	0.031	**100.02**	44.752	47.16	8.087	unkown
P1	19_3	54.877	0.047	1.227	12.308	0.367	0.068	29.583	1.388	0	0.014	**99.88**	2.658	78.838	18.504	tabular
P1	19_30	55.148	0.034	1.27	12.408	0.41	0.142	29.506	1.298	0.006	0.025	**100.25**	2.489	78.724	18.787	tabular
P1	19_31	55.167	0.031	0.977	11.773	0.309	0.137	30.105	0.826	0	0.027	**99.35**	1.588	80.536	17.876	tabular
P1	19_32	55.034	0.003	1.189	12.766	0.365	0.089	29.868	0.845	0	0.006	**100.17**	1.611	79.252	19.137	tabular
P1	19_33	55.018	0.016	1.15	12.096	0.377	0.1	29.542	1.163	0	0.028	**99.49**	2.246	79.371	18.384	tabular
P1	19_34	54.941	0.03	1.192	11.675	0.347	0.059	29.686	1.325	0	0.016	**99.27**	2.558	79.755	17.686	tabular
P1	19_35	53.193	0.015	1.192	3.642	0.622	0.067	16.657	24.812	0.068	0.021	**100.29**	48.762	45.547	5.691	Rim

P1	19_36	53.062	0.043	1.469	4.117	0.594	0.027	16.713	24.078	0.068	0.025	**100.2**	47.616	45.987	6.397	Rim
P1	19_37	52.787	0.073	1.685	3.918	0.666	0.078	16.193	23.847	0.076	0.021	**99.34**	48.178	45.519	6.303	tabular
P1	19_38	52.663	0.024	1.722	5.216	0.664	0.049	17.11	22.383	0.103	0.019	**99.95**	44.499	47.33	8.171	tabular
P1	19_39	52.482	0.04	1.867	4.465	0.646	0.101	15.896	24.101	0.083	0.025	**99.71**	48.412	44.427	7.161	Fluid Necking
P1	19_4	54.875	0.033	1.202	11.85	0.416	0.06	29.608	1.386	0	0.029	**99.46**	2.672	79.408	17.92	tabular
P1	19_42	52.59	0.046	1.812	4.372	0.632	0.055	16.083	24.309	0.102	0.025	**100.03**	48.48	44.628	6.892	necking
P1	19_43	53.08	0.02	1.285	3.987	0.626	0.02	16.636	24.502	0.101	0.025	**100.28**	48.254	45.586	6.16	necking
FTW	19_44	56.098	0.03	1.467	9.106	0.341	0.064	32.245	0.851	0.001	0	**100.2**	1.609	84.852	13.538	tabular
FTW	19_45	55.342	0.026	1.476	9.108	0.431	0.077	30.098	3.736	0.009	0.018	**100.32**	7.078	79.338	13.584	tabular
FTW	19_46	55.788	0.035	1.358	9.57	0.36	0.103	32.168	0.876	0	0.027	**100.29**	1.647	84.155	14.198	tabular
FTW	19_47	55.929	0.024	1.502	8.225	0.343	0.077	33.486	0.692	0.004	0.013	**100.3**	1.287	86.659	12.054	tabular
P1	19_5	54.543	0.038	1.268	12.118	0.414	0.093	29.62	1.415	0.006	0.014	**99.53**	2.713	79.012	18.275	tabular
P4	19_54	54.762	0.023	1.512	9.755	0.455	0.104	29.127	3.257	0.019	0.026	**99.04**	6.327	78.723	14.95	oikocryst
P4	19_55	55.003	0.026	1.417	11.521	0.422	0.092	30.167	0.79	0.004	0.018	**99.46**	1.524	80.985	17.491	oikocryst
P4	19_58	55.342	0.03	1.117	10.495	0.264	0.074	30.524	1.585	0.006	0.026	**99.46**	3.03	81.197	15.773	tabular
P4	19_59	54.588	0.027	1.377	9.326	0.428	0.071	26.977	7.11	0.03	0.028	**99.96**	13.678	72.21	14.112	tabular

P4	19_60	55.573	0.02	1.161	10.966	0.32	0.08	30.577	0.773	0.017	0.028	**99.51**	1.488	81.911	16.601	tabular
P4	19_61	54.68	0.009	1.411	11.139	0.395	0.062	30.128	1.322	0	0.012	**99.16**	2.543	80.638	16.819	tabular
P4	19_62	54.824	0.021	1.18	11.891	0.372	0.077	29.683	1.489	0.009	0.02	**99.57**	2.856	79.223	17.921	tabular
P4	19_65	54.778	0.038	1.331	11.702	0.424	0.093	29.422	1.691	0	0.024	**99.5**	3.262	78.975	17.763	tabular
P1	19_7	52.399	0.053	1.58	4.155	0.743	0.081	16.288	24.823	0.099	0.034	**100.26**	48.871	44.618	6.511	necking
P1	19_8	52.508	0.039	1.524	4.381	0.619	0.05	16.878	23.436	0.063	0.03	**99.53**	46.519	46.614	6.866	unknown
P1	19_9	52.014	0.093	2.045	4.326	0.533	0.052	15.949	24.258	0.081	0.014	**99.365**	48.645	44.501	6.854	tabular
U5	25_5	52.568	0.273	1.751	3.846	0.804	0.107	16.138	23.648	0.001	0.029	99.165	48.076	45.649	6.275	Rim
U5	25_6	52.495	0.253	1.69	3.554	0.802	0.065	16.094	24.429	0.007	0.019	99.408	49.205	45.104	5.691	Rim
U5	25_7	52.896	0.352	1.906	3.775	0.827	0.142	16.167	24.087	0.013	0.011	100.176	48.523	45.315	6.162	Rim
U5	25_8	52.783	0.311	1.807	3.884	0.792	0.176	16.187	23.368	0.008	0.014	99.33	47.63	45.907	6.463	Rim
U5	25_9	52.673	0.325	1.906	4.076	0.877	0.076	15.917	23.593	0.007	0	99.45	48.167	45.215	6.618	Rim
U5	25_10	51.868	0.525	2.434	4.057	0.848	0.127	15.674	23.425	0.011	0.047	99.016	48.298	44.966	6.736	Oikocryst
U5	25_11	53.037	0.276	1.81	4.145	0.841	0.069	16.292	23.76	0.007	0	100.237	47.789	45.594	6.617	Rim
U5	25_12	52.861	0.308	2.235	4.248	0.929	0.108	16.022	23.724	0	0	100.435	48.007	45.111	6.882	Rim
U5	25_14	55.138	0.164	1.342	11.915	0.489	0.214	29.484	1.041	0.013	0.018	99.818	2.02	79.605	18.375	tabular

U5	25_15	54.888	0.161	1.313	11.951	0.532	0.273	29.291	0.997	0.002	0.034	99.442	1.944	79.451	18.606	tabular
U5	25_16	54.676	0.157	1.33	11.304	0.489	0.26	28.852	1.983	0	0.014	99.065	3.876	78.474	17.65	tabular
U5	25_20	55.298	0.146	1.289	11.959	0.433	0.233	29.506	0.879	0	0.048	99.791	1.708	79.791	18.5	tabular
U5	25_23	52.41	0.288	2.02	4.33	0.915	0.16	15.409	23.507	0.01	0.008	99.057	48.515	44.249	7.236	Oikocryst
U5	25_25	52.442	0.291	2.19	3.882	0.89	0.127	16.062	23.603	0.008	0.019	99.514	48.089	45.533	6.378	Rim
U5	25_26	52.474	0.314	2.137	4.396	0.9	0.134	15.834	23.529	0.008	0.008	99.734	47.923	44.873	7.204	Rim
U5	25_27	52.538	0.32	2.223	4.2	0.872	0.119	15.791	23.958	0	0.03	100.051	48.595	44.565	6.84	Oikocryst
U5	25_28	52.79	0.294	2.017	4.035	0.857	0.14	15.762	24.274	0.007	0.017	100.193	49.073	44.336	6.591	Oikocryst
U5	25_29	53.141	0.247	1.532	3.739	0.704	0.132	16.422	24.285	0.006	0.026	100.234	48.418	45.556	6.027	Rim
U5	25_30	52.894	0.273	1.524	3.545	0.776	0.103	16.3	24.161	0.006	0.031	99.613	48.624	45.643	5.733	Rim
U5	25_31	52.783	0.315	1.838	3.905	0.855	0.098	15.998	23.799	0	0.01	99.601	48.388	45.258	6.355	Rim
U5	25_32	54.433	0.167	1.585	11.925	0.459	0.29	29.201	1.153	0.001	0.062	99.276	2.247	79.169	18.584	tabular
U5	25_36	54.903	0.181	1.426	12.113	0.443	0.26	29.505	0.713	0.003	0.02	99.567	1.386	79.829	18.785	tabular
U5	25_37	55.331	0.138	1.324	12.304	0.427	0.277	29.779	0.466	0	0.014	100.06	0.901	80.108	18.991	tabular
U5	25_38	54.696	0.173	1.389	11.029	0.5	0.303	28.999	1.957	0.004	0.044	99.094	3.826	78.877	17.297	tabular
U5	25_40	52.276	0.271	1.978	5.046	0.827	0.143	17.811	20.906	0.007	0.043	99.308	42.031	49.823	8.146	Oikocryst

U5	25_42	52.507	0.327	2.162	4.141	0.91	0.097	15.875	24.096	0.01	0.014	100.139	48.685	44.629	6.686	Oikocryst
U5	25_43	52.566	0.304	1.854	4.2	0.84	0.172	15.94	23.702	0.008	0.023	99.609	48.082	44.992	6.926	Oikocryst
U5	25_46	52.579	0.282	2.047	3.935	0.903	0.139	15.783	23.552	0	0.034	99.254	48.368	45.099	6.533	Oikocryst
U5	25_47	52.497	0.297	2.038	4.438	0.884	0.111	15.609	23.791	0.017	0.023	99.705	48.493	44.268	7.24	Oikocryst
U5	25_51	54.943	0.18	1.306	11.537	0.433	0.205	29.527	0.951	0	0.028	99.11	1.857	80.239	17.904	tabular
U5	25_52	55.135	0.133	1.397	11.712	0.491	0.305	29.056	0.887	0	0.025	99.141	1.75	79.743	18.507	tabular
U5	25_53	55.087	0.147	1.468	12.265	0.45	0.272	29.85	0.891	0	0.032	100.462	1.706	79.546	18.747	tabular
U5	25_55	52.504	0.278	2.384	3.652	1.007	0.108	15.578	23.984	0.011	0.032	99.538	49.355	44.604	6.042	Oikocryst
U5	25_56	52.631	0.314	2.183	5.106	0.975	0.156	17.099	21.247	0.004	0.013	99.728	43.231	48.408	8.36	Oikocryst
U5	25_58	52.092	0.278	2.337	4.113	0.977	0.156	15.848	24.083	0.001	0.023	99.908	48.685	44.576	6.739	Oikocryst
U5	25_59	52.331	0.317	2.172	3.899	1.006	0.095	15.836	23.688	0.007	0.055	99.406	48.501	45.114	6.385	Oikocryst
U5	25_60	52.372	0.267	2.123	3.695	0.924	0.14	15.527	23.954	0.004	0.02	99.026	49.336	44.496	6.168	Oikocryst
U5	25_61	53.074	0.21	1.592	3.494	0.784	0.114	16.022	24.256	0.001	0.002	99.549	49.135	45.158	5.707	Oikocryst
U5	25_62	53.202	0.223	1.703	4.13	0.836	0.116	16.293	23.755	0.008	0.002	100.268	47.758	45.577	6.665	Oikocryst
U5	25_64	54.899	0.169	1.497	11.502	0.482	0.267	29.057	1.185	0.001	0.008	99.067	2.333	79.58	18.087	tabular
U5	25_65	54.956	0.161	1.566	11.698	0.519	0.285	28.923	1.135	0	0.017	99.26	2.237	79.321	18.441	tabular

U5	25_69	54.802	0.152	1.431	11.92	0.081	0.291	29.102	1.285	0	0.008	99.072	2.504	78.915	18.581	tabular
U5	25_70	55.228	0.181	1.507	11.801	0.087	0.267	29.489	1.227	0	0.011	99.798	2.374	79.394	18.232	tabular
U5	25_72	52.918	0.252	1.699	3.971	0.112	0.116	16.183	23.996	0.003	0.014	99.264	48.278	45.302	6.421	Rim
U5	25_73	53.51	0.198	1.47	4.288	0.712	0.135	16.39	23.897	0.004	0.033	100.637	47.646	45.468	6.886	Rim
U5	25_75	52.523	0.31	2.109	3.894	0.941	0.143	15.814	23.78	0	0.035	99.549	48.594	44.964	6.442	Rim
U5	25_76	53.044	0.247	1.882	3.774	0.908	0.119	16.067	23.72	0.012	0.031	99.804	48.294	45.516	6.189	Rim
U5	25_78	52.063	0.448	2.583	4.047	0.964	0.087	15.706	23.864	0.001	0.028	99.791	48.757	44.649	6.594	Rim
U5	25_80	55.058	0.106	1.389	11.974	0.476	0.267	29.732	0.672	0	0.019	99.693	1.302	80.175	18.523	tabular
U5	25_81	54.95	0.135	1.406	11.74	0.45	0.226	29.528	0.988	0.006	0.028	99.457	1.922	79.908	18.17	tabular
U5	25_83	55.221	0.139	1.362	11.862	0.059	0.24	29.427	0.719	0	0.021	99.05	1.407	80.107	18.486	tabular

	8.3 Appendix B: Plagioclase EMP DATA												
Sample	EMP Sample No.	SiO2	Al2O3	Fe2O3	MnO	BaO	CaO	Na2O	K2O	Total	Ab	An	Or	Texture
P1	18_1	50.918	30.531	0.136	0	0	14.778	2.862	0.248	99.473	25.6	73	1.5	zoned/recrystallised
P1	18_10	50.567	31.008	0.127	0	0.006	14.917	2.823	0.255	99.703	25.1	73.4	1.5	zoned/recrystallised
P1	18_12	50.798	30.518	0.186	0	0.001	14.633	2.879	0.239	99.254	25.9	72.7	1.4	zoned/recrystallised
P1	18_13	50.111	31.446	0.124	0	0.001	15.035	2.596	0.197	99.51	23.5	75.3	1.2	zoned/recrystallised
P1	18_14	50.616	31.018	0.191	0	0.013	14.544	2.845	0.235	99.462	25.8	72.8	1.4	zoned/recrystallised

P1	18_15	50.451	31.361	0.224	0	0	15.155	2.552	0.207	99.95	23.1	75.7	1.2	zoned/recrystallised
P1	18_16	50.236	31.402	0.246	0.014	0	15.107	2.506	0.219	99.73	22.8	75.9	1.3	inclusion
P1	18_17	51.283	30.658	0.109	0.003	0.006	14.342	2.9	0.251	99.552	26.4	72.1	1.5	zoned/recrystallised
P1	18_18	50.709	31.206	0.095	0.024	0.017	15.128	2.72	0.23	100.129	24.2	74.4	1.4	zoned/recrystallised
P1	18_19	51.11	30.386	0.134	0.002	0.006	14.292	2.909	0.232	99.071	26.5	72.1	1.4	zoned/recrystallised
P1	18_2	50.925	30.442	0.124	0	0.029	14.656	2.931	0.246	99.353	26.2	72.4	1.4	zoned/recrystallised
P1	18_20	50.706	30.865	0.124	0.038	0	14.698	2.86	0.234	99.525	25.7	72.9	1.4	zoned/recrystallised
P1	18_22	51.029	30.85	0.212	0	0	14.594	2.751	0.211	99.647	25.1	73.6	1.3	zoned/recrystallised
P1	18_23	50.896	30.954	0.13	0.032	0	14.743	2.73	0.241	99.726	24.7	73.8	1.4	zoned/recrystallised
P1	18_27	50.567	30.821	0.14	0	0	14.722	2.705	0.392	99.347	24.4	73.3	2.3	inclusion
P1	18_28	51.202	30.774	0.151	0	0.013	14.501	2.855	0.232	99.728	25.9	72.7	1.4	zoned/recrystallised
P1	18_29	50.759	30.743	0.136	0	0.002	14.497	2.851	0.238	99.226	25.9	72.7	1.4	zoned/recrystallised
P1	18_3	50.433	31.205	0.237	0	0	14.867	2.677	0.229	99.648	24.2	74.4	1.4	inclusion
P1	18_30	49.881	31.408	0.278	0	0.009	15.286	2.538	0.181	99.581	22.9	76.1	1.1	inclusion
P1	18_31	49.82	31.111	0.326	0.012	0	15.137	2.527	0.208	99.141	22.9	75.8	1.3	zoned/recrystallised
P1	18_32	50.85	30.839	0.166	0.005	0.009	14.672	2.718	0.22	99.479	24.8	73.9	1.3	inclusion
P1	18_33	50.509	30.973	0.22	0.018	0	15.027	2.722	0.281	99.75	24.3	74.1	1.7	inclusion
P1	18_34	50.951	30.754	0.027	0.021	0.01	14.56	2.855	0.223	99.401	25.8	72.8	1.3	zoned/recrystallised
P1	18_36	50.696	31.021	0.215	0	0	14.539	2.786	0.237	99.494	25.4	73.2	1.4	inclusion
P1	18_37	51.221	30.598	0.153	0.005	0	14.438	2.778	0.228	99.421	25.5	73.1	1.4	zoned/recrystallised
P1	18_4	50.424	31.349	0.302	0.017	0	15.109	2.489	0.219	99.909	22.7	76	1.3	inclusion
C1	18_43	51.484	30.613	0.087	0	0.019	14.524	2.926	0.275	99.928	26.3	72.1	1.6	zoned/recrystallised
C1	18_44	51.303	30.502	0.096	0	0	14.231	3.294	0.136	99.562	29.3	69.9	0.8	zoned/recrystallised
C1	18_45	51.247	30.736	0.11	0.029	0.012	14.245	3.049	0.265	99.693	27.5	70.9	1.6	zoned/recrystallised
C1	18_46	51.249	30.413	0.102	0	0	14.335	3.208	0.111	99.418	28.7	70.7	0.7	zoned/recrystallised
P1	18_5	51.187	30.969	0.232	0.006	0	14.715	2.941	0.238	100.288	26.2	72.4	1.4	inclusion
P1	18_6	51.101	30.757	0.182	0	0.013	14.563	2.986	0.223	99.825	26.7	72	1.3	inclusion
P1	18_7	51.249	31.277	0.144	0	0.009	14.451	2.928	0.248	100.306	26.4	72.1	1.5	inclusion
P1	18_8	50.695	31.127	0.22	0.002	0.004	14.37	2.759	0.275	99.452	25.4	73	1.7	zoned/recrystallised

P1	18_9	51.09	31.091	0.248	0	0	14.574	2.848	0.286	100.137	25.7	72.6	1.7	inclusion
P1	19_1	50.857	30.999	0.102	0	0	14.729	2.91	0.209	99.806	26	72.8	1.2	zoned/recrystallised
P1	19_10	50.61	30.666	0.111	0	0	14.613	3.016	0.233	99.249	26.8	71.8	1.3	zoned/recrystallised
P1	19_11	50.727	30.771	0.18	0	0.001	14.61	3.021	0.221	99.531	26.9	71.8	1.3	zoned/recrystallised
P1	19_12	51.111	31.048	0.208	0	0.019	14.629	2.99	0.222	100.227	26.6	72	1.3	inclusion
P1	19_13	50.232	30.993	0.165	0.006	0	14.978	2.902	0.229	99.505	25.6	73.1	1.3	inclusion
P1	19_14	50.036	31.672	0.34	0	0	15.332	2.608	0.201	100.189	23.3	75.6	1.2	inclusion
P1	19_15	50.18	31.307	0.215	0.012	0.002	15.079	2.733	0.138	99.666	24.5	74.7	0.8	inclusion
P1	19_16	51.093	30.465	0.083	0.011	0	14.566	3.109	0.244	99.571	27.5	71.1	1.4	zoned/recrystallised
P1	19_17	50.899	30.883	0.193	0.012	0	14.473	3.071	0.213	99.744	27.4	71.3	1.3	inclusion
P1	19_18	50.134	31.403	0.237	0	0	15.107	2.716	0.224	99.821	24.2	74.4	1.3	inclusion
P1	19_19	50.87	30.626	0.105	0	0	14.529	2.922	0.252	99.304	26.3	72.2	1.5	zoned/recrystallised
P1	19_2	51.707	30.171	0.186	0.009	0	14.03	3.218	0.319	99.64	28.8	69.4	1.9	inclusion
P1	19_20	51.068	30.778	0.217	0.041	0	14.149	3.164	0.235	99.652	28.4	70.2	1.4	inclusion
P1	19_21	50.746	30.926	0.175	0.024	0	14.454	3.009	0.231	99.565	27	71.7	1.4	inclusion
P1	19_22	51.163	30.656	0.137	0	0	14.585	3.133	0.227	99.901	27.6	71	1.3	zoned/recrystallised
P1	19_23	50.612	30.703	0.117	0.046	0	14.784	2.97	0.235	99.467	26.3	72.3	1.4	zoned/recrystallised
P1	19_24	50.379	31.369	0.298	0.03	0	15.055	2.631	0.225	99.987	23.7	75	1.3	inclusion
P1	19_25	50.876	30.59	0.149	0	0	14.567	2.932	0.244	99.358	26.3	72.2	1.5	zoned/recrystallised
P1	19_26	50.405	30.887	0.18	0.043	0	14.798	2.914	0.188	99.415	26	72.9	1.1	zoned/recrystallised
P1	19_27	51.503	30.377	0.157	0.067	0.008	14.05	3.307	0.273	99.742	29.4	69	1.6	zoned/recrystallised
P1	19_28	50.213	30.909	0.105	0	0	14.938	2.889	0.223	99.277	25.6	73.1	1.3	zoned/recrystallised
P1	19_29	52.046	29.833	0.162	0.014	0	13.684	3.578	0.402	99.719	31.4	66.3	2.3	inclusion
P1	19_3	49.765	31.789	0.302	0.015	0.002	15.313	2.371	0.152	99.709	21.7	77.4	0.9	zoned/recrystallised
P1	19_31	50.034	31.033	0.272	0.029	0.013	15.135	2.831	0.239	99.586	24.9	73.7	1.4	zoned/recrystallised
P1	19_32	50.572	30.911	0.151	0.006	0	14.668	3.077	0.264	99.649	27.1	71.4	1.5	zoned/recrystallised
P1	19_33	50.92	30.413	0.151	0	0	14.381	3.081	0.241	99.187	27.6	71.1	1.4	inclusion
P1	19_34	50.503	30.451	0.125	0.017	0	14.727	3.063	0.219	99.105	27	71.7	1.3	zoned/recrystallised
P1	19_35	50.827	30.787	0.069	0.006	0	14.6	2.998	0.229	99.516	26.7	71.9	1.4	zoned/recrystallised

P1	19_36	50.646	30.651	0.092	0	0.019	14.753	2.967	0.227	99.355	26.3	72.3	1.3	zoned/recrystallised
P1	19_37	50.528	31.16	0.212	0	0	14.943	2.886	0.247	99.976	25.5	73	1.4	zoned/recrystallised
P1	19_4	50.621	30.76	0.126	0	0.002	14.604	3.038	0.227	99.378	27	71.7	1.3	zoned/recrystallised
C2	19_43	51.376	30.521	0.06	0.005	0	14.348	3.546	0.183	100.039	30.6	68.4	1	zoned/recrystallised
C2	19_44	51.847	30.028	0.085	0	0	13.686	3.705	0.169	99.52	32.6	66.5	1	zoned/recrystallised
C2	19_45	52.506	29.667	0.065	0.012	0.013	13.155	3.871	0.241	99.53	34.3	64.3	1.4	zoned/recrystallised
C2	19_46	52.409	29.977	0.083	0.014	0	13.176	3.75	0.22	99.629	33.5	65.1	1.3	zoned/recrystallised
C2	19_47	51.328	30.379	0.125	0	0	13.925	3.262	0.173	99.192	29.5	69.5	1	zoned/recrystallised
C2	19_48	51.415	30.495	0.091	0	0	14.073	3.478	0.206	99.758	30.5	68.3	1.2	zoned/recrystallised
C2	19_49	52.15	30.25	0.08	0	0.007	13.703	3.697	0.197	100.084	32.4	66.4	1.1	zoned/recrystallised
P1	19_5	50.878	30.843	0.18	0	0.005	14.801	3.032	0.249	99.988	26.6	71.9	1.4	inclusion
C2	19_52	51.674	30.578	0.095	0	0	14.308	3.452	0.201	100.308	30.1	68.8	1.1	zoned/recrystallised
FTW	19_53	51.758	30.286	0.094	0	0.002	13.827	3.702	0.174	99.843	32.3	66.7	1	zoned/recrystallised
FTW	19_54	51.894	30.146	0.066	0	0.008	14.035	3.63	0.12	99.899	31.7	67.6	0.7	zoned/recrystallised
FTW	19_55	50.864	30.47	0.063	0	0	14.109	3.495	0.138	99.139	30.7	68.5	0.8	zoned/recrystallised
FTW	19_56	51.939	30.211	0.091	0.02	0.032	13.657	3.85	0.197	99.997	33.4	65.5	1.1	zoned/recrystallised
FTW	19_57	51.774	30.024	0.097	0.014	0	13.719	3.462	0.073	99.163	31.2	68.4	0.5	zoned/recrystallised
P4	19_58	52.744	29.512	0.06	0.018	0	12.948	3.863	0.474	99.619	34.1	63.1	2.7	Zoned/recrystallised
P4	19_59	53.168	29.179	0.057	0	0	12.483	4.066	0.52	99.473	36	61	3	Zoned/recrystallised
P1	19_6	50.859	30.822	0.145	0	0	14.277	3.027	0.27	99.4	27.3	71.1	1.6	inclusion
P4	19_60	53.118	29.127	0.1	0	0.018	12.751	3.895	0.483	99.492	34.6	62.6	2.8	Zoned/recrystallised
P4	19_61	53.144	29.037	0.096	0	0	12.653	4.161	0.387	99.478	36.5	61.3	2.2	Zoned/recrystallised
P1	19_7	50.938	30.793	0.165	0	0	14.449	3.163	0.25	99.758	28	70.6	1.4	inclusion
P1	19_8	50.302	31.306	0.183	0	0	15.286	2.775	0.223	100.075	24.4	74.3	1.3	inclusion
P1	19_9	50.864	30.861	0.219	0.024	0	14.55	3.011	0.228	99.757	26.9	71.8	1.4	zoned/recrystallised
U5	25_1	53.104	29.336	0.083	0.029	0	11.899	4.609	0.391	99.451	40.3	57.5	2.3	zoned/recrystallised
U5	25_3	52.511	29.457	0.051	0.003	0	12.342	4.328	0.41	99.102	37.9	59.7	2.4	zoned/recrystallised
U5	25_5	51.946	30.046	0.065	0.019	0.012	13.006	3.778	0.357	99.229	33.7	64.2	2.1	zoned/recrystallised
U5	25_6	51.847	29.961	0.003	0	0	12.872	3.969	0.371	99.023	35	62.8	2.2	zoned/recrystallised

U5	25_7	52.981	29.602	0.091	0	0	12.067	4.48	0.416	99.637	39.2	58.4	2.4	zoned/recrystallised
U5	25_8	53.141	29.424	0.119	0	0.001	11.915	4.482	0.415	99.497	39.5	58.1	2.4	zoned/recrystallised
U5	25_9	53.051	29.349	0.089	0	0	11.908	4.602	0.4	99.399	40.2	57.5	2.3	zoned/recrystallised
U5	25_10	53.667	28.853	0.071	0	0.007	11.561	4.923	0.223	99.305	43	55.7	1.3	inclusion
U5	25_14	50.773	30.697	0.037	0.002	0.014	13.749	3.558	0.315	99.145	31.3	66.9	1.8	zoned/recrystallised
U5	25_16	53.276	29.332	0.168	0.024	0.01	11.604	4.379	0.324	99.117	39.8	58.3	1.9	zoned/recrystallised
U5	25_17	51.599	30.745	0.051	0	0.008	13.349	3.779	0.282	99.813	33.3	65.1	1.6	zoned/recrystallised
U5	25_19	49.663	31.329	0.122	0.005	0	14.556	3.118	0.208	99.001	27.6	71.2	1.2	zoned/recrystallised
U5	25_22	52.586	29.469	0.051	0.019	0.005	12.193	4.32	0.417	99.06	38.1	59.5	2.4	zoned/recrystallised
U5	25_23	53.719	29.379	0.025	0.01	0	11.658	4.245	0.488	99.524	38.6	58.5	2.9	zoned/recrystallised
U5	25_24	52.731	29.686	0.04	0.015	0	12.397	4.19	0.362	99.421	37.2	60.7	2.1	zoned/recrystallised
U5	25_26	52.942	29.517	0.04	0	0.011	12.004	4.401	0.328	99.243	39.1	59	1.9	zoned/recrystallised
U5	25_27	51.58	30.178	0.063	0.016	0	13.292	3.875	0.296	99.3	34	64.3	1.7	zoned/recrystallised
U5	25_31	52.37	29.781	0.052	0.042	0.013	12.605	3.985	0.364	99.212	35.6	62.2	2.1	zoned/recrystallised
U5	25_36	53.511	28.987	0.04	0.008	0.008	11.561	4.769	0.397	99.281	41.8	55.9	2.3	inclusion

	8.3 Appendix C: Chromite EMP DATA												
Sample	EMP sample no.	SiO2	TiO2	Al2O3	Cr2O3	FeO	MnO	MgO	V2O3	NiO	Total	Fe3 tot	Texture
C2	18_1	0	1.068	16.647	43.812	27.957	0.388	9.698	0.36	0.114	100.04	0.18	Coalescent
C2	18_10	0.025	1.012	16.349	43.799	29.092	0.381	9.389	0.392	0.157	100.6	0.2	Coalescent
C2	18_11	0.007	1.016	16.819	43.045	28.646	0.375	9.732	0.361	0.137	100.14	0.2	Coalescent
C2	18_12	0	1.083	16.767	43.107	27.677	0.316	9.512	0.368	0.152	98.98	0.18	Coalescent
C2	18_13	0.035	1.062	16.731	42.798	28.494	0.283	9.42	0.381	0.17	99.37	0.19	Coalescent
C2	18_14	0.012	0.897	17.179	43.267	28.499	0.315	9.669	0.339	0.188	100.37	0.19	Coalescent
C2	18_15	0.004	0.825	16.953	43.472	27.152	0.441	9.629	0.368	0.145	98.99	0.17	Coalescent
C2	18_16	0.009	0.949	16.955	43.332	28.356	0.224	9.582	0.376	0.161	99.94	0.18	Coalescent

C2	18_17	0	1.012	16.796	43.468	27.887	0.329	9.717	0.364	0.135	99.71	0.18	Coalescent
C2	18_18	0	0.998	16.891	42.982	28.585	0.263	9.518	0.37	0.137	99.74	0.19	Coalescent
C2	18_19	0.005	0.947	17.049	43.276	27.509	0.414	9.636	0.344	0.07	99.25	0.17	Coalescent
C2	18_20	0.001	0.963	17.073	43.214	28.035	0.283	9.712	0.399	0.112	99.79	0.18	Coalescent
C2	18_21	0.028	0.617	16.293	44.845	28.017	0.309	9.435	0.337	0.116	100	0.17	Coalescent
C2	18_22	0	0.975	17.012	43.645	28.061	0.27	9.462	0.378	0.121	99.92	0.17	Coalescent
C2	18_23	0	0.948	17.051	43.616	27.171	0.204	9.636	0.376	0.123	99.13	0.17	Coalescent
C2	18_4	0	0.861	16.505	43.142	28.953	0.374	8.849	0.164	0.141	98.99	0.19	Coalescent
C2	18_5	0	1.038	16.649	43.254	28.387	0.315	9.516	0.345	0.213	99.72	0.19	Coalescent
C2	18_6	0	1.07	16.499	43.033	28.394	0.421	9.425	0.368	0.117	99.33	0.19	Coalescent
C2	18_7	0.019	1.072	16.45	43.157	27.957	0.29	9.683	0.366	0.21	99.2	0.19	Coalescent
C2	18_8	0.008	1.036	16.357	43.927	27.585	0.382	9.261	0.375	0.217	99.15	0.17	Coalescent
C2	18_9	0	1.068	16.779	42.996	29.147	0.381	9.281	0.386	0.143	100.18	0.19	Coalescent
C2	19_1	0	1.026	16.71	43.322	27.696	0.425	9.909	0.393	0.144	99.63	0.19	Coalescent
C2	19_10	0	1.062	17.075	43.435	28.053	0.353	9.895	0.388	0.165	100.43	0.19	Coalescent
C2	19_11	0	0.949	16.685	43.425	27.82	0.278	9.758	0.39	0.173	99.48	0.18	Coalescent
C2	19_12	0	1.002	16.606	43.179	28.09	0.491	9.813	0.405	0.12	99.71	0.2	Coalescent
C2	19_13	0	1.008	16.707	43.302	28.575	0.159	9.765	0.389	0.123	100.03	0.19	Coalescent
C2	19_14	0	0.953	16.197	43.629	28.319	0.199	9.631	0.383	0.126	99.44	0.19	Coalescent
C2	19_15	0.014	1.055	16.495	43.409	28.095	0.378	9.699	0.394	0.154	99.69	0.19	Coalescent
C2	19_16	0.002	0.988	16.261	43.571	26.34	0.377	9.348	0.38	0.205	97.47	0.16	Coalescent
C2	19_17	0	1.033	16.817	43.257	26.87	0.319	9.564	0.407	0.164	98.43	0.17	Coalescent
C2	19_2	0.014	1.002	16.471	43.973	26.645	0.365	9.799	0.383	0.132	98.78	0.17	Coalescent
C2	19_22	0	0.992	16.707	43.706	27.459	0.305	9.628	0.403	0.153	99.35	0.17	Coalescent
C2	19_23	0.032	0.894	16.417	43.768	27.483	0.239	9.475	0.399	0.134	98.84	0.18	Coalescent
C2	19_24	0.034	0.932	16.585	43.808	27.044	0.352	9.839	0.39	0.158	99.14	0.18	Coalescent
C2	19_25	0	1.152	16.456	43.648	27.129	0.331	9.777	0.393	0.148	99.03	0.18	Coalescent
C2	19_26	0	1.07	16.434	43.294	27.865	0.232	9.903	0.403	0.087	99.29	0.19	Coalescent
C2	19_27	0	1.069	16.44	43.253	27.889	0.086	9.793	0.398	0.121	99.05	0.19	Coalescent

C2	19_28	0	1.117	16.531	43.349	28.294	0.358	9.756	0.397	0.132	99.93	0.19	Coalescent
C2	19_29	0.003	1.136	16.434	43.677	27.365	0.239	9.856	0.397	0.168	99.28	0.18	Coalescent
C2	19_3	0.004	1.056	16.42	43.673	28.03	0.292	9.672	0.39	0.159	99.7	0.19	Coalescent
C2	19_30	0	1.055	16.613	43.46	28.297	0.318	9.862	0.412	0.129	100.15	0.19	Coalescent
C2	19_31	0.052	1.059	16.697	42.907	27.944	0.325	9.759	0.43	0.119	99.29	0.19	Coalescent
C2	19_32	0.034	1.1	16.64	43.479	27.902	0.278	9.851	0.385	0.195	99.86	0.19	Coalescent
C2	19_33	0	1.09	16.36	43.529	27.708	0.345	9.737	0.396	0.146	99.31	0.19	Coalescent
C2	19_34	0	0.904	16.607	43.922	27.587	0.345	9.636	0.394	0.109	99.5	0.18	Coalescent
C1	19_37	0	1.11	15.579	44.366	28.009	0.324	9.359	0.44	0.127	99.31	0.18	Sub-Coalescent
C1	19_38	0	0.999	15.877	44.354	27.411	0.338	9.36	0.423	0.161	98.92	0.17	Sub-Coalescent
C1	19_39	0	1.057	15.668	43.76	27.33	0.456	9.308	0.43	0.164	98.17	0.18	Sub-Coalescent
C2	19_4	0.029	1.016	16.545	43.384	27.43	0.219	9.616	0.401	0.171	98.81	0.18	Sub-Coalescent
C1	19_40	0.056	1.244	14.837	44.836	28.621	0.33	9.103	0.423	0.154	99.6	0.19	Sub-Coalescent
C1	19_41	0.016	1.12	15.422	44.795	27.96	0.317	9.205	0.438	0.155	99.43	0.18	Sub-Coalescent
C1	19_42	0	1.089	15.626	44.836	27.872	0.351	9.141	0.424	0.187	99.53	0.17	Sub-Coalescent
C1	19_43	0.005	0.796	15.814	44.605	27.68	0.297	9.226	0.428	0.122	98.97	0.17	Sub-Coalescent
C1	19_44	0.013	1.006	15.292	44.504	27.812	0.244	9.308	0.397	0.124	98.7	0.18	Sub-Coalescent
C1	19_45	0	1.076	15.621	44.564	28.283	0.284	9.326	0.431	0.157	99.74	0.18	Sub-Coalescent
C1	19_46	0	0.855	15.754	44.807	28.159	0.503	9.421	0.428	0.12	100.05	0.18	Sub-Coalescent
C1	19_47	0	1.117	13.731	46.359	28.627	0.297	8.96	0.431	0.131	99.65	0.19	Sub-Coalescent
C1	19_48	0	0.89	14.969	45.191	28.626	0.383	9.154	0.434	0.17	99.82	0.19	Sub-Coalescent
C1	19_49	0	1.077	14.353	45.677	29.175	0.185	9.028	0.438	0.152	100.09	0.2	Sub-Coalescent
C2	19_5	0.015	1.032	16.55	43.756	27.661	0.272	9.725	0.399	0.145	99.56	0.18	Annealed
C1	19_50	0	0.976	15.055	45.079	28.052	0.311	9.172	0.416	0.13	99.19	0.18	Sub-Coalescent
C1	19_51	0	1.168	15.043	44.737	28.712	0.429	9.15	0.433	0.198	99.87	0.19	Sub-Coalescent
C1	19_52	0	1.22	14.831	45.108	28.423	0.317	9.217	0.437	0.133	99.69	0.19	Sub-Coalescent
C1	19_53	0	1.156	14.808	44.846	28.348	0.251	9.052	0.453	0.115	99.03	0.19	Sub-Coalescent
P4	19_54	0.001	0.992	14.6	43.985	30.949	0.343	7.66	0.425	0.143	99.1	0.2	Disseminated
P4	19_55	0.004	0.853	14.359	44.114	30.31	0.343	7.702	0.375	0.148	98.21	0.19	Disseminated

P4	19_56	0.015	0.98	12.296	46.569	31.003	0.382	7.361	0.454	0.162	99.22	0.2	Disseminated
P4	19_57	0.001	1.036	11.978	46.03	31.398	0.427	6.721	0.419	0.118	98.13	0.2	Disseminated
P4	19_58	0	1.01	12.154	46.043	31.562	0.42	6.719	0.425	0.177	98.51	0.2	Disseminated
P4	19_59	0.014	0.912	14.129	44.023	31.503	0.395	7.615	0.412	0.159	99.16	0.21	Disseminated
C2	19_6	0	1.02	16.482	43.597	27.077	0.465	9.686	0.419	0.136	98.88	0.18	Coalescent
P4	19_61	0	1.351	11.694	45.161	32.054	0.315	6.97	0.478	0.151	98.17	0.23	Disseminated
P4	19_62	0.019	1.273	10.358	46.033	34.636	0.386	5.651	0.451	0.173	98.98	0.24	Disseminated
P4	19_64	0	1.233	11.914	44.996	32.834	0.388	6.814	0.461	0.147	98.79	0.23	Disseminated
P4	19_65	0.006	1.091	10.252	47.267	33.113	0.308	5.686	0.497	0.138	98.36	0.21	Disseminated
P4	19_67	0	1.356	9.57	46.076	34.856	0.242	5.615	0.484	0.114	98.31	0.25	Disseminated
P4	19_68	0	1.398	10.451	46.703	32.43	0.341	6.223	0.448	0.116	98.11	0.22	Disseminated
C2	19_7	0	1.079	16.815	43.129	27.566	0.239	9.551	0.407	0.166	98.95	0.18	Coalescent
P4	19_71	0	1.053	10.32	46.918	33.543	0.42	5.918	0.48	0.186	98.84	0.23	Disseminated
P4	19_73	0	1.311	8.027	48.844	34.868	0.398	4.775	0.506	0.155	98.88	0.23	Disseminated
C2	19_9	0	1.059	16.822	43.074	27.787	0.352	9.553	0.392	0.156	99.19	0.18	Coalescent
U2	25_1	0.01	1.058	13.903	41.803	34.559	0.337	5.952	0.499	0.059	98.18	0.236	Coalescent
U2	25_10	0.024	0.762	19.104	42.549	27.302	0.447	9.659	0.407	0.099	100.35	0.156	Coalescent
U2	25_11	0.021	0.811	19.051	42.788	26.838	0.167	9.371	0.384	0.091	99.52	0.138	Coalescent
U2	25_12	0	0.808	18.975	42.492	25.593	0.447	9.382	0.352	0.087	98.14	0.128	Coalescent
U2	25_14	0	0.771	18.169	43.398	26.048	0.32	9.409	0.384	0.018	98.52	0.135	Annealed
U2	25_15	0.012	0.755	19.696	41.873	26.876	0.34	9.728	0.377	0.087	99.74	0.148	Coalescent
U2	25_16	0	0.774	18.43	43.282	26.468	0.393	9.512	0.402	0.051	99.31	0.143	Coalescent
U2	25_17	0	0.812	18.841	42.233	27.05	0.173	9.395	0.385	0.068	98.96	0.148	Annealed
U2	25_18	0.013	0.833	18.268	43.038	27.689	0.366	9.297	0.412	0.081	100	0.158	Annealed
U2	25_19	0	0.797	18.567	42.74	26.528	0.367	9.548	0.348	0.068	98.96	0.146	Annealed
U2	25_2	0	1.248	13.178	41.467	35.09	0.522	6.082	0.484	0.021	98.09	0.261	Coalescent
U2	25_20	0.01	0.792	17.922	43.412	26.537	0.14	9.483	0.383	0.037	98.72	0.144	Coalescent
U2	25_3	0	1.355	13.337	41.321	33.595	0.297	6.295	0.517	0.046	96.76	0.243	Annealed
U2	25_4	0	1.277	12.882	41.752	34.06	0.31	6.219	0.49	0.034	97.02	0.249	Coalescent

U2	25_5	0	0.829	19.297	42.05	27.258	0.44	9.601	0.408	0.064	99.95	0.154	Coalescent
U2	25_6	0	0.831	18.894	42.632	26.797	0.3	9.458	0.378	0.031	99.32	0.143	Coalescent
U2	25_7	0	0.817	19.312	41.853	25.902	0.307	9.551	0.41	0.084	98.24	0.137	Coalescent
U2	25_8	0	0.833	19.576	42.084	26.832	0.267	9.672	0.379	0.041	99.68	0.144	Coalescent
U2	25_9	0.017	0.836	20.506	40.63	26.728	0.2	9.781	0.42	0.049	99.17	0.147	Coalescent

Appendix 8.3: Electron microprobe images with sample points.

Some photomicrographs have been left out due to them being unclear.

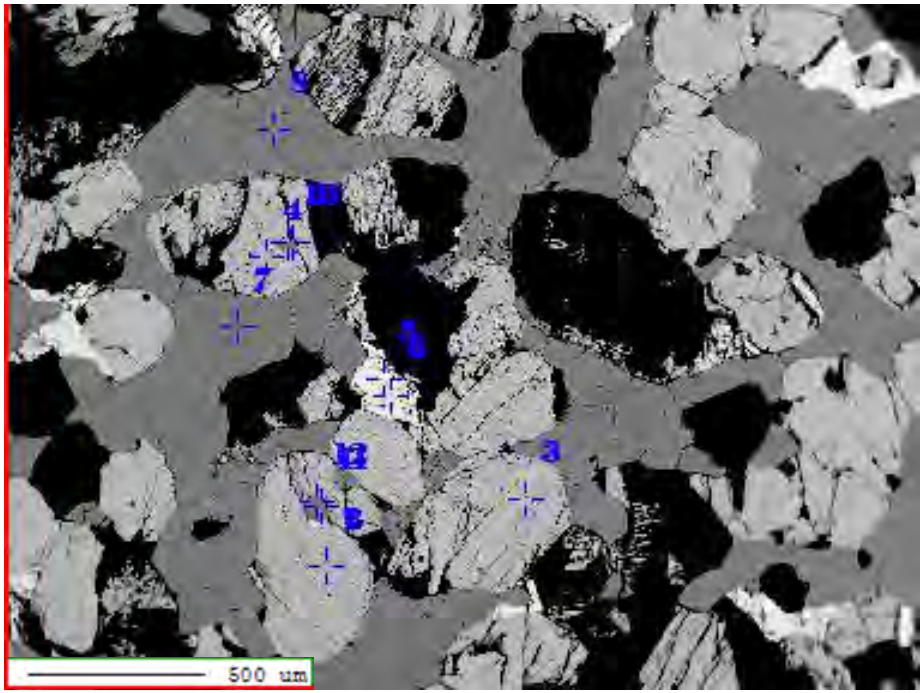

Sample P1 image 1 showing plagioclase and pyroxene sample points.

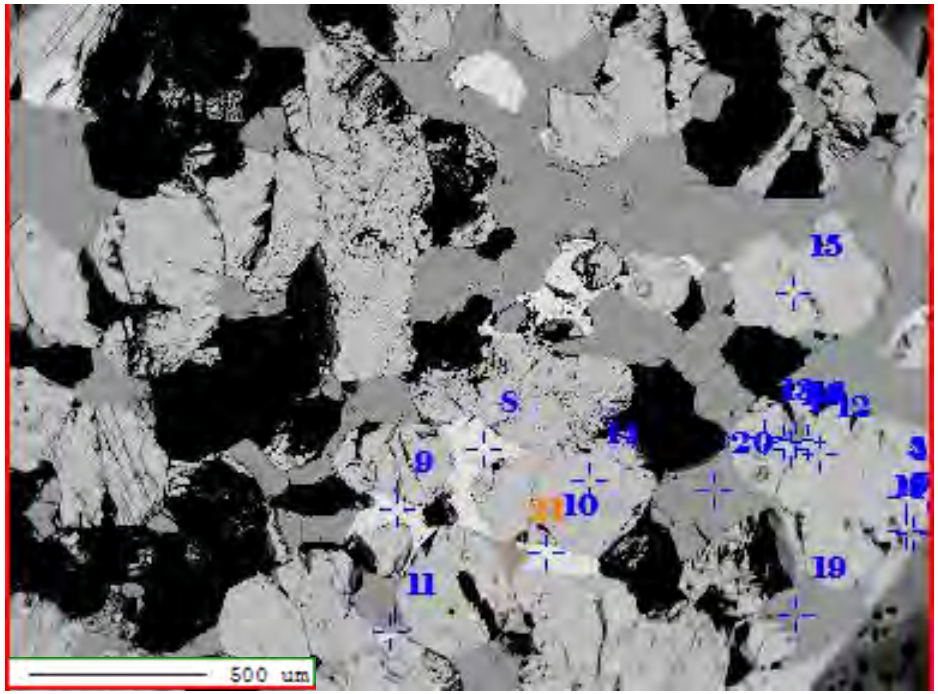

Sample P1 image 2 showing plagioclase and pyroxene sample points.

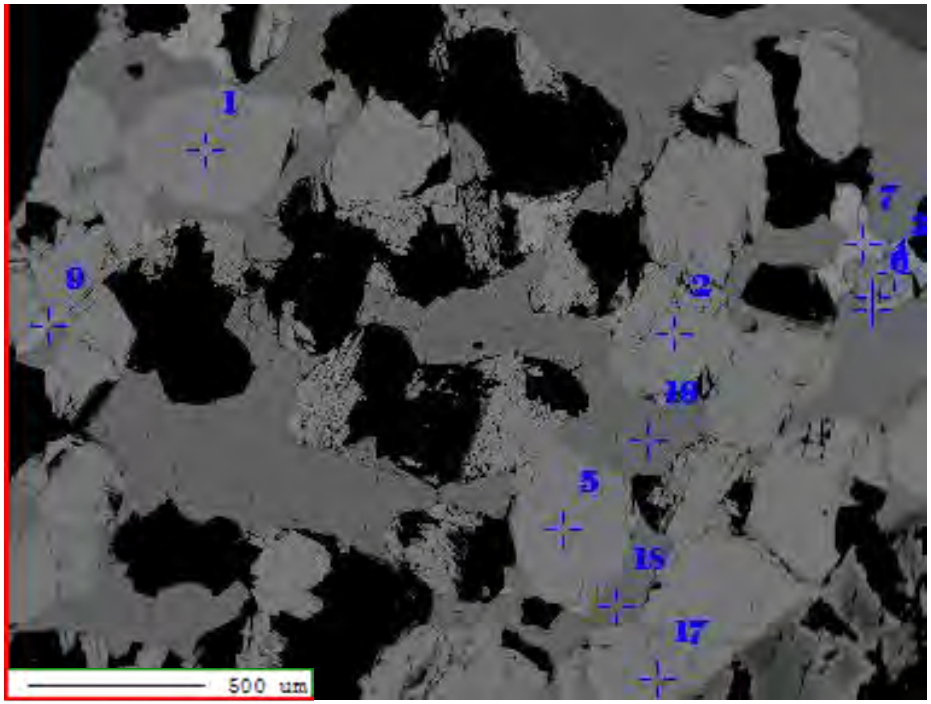

Sample P1 image 3 showing plagioclase and pyroxene sample points.

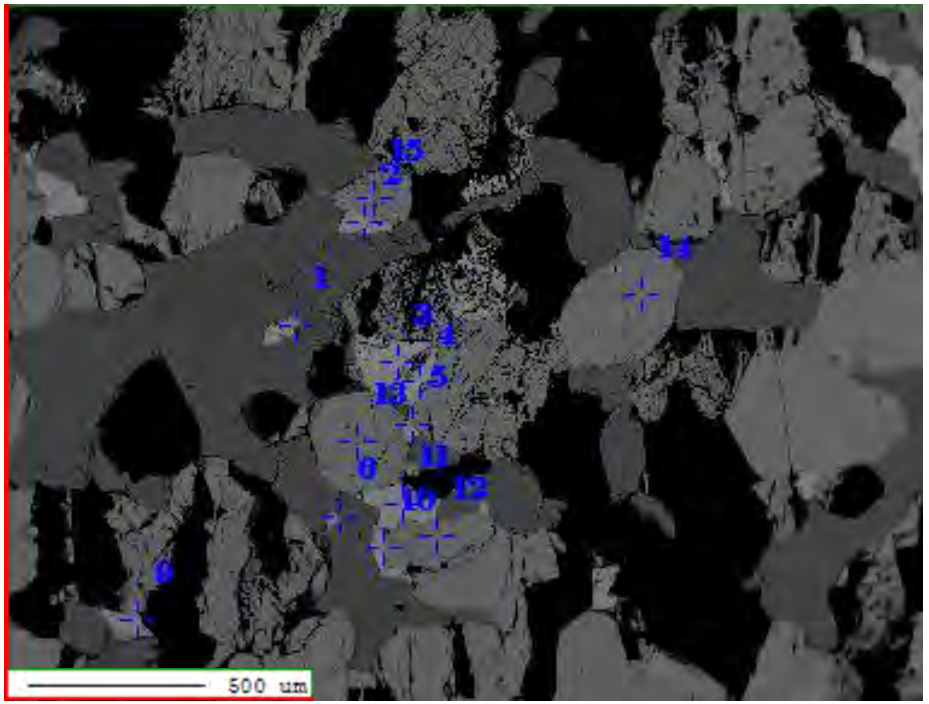

Sample P1 image 4 showing plagioclase and pyroxene sample points.

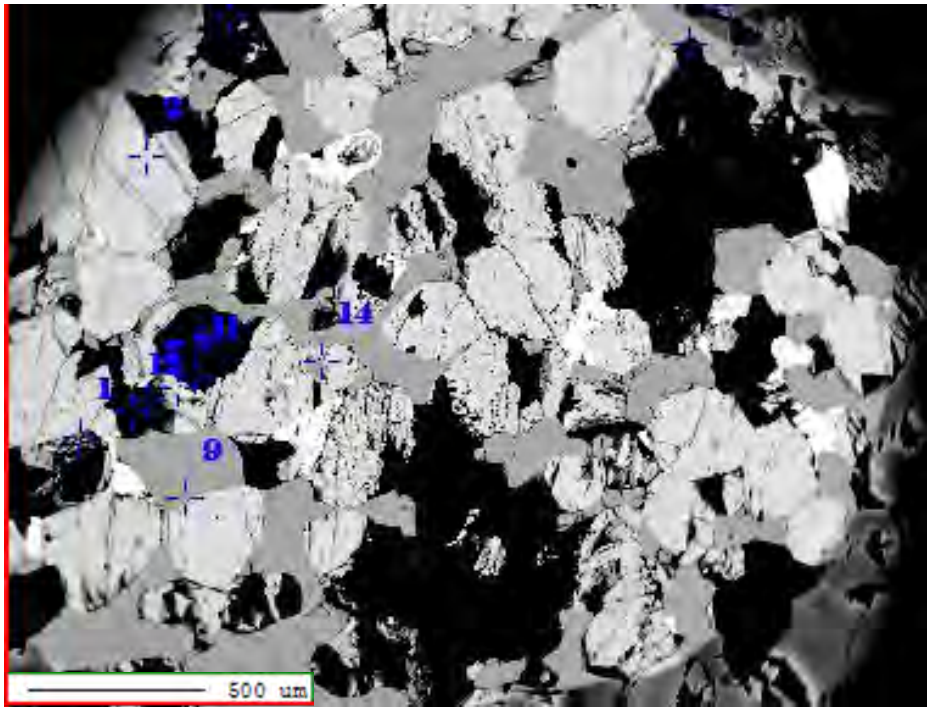

Sample P1 image 5 showing plagioclase and pyroxene sample points.

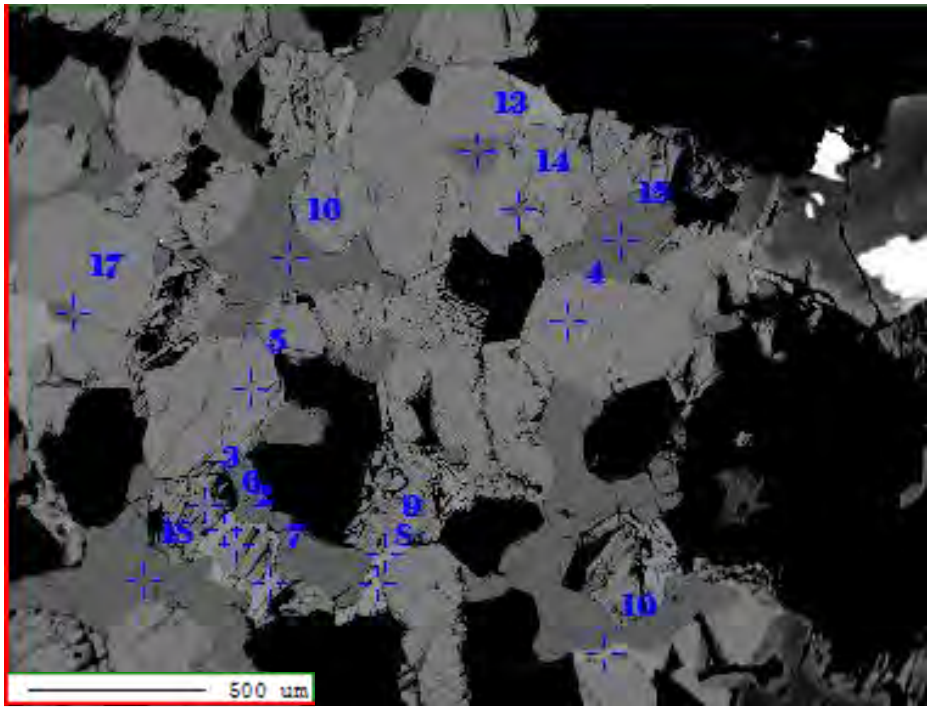

Sample P1 image 6 showing plagioclase and pyroxene sample points.

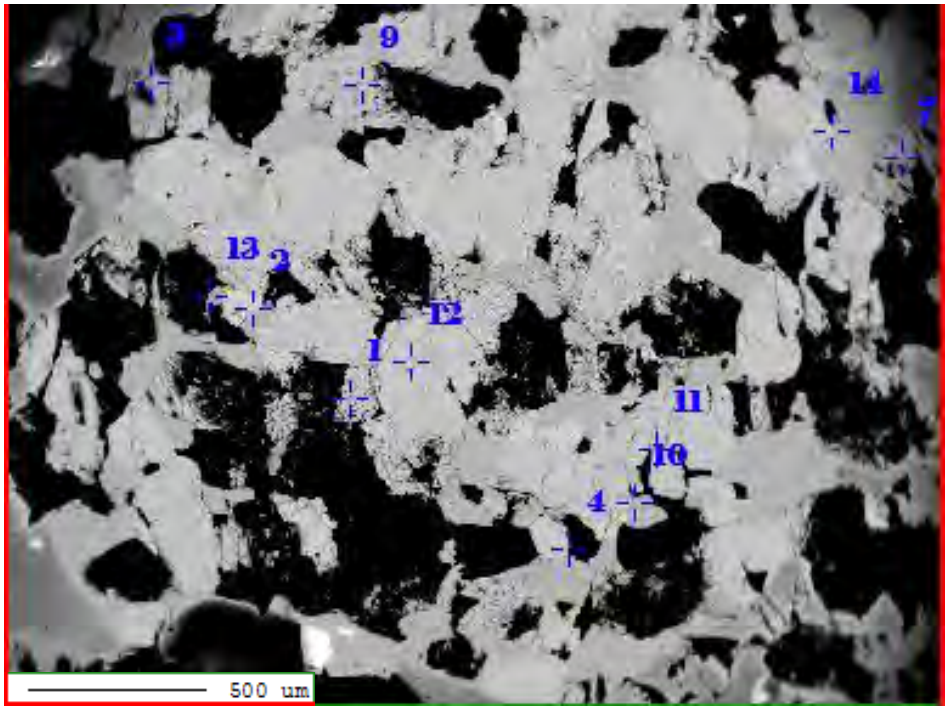

Sample P1 image 7 showing plagioclase and pyroxene sample points.

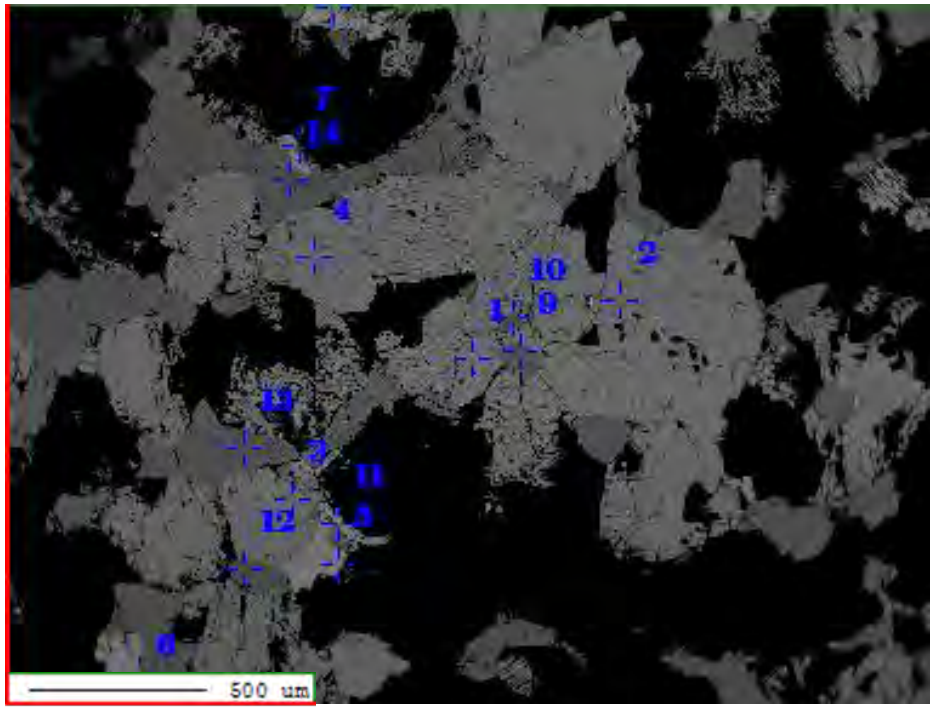

Sample P1 image 8 showing plagioclase and pyroxene sample points.

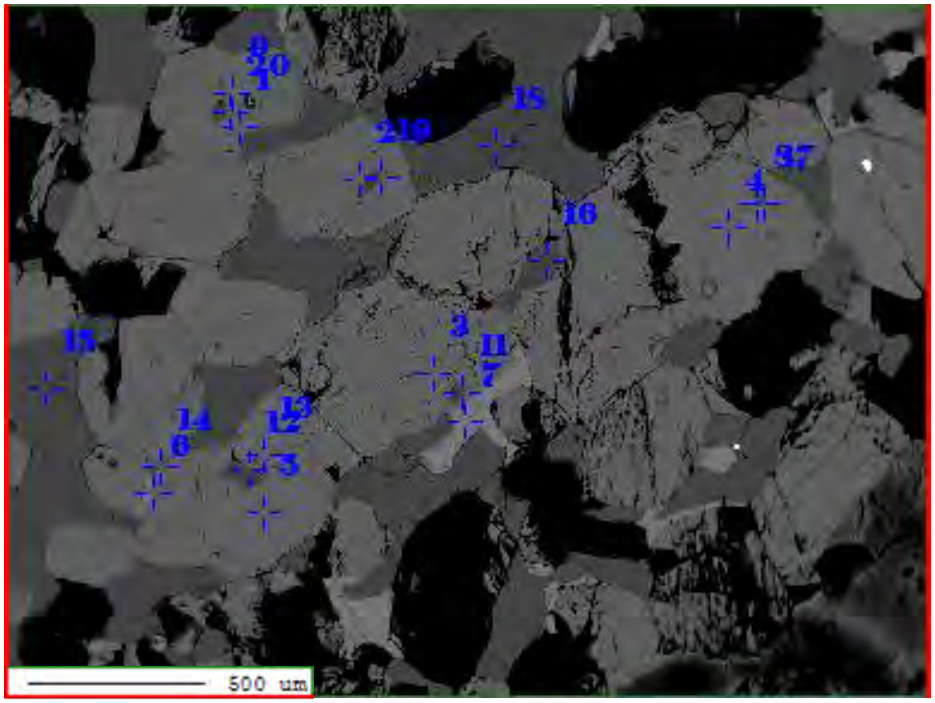

Sample P1 image 9 showing plagioclase and pyroxene sample points.

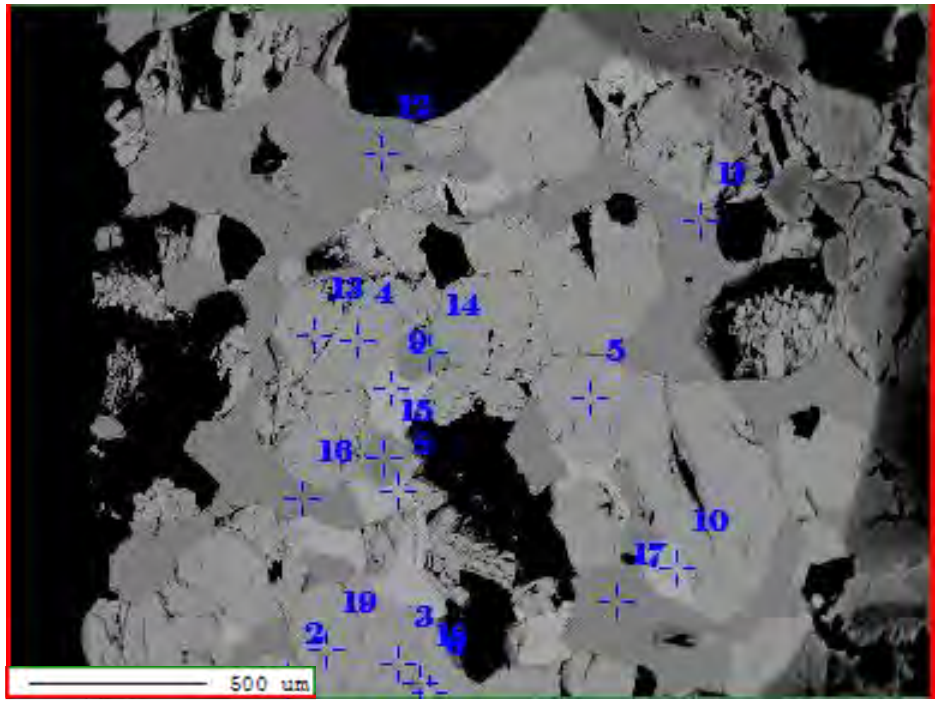

Sample P1 image 10 showing plagioclase and pyroxene sample points.

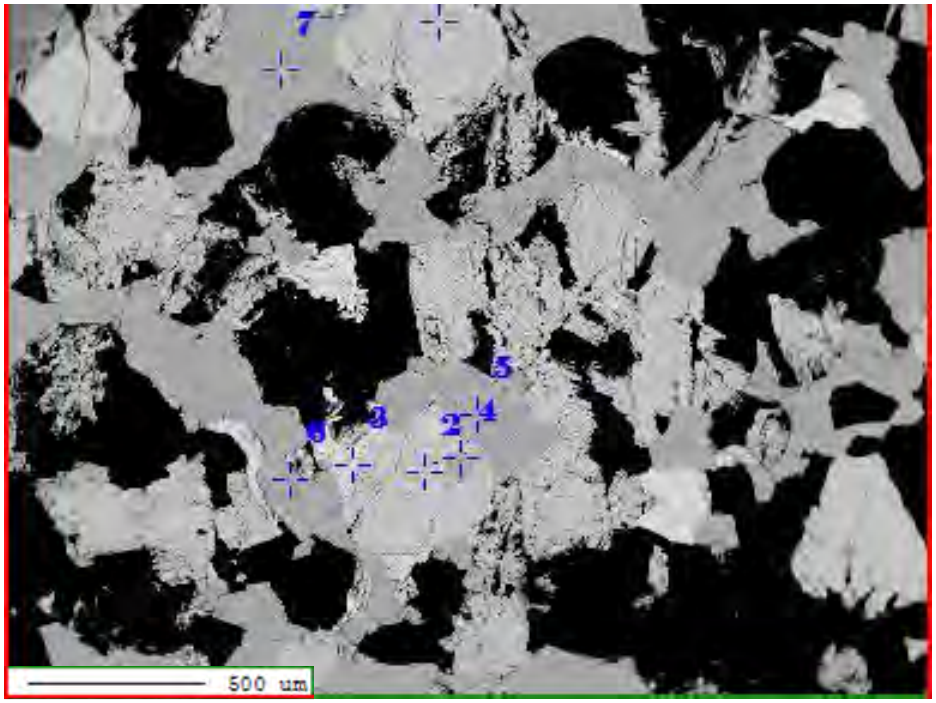

Sample P1 showing plagioclase and pyroxene sample points.

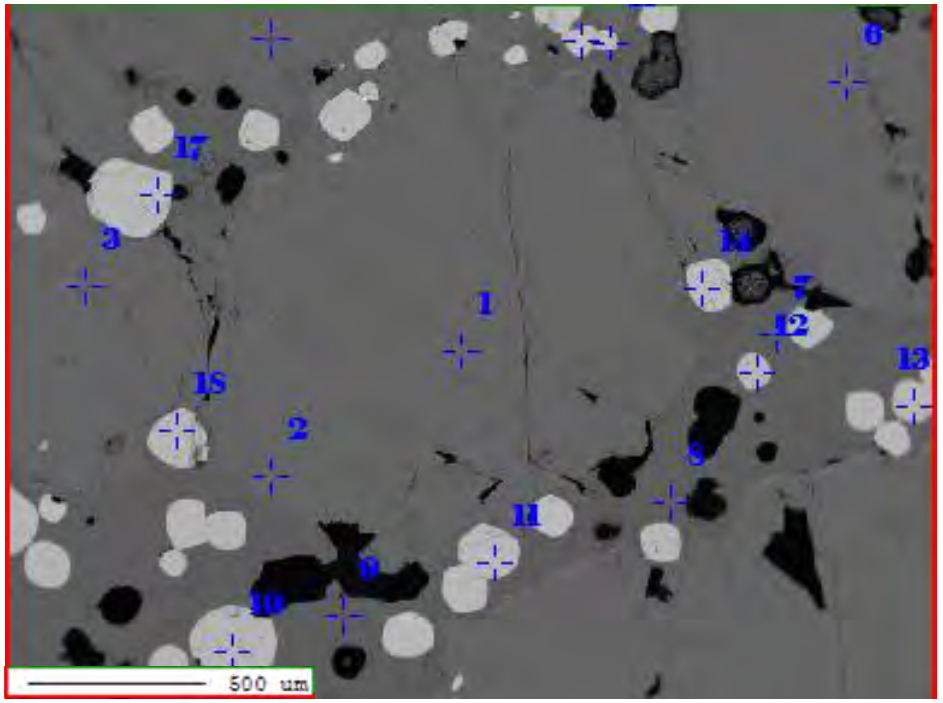

Sample P4 image 1 showing plagioclase, pyroxene and chromite sample points.

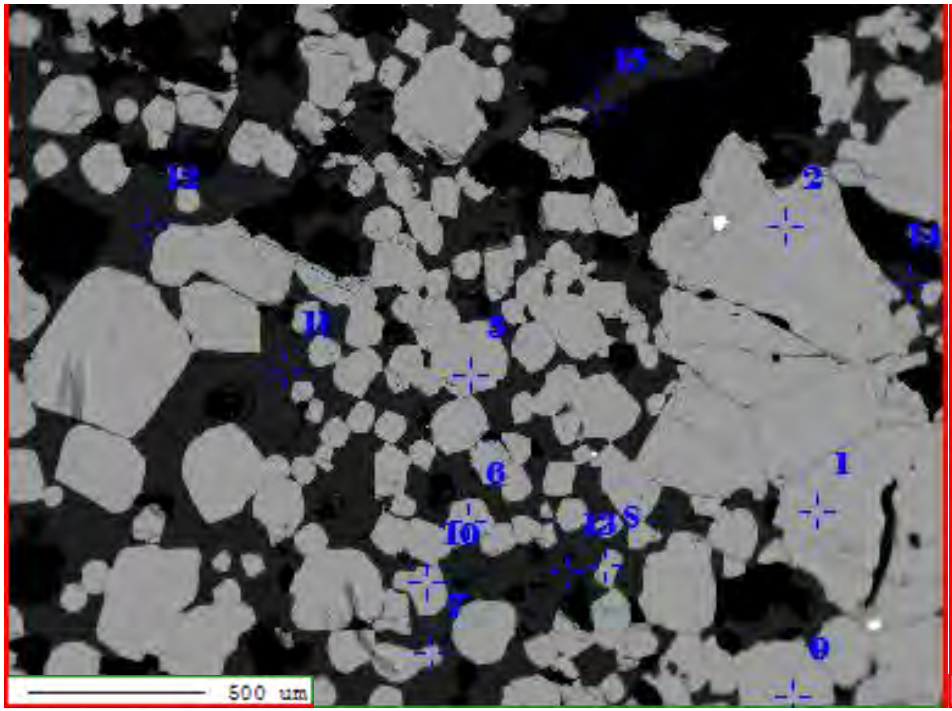

Sample C1 showing plagioclase and chromite sample points.

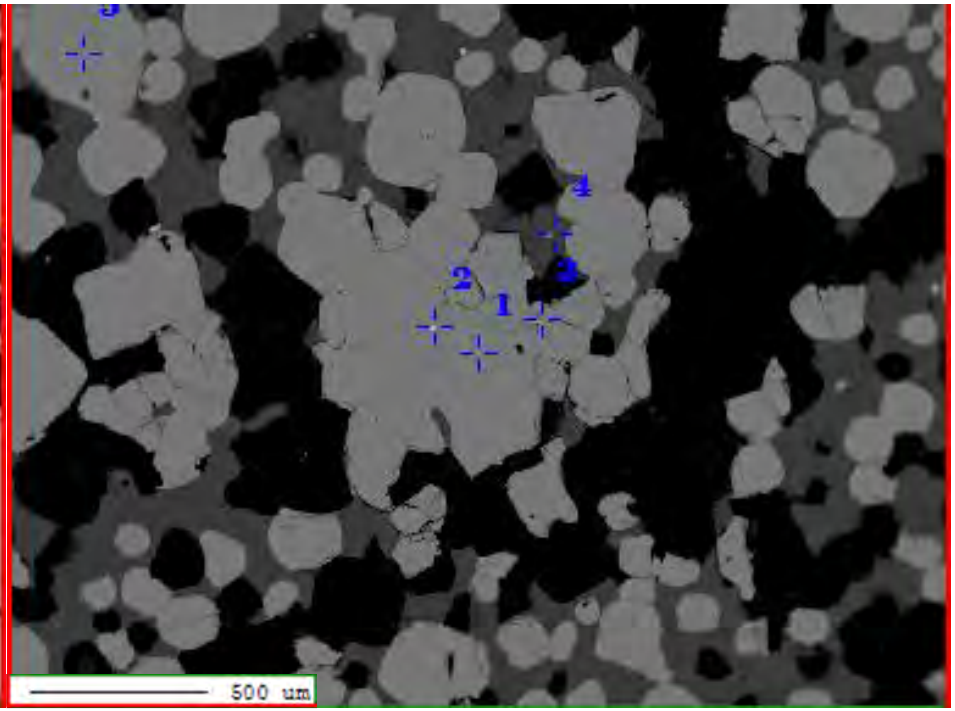

Sample C1 showing chromite sample points.

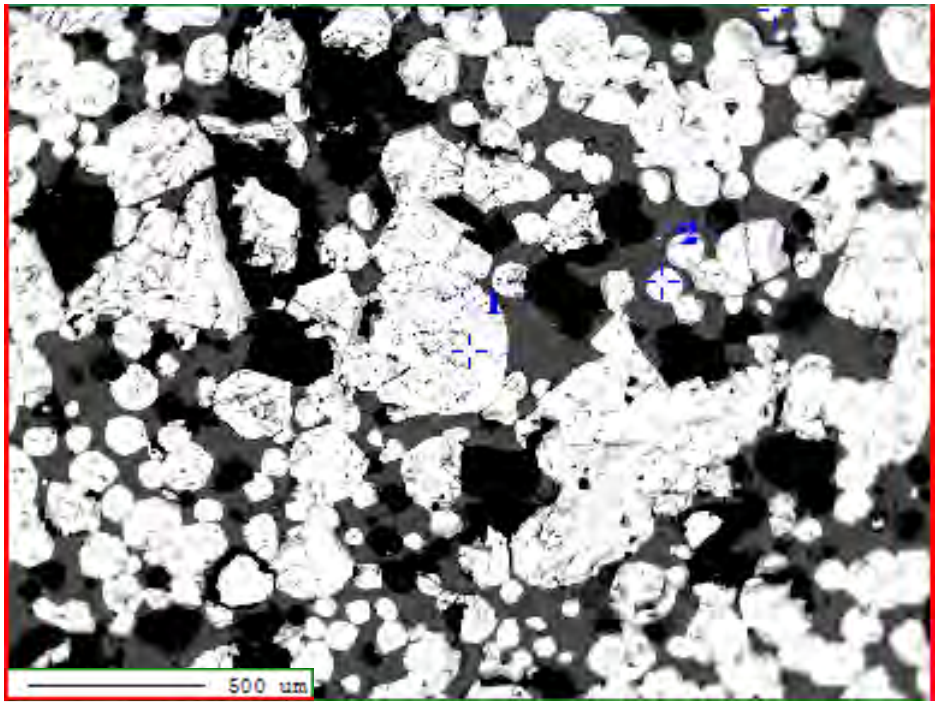

Sample C2 image 1 showing chromite sample points. Some points do not appear on the image due to the probe imager being slightly off and some of the points being taken just off the edges of the picture.

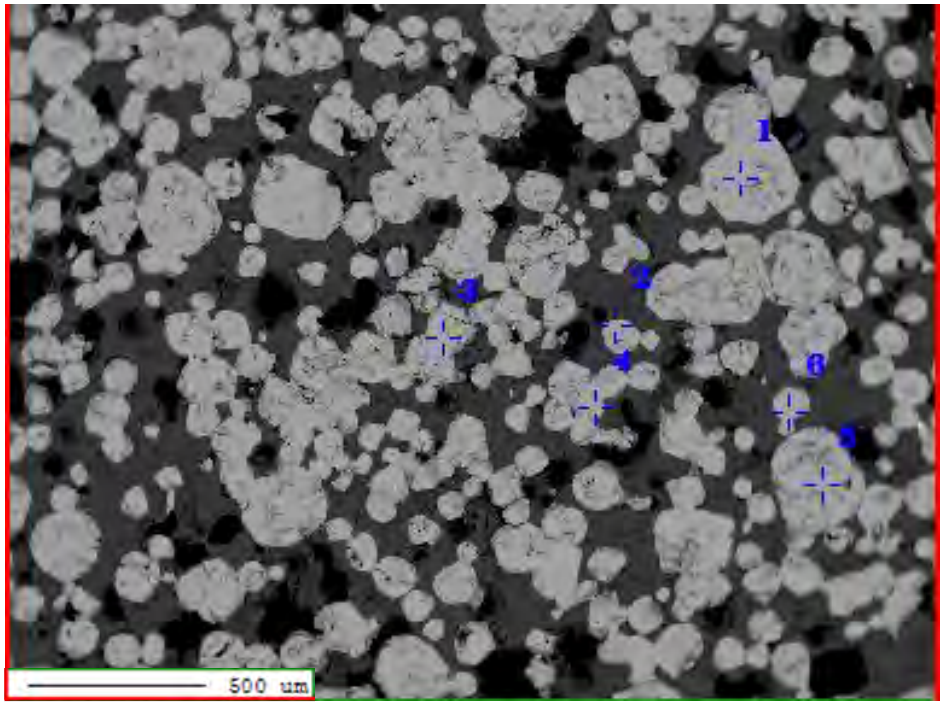

Sample C2 showing chromite sample points.

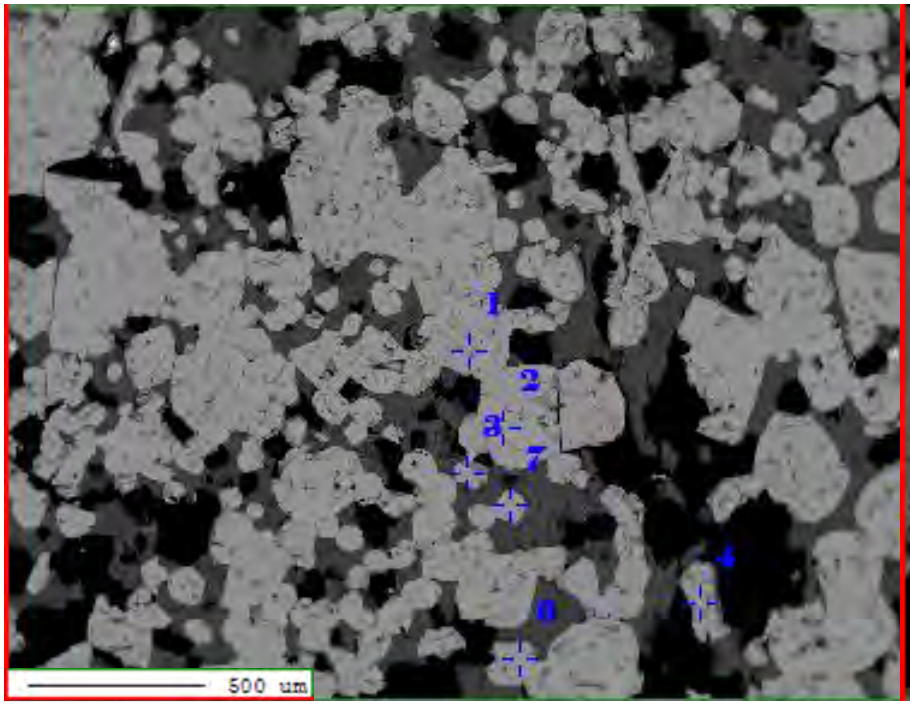

Sample C2 showing chromite sample points.

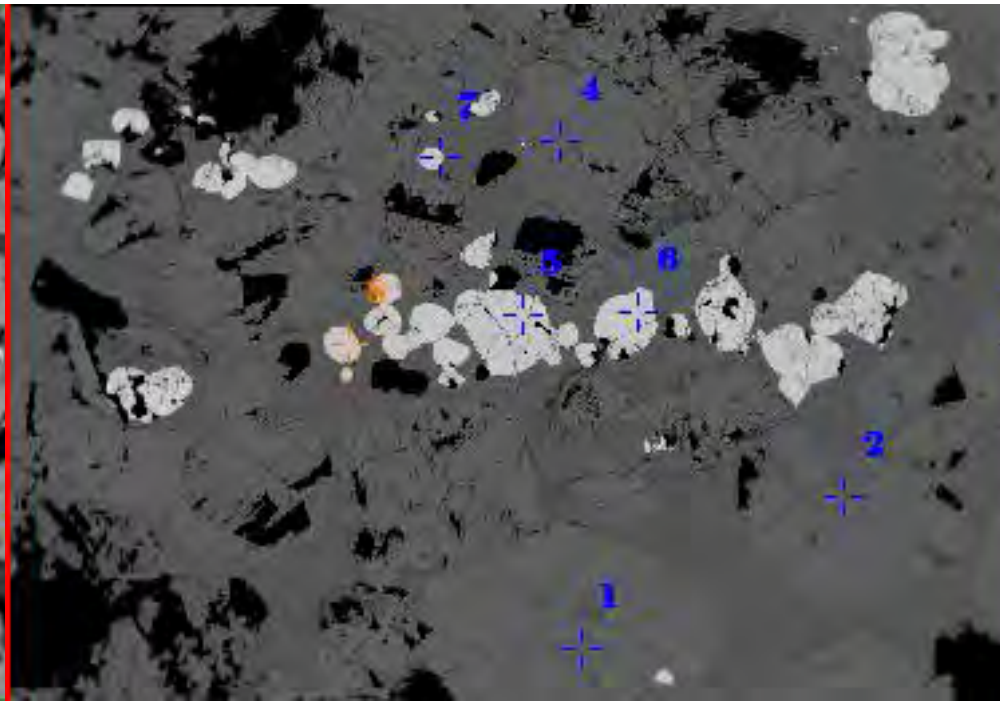

Sample U2 showing chromite and pyroxene sample points.

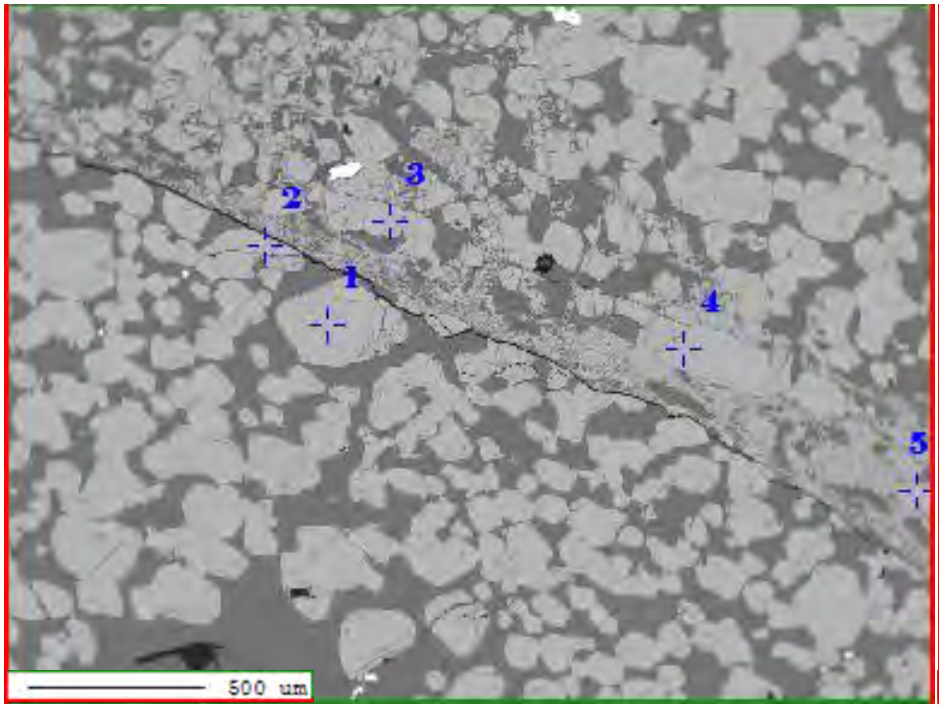

Sample U2 showing chromite sample points. Photomicrograph also shows chromite following a fracture.

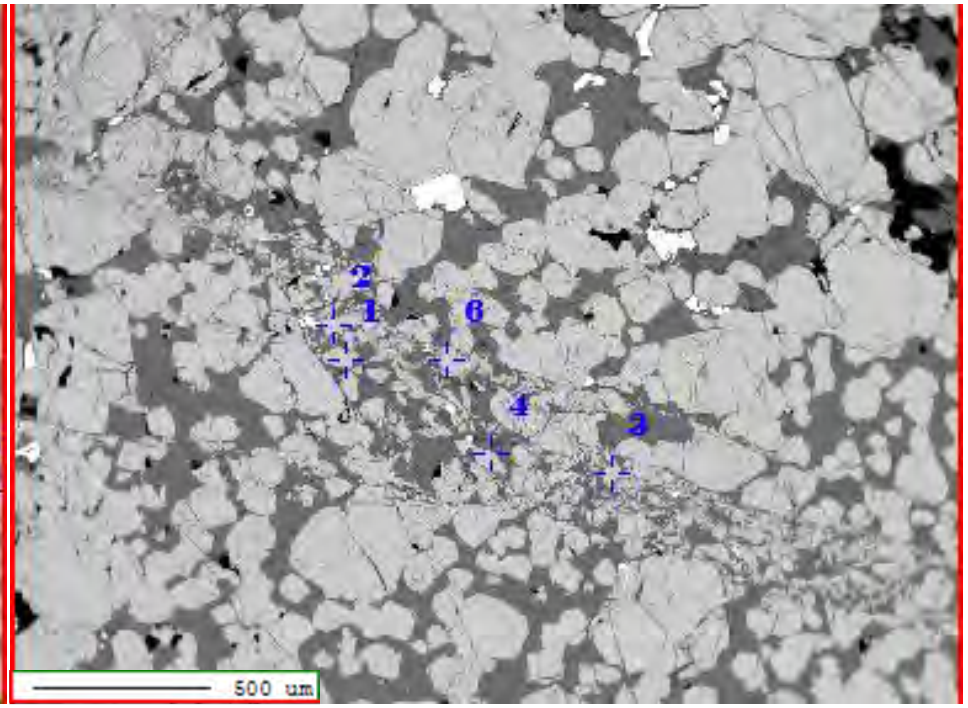

Sample U2 showing chromite sample points. Photomicrograph again showed chromite following the same fracture as the previous photomicrograph.

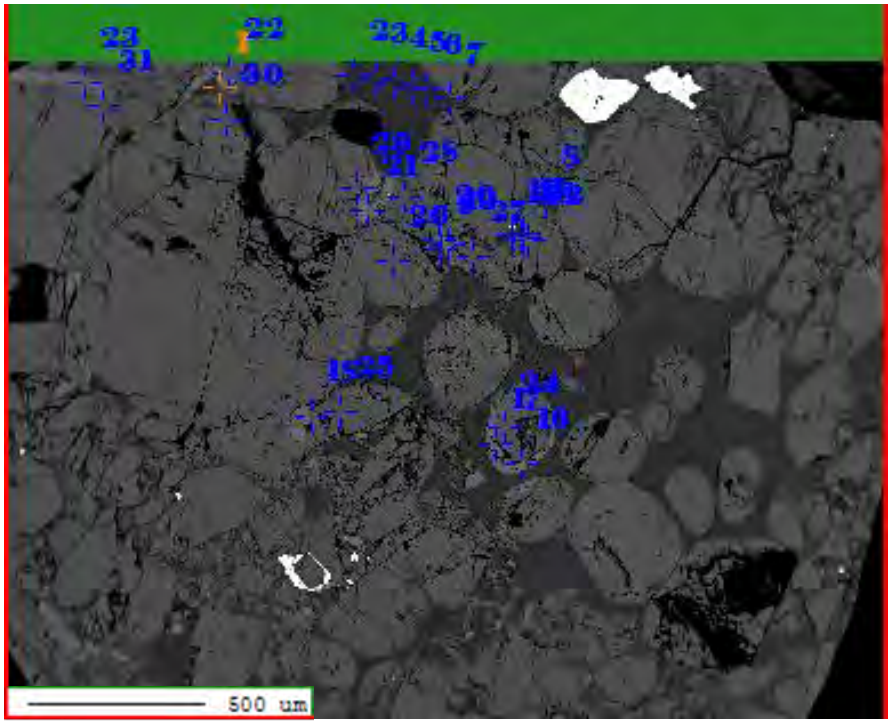

Sample U5 image 1 showing plagioclase and pyroxene sample points.

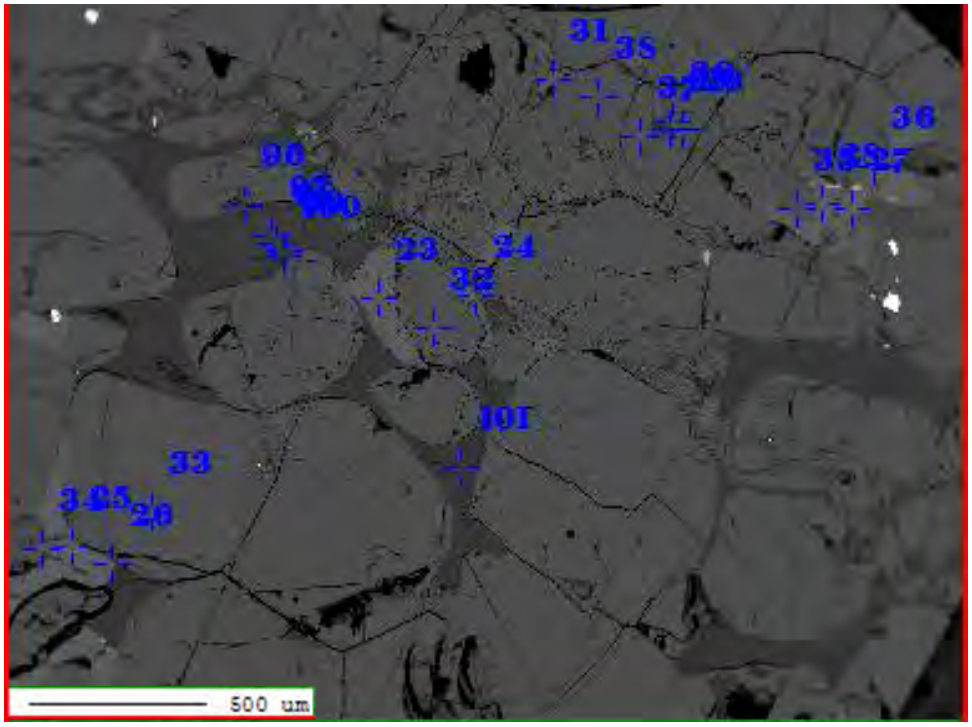

Sample U5 image 2 showing plagioclase and pyroxene sample points. Photomicrograph shows rounded zone of norite.

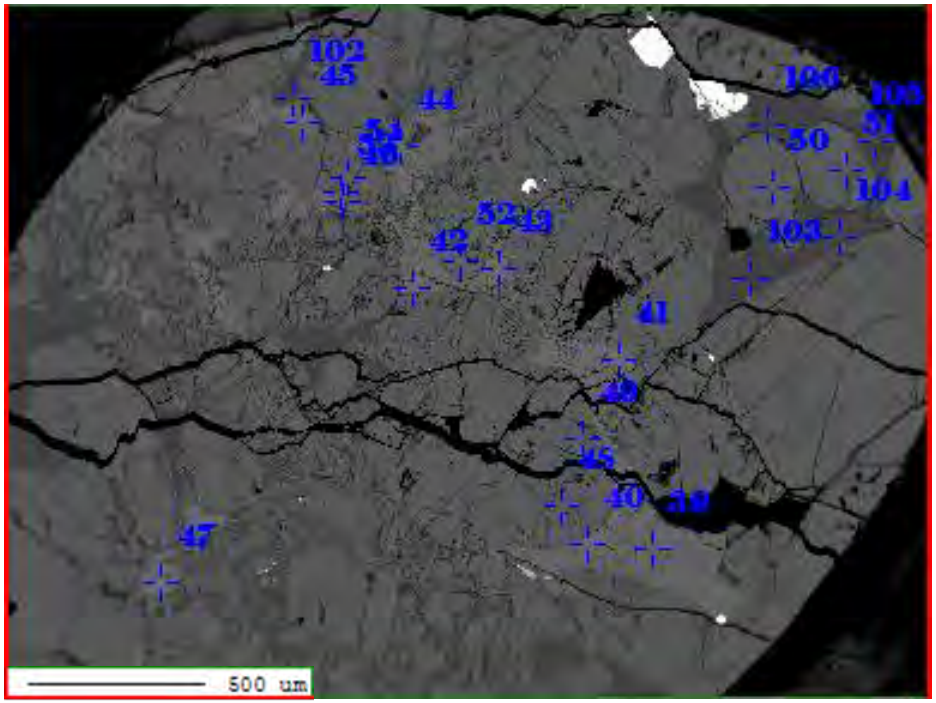

Sample U5 image 3 showing plagioclase and pyroxene sample points.

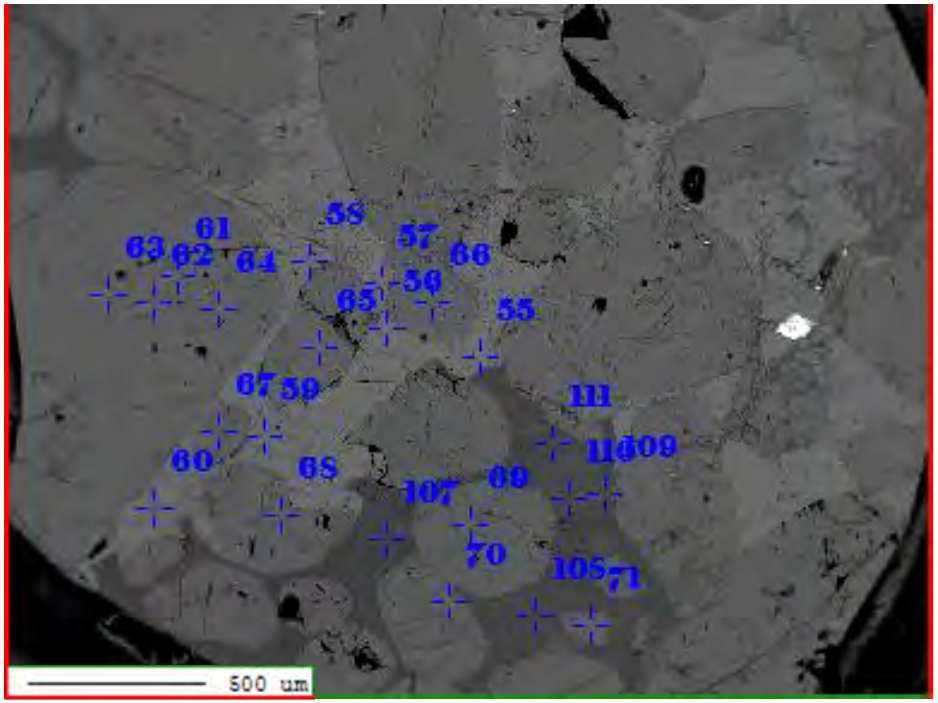

Sample U5 image 4 showing plagioclase and pyroxene sample points. Photomicrograph again shows rounder norite zone. Also shows fluid boundary between clinopyroxene and plagioclase.

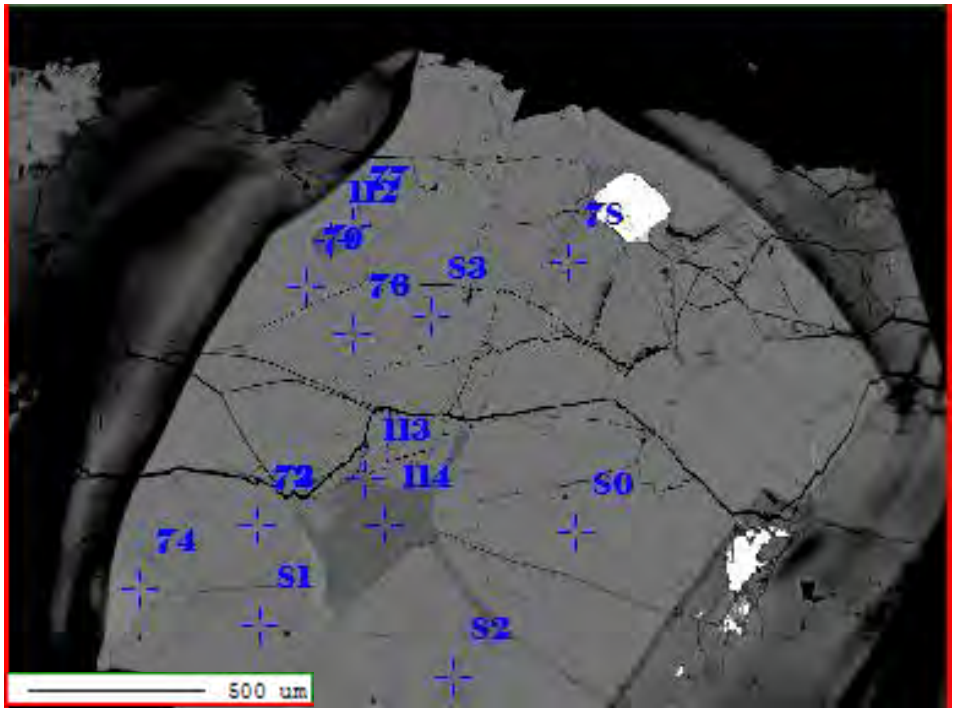

Sample U5 image 5 showing plagioclase and pyroxene sample points.